ELASTIC ELECTRON SCATTERING MEASUREMENTS OF THE NEUTRON CHARGE FORM FACTOR AT VERY LOW MOMENTUM TRANSFERS

Jake W. Stewart

United States
Naval Postgraduate School

THESIS

ELASTIC ELECTRON SCATTERING MEASUREMENTS
OF THE NEUTRON CHARGE FORM FACTOR
AT VERY LOW MOMENTUM TRANSFERS

by

Jake W. Stewart, Jr.

June 1970

Elastic Electron Scattering Measurements of the Neutron Charge Form Factor at Very Low Momentum Transfers

by

Jake W. Stewart, Jr.
Lieutenant Commander, United States Navy
B.S., Georgia Institute of Technology, 1962

Submitted in partial fulfillment of the
requirements for the degree of

DOCTOR OF PHILOSOPHY

from the

NAVAL POSTGRADUATE SCHOOL
June 1970

ABSTRACT

Measurements of the ratio of the neutron-proton electric form factors, G_{E_n}/G_{E_p}, were made from elastic electron-deuteron scattering to a precision of approximately 1 to 2% for the range of momentum transfers, q^2, of $0.10 \leq q^2 \leq 0.8\ F^{-2}$, and for electron scattering angles of 45° to 120°. It was found that within experimental errors the slope as determined from the ratio G_{E_n}/G_{E_p}, agrees with the thermal neutron-electron interaction slope when relativistic corrections and proper deuteron wave functions are applied to the electron-deuteron scattering results.

TABLE OF CONTENTS

LIST OF TABLES

LIST OF FIGURES

Figure

ACKNOWLEDGEMENTS

It is a pleasure to mention some of those people who have contributed so much to the completion of this thesis. The author owes a great debt of thanks to Professor Franz Bumiller. It was his persistence, encouragement, and unfailing help that made the accomplishment of this work possible. To Dr. Ed Dally and Professor Bumiller many thanks for their help with the experiment at the High Energy Physics Laboratory, Stanford University. Much credit is due to Professors Fred Buskirk and John Dyer for their herculean efforts in keeping the Naval Postgraduate School LINAC running through many troublesome days.

Fellow students also should share the credit for this thesis: 1st Lieutenant L. P. Gaby, USAF, for his continuing work in computer programming; 1st Lieutenant John Gordon, USAF, for many stimulating discussions and hours of assistance in running the machine.

Experimental setups were accomplished with the aid of Mr. Don Snyder of the LINAC group and Mr. Mike O'Dea of the Machine Shop.

I. INTRODUCTION

A. EXPERIMENTAL OBJECTIVES

The charge form factor of the neutron, G_{E_n}, as determined by electron scattering is found to be essentially zero in the range of momentum transfers, q^2, of $0.3 \leq q^2 \leq 100\ F^{-2}$. This fact is in apparent conflict with the results obtained by the scattering of thermal neutrons from atomic electrons. By methods to be described later, measurements of the slope of the neutron charge form factor at very low momentum transfers of $q^2 \simeq 10^{-9}\ F^{-2}$, show that

$$\left[\frac{dG_{E_n}}{d(q^2)}\right]_{q^2\to 0} = +0.0193 \pm 0.0004\ F^2 \qquad (1\text{-}1)$$

It is very doubtful that a non-zero slope for G_{E_n} at $q^2 \to 0$ can be reconciled with $G_{E_n} \simeq 0$ at $q^2 \geq 0.3\ F^{-2}$.

Drickey and Hand [1] in 1962 measured G_{E_n}/G_{E_p} for values of q^2, $0.3 \leq q^2 \leq 2.2\ F^{-2}$ to an accuracy of about 2%. Their results yielded $G_{E_n} \simeq 0$, but when reanalyzed by Casper and Gross [2] (1966) using recently developed deuteron relativistic corrections and new deuteron wave functions, the value of G_{E_n} was brought into fair agreement with the value of (1-1). Thus the entire problem is further complicated by the extreme sensitivity of G_{E_n} to the different deuteron models assumed. Hence, if very accurate measurements of G_{E_n}, for q^2 small, can be made by electron-scattering

techniques, a comparison with the value (1-1) could be made, which might yield an answer to the "correct" deuteron model to be chosen.

It is the purpose of this experiment to (a) demonstrate the basic agreement between the thermal neutron-electron slope value of G_{E_n} and the electron scattering G_{E_n}; and (b) try to determine which deuteron wave function (model), best describes the deuteron.

B. NUCLEAR STRUCTURE FROM ELECTRON SCATTERING

Since the early 1950's production of beams of high energy electrons by linear accelerators (LINACS) has made possible the study of the electromagnetic structure of the nucleon. It is expected that the dimensions of any particle of mass m is of the order of $\hbar/mc$, which for a nucleon is about 2×10^{-14} cm. Hence, to investigate the structure in this size range it is necessary to use a probe having about these wave lengths or shorter. Linacs produce electrons with just such wave lengths. The 100 MeV NPS Linac thus "sees" only the outer structure or surface of the nucleus.

Electron scattering has several definite advantages over other methods of nuclear structure research. Briefly, the important reasons that electron scattering is such a useful tool are the following:

(a) The basic interaction between the electron and target nucleus is known; the electron interacts with the charge-current density and magnetization density of the

nucleus. Since the electromagnetic interaction is relatively weak, of the order of $\alpha = 1/137$, the fine structure constant, measurements on the target nucleus can be made without greatly disturbing its structure.

This is in contrast to the situation with protons, neutrons and alpha particles, since they are strongly interacting particles, and the scattering mechanism cannot be clearly separated from structure effects in the target.

(b) Photons interact electromagnetically with the nucleus, but since a real photon has rest mass zero, it can transfer only a definite amount of momentum to the struck nucleus. This is in contrast to electron scattering where the momentum transferred to the nucleus is limited only by the energy lost to the nucleus.

The probability that an incident electron of total energy E is scattered elastically at an angle θ (i.e., σ, the cross section for elastic scattering at angle θ) can be calculated precisely on the assumption that the target nucleus consists of point nucleons. That means the charge and magnetization densities are delta functions. The actual cross sections differ from the predicted cross section if the charge and magnetic moment are spread out, and the difference is usually in the direction of smaller values of the cross section since the smeared out structure reduces the field against which the particles scatter. The deviation becomes greater as the parameter, q, the momentum

transferred to the struck nucleon increases. The (three) momentum transfer is defined by

$$\vec{q} = \vec{p}_f - \vec{p}_i \qquad (1\text{-}2)$$

where $\vec{p}_i$ and $\vec{p}_f$ are the incident and final values of the electron momentum. The effect of structure of the nucleons is normally expressed by the use of form factors, G, which are believed to be functions of the structure and momentum transfer only;

$$G^2(q^2) = \frac{\text{cross section for scattering from physical particles}}{\text{cross section for scattering from point particles}} . \qquad (1\text{-}3)$$

Note that similar ideas occur in all scattering situations in which the structure of the scattering center has an influence, e.g., x-ray scattering form factors reflecting the electronic structure of atoms.

C. ELECTRON SCATTERING FROM DEUTERIUM

The deuteron, as the only bound two-nucleon state, has been the source of much information for nuclear physics, due initially to the great interest in the two-nucleon problem. Originally the two-body problem was thought to be of great importance because of its relative mathematical simplicity, and because of the hope that the inter-nucleon force was additive, so that knowledge of this system's solution would allow extension to more complex nuclei. It is now generally assumed that the nuclear force is not additive (e.g., the nuclear force, unlike the electromagnetic

force, "saturates") and hence the two-nucleon interaction is not necessarily the best source through which understanding of the nature of the nuclear force can be gained.

Since free neutrons are unstable and decay with a half-life of 17 minutes to a proton and electron, deuterium is a convenient source for neutrons as targets. For this experiment deuterium in the form of solid deuterized polyethylene $(CD_2)_n$, was used as a target. Assuming that deuteron wave functions are known from theory, neutron structure is inferred through a comparison of electron-proton and electron-deuteron scattering results. Conversely, knowing the nucleon form factors from theory makes comparisons of different deuteron wave functions possible.

There are several possible outcomes to an electron-deuteron scattering experiment:

(1) $e + D \rightarrow e' + D'$ (elastic scattering)

(2) $e + D \rightarrow e' + P + N$ (inelastic scattering, break-up)

(3) Radiative scattering

(4) Reactions with pion production.

Now (2) occurs only above 2.2 MeV excitation energy and is not of interest here; (3) can be calculated; (4) is not a problem for incident energies smaller than 150 MeV. The theory for process (1) was developed initially by Jankus [3] (1956) in the first Born approximation, which should be adequate because of the small deuteron charge. The deuteron is described by nonrelativistic wave functions while the electron is treated relativistically. Jankus's result will be presented in Section II, part B3.

Attempts at a relativistic deuteron theory were initiated by Jones and carried forward by several authors, principally Gourdin, Adler and Gross [4, 5, 6, 7, 8, 9, 10, 11]. Results of their attempts will be presented in Section II, part B5.

D. THE NEUTRON-ELECTRON INTERACTION

The neutron-electron (n-e) interaction is the term used to describe part of the electromagnetic interaction between the neutron and the electron. This interaction may not only be a specific interaction between neutron and electron, but between any charged particle and the neutron. Furthermore, there exists the possibility of some n-e interaction of a nonelectromagnetic (weak) nature. For the present case however, results that stem from the interaction of an electron with the internal electromagnetic structure of the neutron will be termed "the neutron-electron interaction."

Since the neutron has zero total charge there is no Coulomb interaction between a neutron and an electron. Both particles have magnetic moments and hence there exists a spin- dependent magnetic dipole - dipole interaction between them and also a velocity-dependent interaction between the magnetic moment of the neutron and the magnetic field associated with the convection current of an electron in motion. These interactions have been well documented and are not of interest here [12]. If there are regions of non-zero charge-density in the neutron, (i.e., a charge separation exists) then any charged particle probing the

neutron will experience spin and velocity- independent electrostatic forces. These are the forces of interest in the n-e interaction.

At least some charge separation in the neutron is expected on the basis that the free neutron possesses an anomalous magnetic moment. This contribution to the interaction is called the magnetic or Foldy term [13]. The remainder of the interaction (due to charge separation) is the result of the fact that a neutron can be part of the time dissociated into a negative pion and a proton,

$$n \leftrightarrow p^{+} + \pi^{-}.$$

If the neutron spends 80% of the time as a neutron and 20% of the time as a proton + negative pion, then an electron penetrating the 'neutron' would see an electric field strength equal to that produced by a charge of 0.2e, e the proton charge. The force resulting from the field would have a very short range since the π^{-} would screen the positive charge at distances greater than the π^{-} p^{+} separation. (The separation can be on the order of the pion's Compton wave length $\hbar/m_{\pi}C \sim 10^{-13}$ cm.) The force should be attractive and can be represented as an extremely narrow potential well. The purpose of all the experiments described below was to determine the well depth V_{o}, essentially by measuring the scattering amplitude.

The first of three techniques to measure the n-e interaction was introduced by Havens, Rabi, and Rainwater [14]

in 1947. It consisted of scattering low energy neutrons (~0.1 eV) from liquid lead and bismuth, noting that the total scattering cross section of an atom includes an observable term arising from interference between the nucleus and the electrons scattering coherently, while at higher neutron energies (~10 eV) this interference term is almost absent. Results on liquid bismuth yield

$$dG_{E_n}/d(q^2)_{q^2\to 0} = 0.0225 \pm 0.0070\ F^2.$$

The work of Hughes, Harvey, Goldberg, and Stafne [15] depends on the fact that the difference in the refractive indices for neutrons at an interface between bismuth and liquid oxygen (liquid mirror) comes largely from the neutron-electron scattering amplitude. The measurement of the angle of total external reflection gives the difference between the two scattering amplitudes and hence the n-e interaction. Here the results are

$$dG_{E_n}/d(q^2)_{q^2\to 0} = 0.0200 \pm 0.0019\ F^2.$$

The most recent and most accurate measurements have been by Krohn and Ringo [16] (1966) utilizing a technique of Fermi and Marshall [17] (1947). It depends on the fact that in scattering neutrons, the interference between the scattering from the nucleus and from the electrons in an atom leads to an asymmetric angular distribution of scattered neutrons in the center-of-mass system. This

occurs because the atomic form factor depends on the scattering angle. A summary of the Krohn and Ringo results are shown in Table I.

TABLE I

Gas	V_o(eV)	$dG_{E_n}/d(q^2)\ F^2$	Statistical weight
Argon	-3780 ± 250	0.0196 ± 0.0013	0.13
Krypton	-3800 ± 130	0.0197 ± 0.0007	0.30
Xenon	-3670 ± 90	0.0190 ± 0.0005	0.57
Weighted mean	-3720 ± 90	0.0193 ± 0.0004	

It is important to note that all measurements agree that $dG_{E_n}/d(q^2)$ is not zero or negative. See Appendix A for the details of the calculation of $\frac{dG_{E_n}}{d(q^2)}$ from V_o.

II. THEORY

A. THE NONRELATIVISTIC DEUTERON

1. The Ground State of the Deuteron

There are three possible states of the two-nucleon system, the di-proton (pp), the di-neutron (nn), and the deuteron (np), of which only the deuteron is known to be stable. Experimentally measured static properties are:

(1) Binding Energy $W = 2.226 \pm 0.003$ MeV

(2) Magnetic Moment $\mu_d = 0.85735 \pm 0.00003$ nm
where 1nm = 1 nuclear magneton = $eh/2m_pc$ and m_p is the proton mass

(3) Electric Quadrupole Moment, $Q_d = 2.82 \times 10^{-27} cm^2$
$= 28.2\ F^2$, where $1F = 10^{-13}$ cm.

(4) Spin Angular Momentum, $S = 1\hbar$

(5) Radius $r_d = 4.3$ F (see page 23 for definition of r_d)

(6) Mass $M_d = 2.01410$ umu (unified mass units)
$= 9.50\ F^{-1}$

Because the neutron has zero charge, the nuclear force binding the deuteron cannot be electrical and neither can it be gravitational, for this force is far too weak to provide a 2.2 MeV binding energy. Thus a nuclear force that is strong and attractive is postulated. By ignoring some experimentally determined parameters a simple quantum mechanical treatment of the deuteron is possible.

Assume that the nuclear force is central, i.e. the interaction potential between the neutron and proton is some function V(r), where r is the separation of the two

nucleons. This assumption is in conflict with (3) above because a non-zero quadrupole moment implies a nonsymmetric charge distribution. Nevertheless, assume the central potential, and take the ground state of the deuteron to be $^3S_1$. Hence the Schroedinger equation in the center-of-mass system is,

$$\frac{-h^2}{2m} \nabla^2\psi(\vec{r}) + V(r)\ \psi(\vec{r}) = E\psi(\vec{r}) \qquad (2\text{-}1)$$

where the reduced mass is,

$$m = \frac{m_p m_n}{m_p + m_n} \simeq \frac{M}{2} \qquad (2\text{-}2)$$

and m_p, m_n are the masses of the proton and neutron. The average of these masses is M, and $\vec{r}$ is the relative vector coordinate between nucleons. E is the energy of the relative motion of the two particles. Since the ground state is spherically symmetric (S state), $\psi(\vec{r})$ depends only on $r = |\vec{r}|$, so that

$$\psi(\vec{r}) \longrightarrow \psi(r) = \frac{u(r)}{r} \qquad (2\text{-}3)$$

The quantity u(r) is called the reduced radial wave function. Now using (2-3) and (2-2), (2-1) can be rewritten as

$$\frac{-h^2}{M} u''(r) + V(r)u(r) = Eu(r) \qquad (2\text{-}4)$$

where $u''(r) \equiv \frac{d^2u(r)}{dr^2}$ and E = -W = -2.226 MeV. For the square-well potential

$$V(r) = \begin{cases} -V_o & r \leq r_o \\ 0 & r > r_o \end{cases} \qquad (2\text{-}5)$$

(2-4) becomes

Case I $r < r_o$

$$u''(r) + \alpha^2 u(r) = 0 \qquad (2\text{-}6a)$$

where

$$\alpha = \sqrt{\frac{M}{h^2}(V_o+E)} = \sqrt{\frac{M}{h^2}(V_o-W)} \qquad (2\text{-}6b)$$

The general solution of (2-6a) is

$$u(r) = A \sin \alpha r + B \cos \alpha r \qquad (2\text{-}7)$$

Requiring that $\psi(r)$ be finite at $r \to 0$ and $\psi(r) = 0$ at $r \to \infty$ forces $B = 0$ in (2-7), hence,

$$u(r) = A \sin \alpha r \qquad (2\text{-}8)$$

Case II $r > r_o$

$$u''(r) - \gamma^2 u(r) = 0 \qquad (2\text{-}9a)$$

where

$$\gamma = \sqrt{\frac{MW}{h^2}} \qquad (2\text{-}9b)$$

The general solution of (2-9a) is

$$u(r) = Ce^{-\gamma r} + De^{\gamma r} \qquad (2\text{-}10)$$

the boundary condition at ∞ requires $D = 0$ so that

$$u(r) = Ce^{-\gamma r} \qquad (2\text{-}11)$$

Now at $r = r_o$ both ψ and ψ' (the slope) must be continuous, thus (2-8) and (2-11) state

$$A \sin \alpha r_o = Ce^{-\gamma r_o} \qquad (2\text{-}12)$$

and

$$A\alpha \cos \alpha r_o = -\gamma Ce^{-\gamma r_o} \qquad (2\text{-}13)$$

The ratio of (2-13) for (2-12) yields

$$\alpha \cot \alpha r_o = \gamma = -\sqrt{\frac{MW}{h^2}} \qquad (2\text{-}14)$$

This is a transcendental equation relating the range of the potential r_o to its depth V_o. Typical solutions of (2-14) for r_o vs depth are given in Table II.

TABLE II

Range r_o(F)	Depth of Potential (MeV)
1.0	120
1.5	59
2.0	36
2.5	25
∞	5.83

The results of this rough calculation are quite good. Independent measurements of r_o yield numbers on the order of 1 Fermi. If r_o = 2.0 F is accepted, the size of the deuteron can be specified by $1/\gamma$ = 4.3F, which is about twice that of the range r_o of the potential. This explains why the deuteron is a loosely bound system (its binding energy is 1.113 MeV/nucleon, vs. 8.0 MeV/nucleon in the average nucleus).

There is no experimental evidence for any excited state of the deuteron. It can be shown by simple theoretical arguments that in order to produce a bound excited state the potential well depth must be much greater than in the ground state. It must be concluded that no bound state exists for $\ell \neq 0$ in the deuteron.

2. Review of Low Energy Neutron-Proton Scattering

Certain parameters pertaining to the deuteron have been established by investigation of the unbound n-p state, that is through neutron-proton scattering experiments. It is clear that these parameters should be predicted by any good theory of the deuteron. With this in mind this brief review is given.

The n-p scattering cross section has been examined closely, both at high and low energies. The cross section depends strongly on the energy of the incident neutrons. At low energies, below 10 MeV, the scattering is essentially due to neutrons with angular momentum $\ell = 0$ (S-wave scattering). Thus the angular distribution of the scattered neutrons is isotropic in the center-of-mass system. Since the proton has molecular binding energy of about 0.1 eV, only neutrons with incident energy greater than 1.0 eV are considered. Hence the neutrons strike essentially free protons.

The Schroedinger equation for the scattering problem is

$$\nabla^2\psi(\vec{r}) + \frac{2m}{\hbar^2}\left[E - V(\vec{r})\right]\psi(\vec{r}) = 0.$$

For a central potential and for neutrons incident along the z-axis the above becomes

$$\nabla^2\psi(r,\theta) + \frac{2m}{\hbar^2}\left[E - V(r)\right]\psi(r\theta) = 0 \qquad (2\text{-}15)$$

which has the asymptotic solution

$$\psi(r,\theta) \xrightarrow[r\to\infty]{} A\left[e^{ikz} + f(\theta)\,\frac{e^{ikr}}{r}\right]. \qquad (2\text{-}16)$$

The $f(\theta)$ is called the scattering amplitude representing the scattered neutrons (waves); Ae^{ikz} represents the incoming plane wave. It is not difficult to show that

$$\frac{d\sigma}{d\Omega} = |f(\theta)|^2. \qquad (2\text{-}17)$$

Using separation of variables, $\psi(r,\theta) = R(r)\,Y(\theta)$, (2-15) divides into a radial and angular equation. The angular part is

$$\frac{1}{\sin\theta}\frac{d}{d\theta}\left(\sin\theta\,\frac{dY}{d\theta}\right) + \ell(\ell+1)\,Y = 0 \qquad (2\text{-}18)$$

with solutions $Y_\ell(\theta) = P_\ell(\cos\theta)$, the Legendre polynomials of order ℓ. Since the potential is central these solutions are independent of the potential $V(r)$. The radial equation is

$$u_\ell''(r) + \left[k^2 - U(r) - \frac{\ell(\ell+1)}{r^2}\right]u_\ell(r) = 0 \qquad (2\text{-}19)$$

where

$$k^2 = \frac{2mE}{\hbar^2} \quad \text{and} \quad U(r) = \frac{2mV(r)}{\hbar^2}$$

and $R(r) = u(r)/r$. Let the potential $V(r)$ be "turned off." Then the solutions of (2-19) are again the spherical Bessel functions $j_\ell(kr)$. It can be shown that as $r \to \infty$

$$j_\ell(kr) \xrightarrow[r\to\infty]{} \frac{\sin(kr - \ell\,\pi/2)}{kr} \quad \text{"V off"}$$

and hence

$$u_\ell(r) \xrightarrow[r \to \infty]{} \sin(kr - \ell\pi/2). \tag{2-20}$$

When V is "turned on" but r is still greater than r_o, the solution of (2-19) must still correspond to that of a free particle, and hence be the same as (2-20) except for possibly a phase factor. Thus

$$u_\ell(r) \xrightarrow[r \to \infty]{} \sin(kr - \frac{\ell\pi}{2} + \delta_\ell) \quad \text{"V on".} \tag{2-21}$$

The general solution to (2-19) for "V on" at $r > r_o$ is

$$\psi(r,\theta) = \sum_{\ell=0}^{\infty} C_\ell \frac{\sin(kr - \ell\pi/2 + \delta\ell)}{r} P_\ell(\cos\theta) \tag{2-22}$$

$$= \sum_{\ell=0}^{\infty} B_\ell P_\ell(\cos\theta).$$

But this must be the same as (2-16). Now using a Rayleigh expansion on e^{ikz} in (2-16), and writing all quantities as complex exponentials, equating (2-16) and (2-22) yields

$$C_\ell = \frac{i^\ell(2\ell+1)e^{i\delta_\ell}}{k}$$

and

$$f(\theta) = \frac{1}{k}\sum_\ell (2\ell+1)e^{i\delta_\ell} \sin\delta_\ell P_\ell(\cos\theta). \tag{2-23}$$

The square of the scattering amplitude is the differential scattering cross section (2-17), hence

$$\sigma_T = \int \frac{d\sigma(\theta)}{d\Omega} \sin\theta \, d\theta = \frac{4\pi}{k^2}\sum_\ell (2\ell+1)\sin^2\delta_\ell. \tag{2-24}$$

Note that S-wave scattering ($\ell = 0$) is predominant for energies less than 10 MeV. By taking the range of nucleon force to be 2F and assuming a 0.5 MeV incident neutron (in center-of-mass frame or 1 MeV in the lab) it can be seen by forming the ratio of the coefficients B_ℓ in (2-22) that

$$\left|\frac{B_1}{B_o}\right|^2 = (kr_o)^2$$

This states that only about 9% of the scattering is due to neutrons with $\ell = 1$.

In (2-24) let $\ell = 0$, then

$$\sigma_T = \frac{4\pi}{k^2} \sin^2\delta_o = 4\pi\left(\frac{\sin \delta_o}{k}\right)^2. \qquad (2\text{-}25)$$

As $k \to 0$, $\sin \delta_o$ approaches δ_o. In order that σ_T remain finite δ_o/k must approach some constant, called -a by convention. Thus

$$\sigma_T = 4\pi a^2 \qquad (2\text{-}26)$$

where a is called the scattering length. Consideration of the solution

$$u_o(r) \sim \sin(kr + \delta_o) = \sin k(r + \frac{\delta_o}{k}) \xrightarrow[k \to 0]{} k(r-a)$$

demonstrates the fact that the asymptotic solution becomes a straight line, and that the scattering length, a, is the intercept on the r-axis and is obtained by extrapolating the radial wave function inside the potential, well beyond

the range of force r_o. Figure 1 illustrates the significance of the sign of the scattering length. The scattering length a is positive if the state is a bound state.

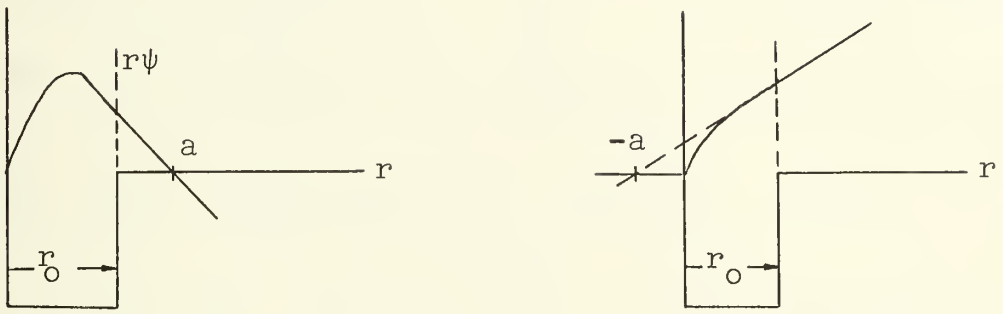

(a) Figure 1 (b)

Positive scattering length indicates a bound state

Negative scattering length indicates an unbound state

The energy dependence of the scattering cross section can be expressed in terms of the scattering length a, and another parameter which has the dimensions of length and is known as the effective range. Denote this parameter by ρ, where ρ is of the same magnitude as the range of nuclear force r_o. Effective range theory predicts the phase shifts δ_ℓ as a function of energy. Consider S-wave scattering only. The wave equations for two energies $E = \hbar^2k^2/2m$ and $E = 0$ are

Case I $V \neq 0$	Case II $V = 0$
$u'' + (k^2 - \frac{2mV}{\hbar^2})u = 0$ (2-27a)	$v'' + k^2 v = 0$ (2-29a)
$u_o'' - \frac{2mV}{\hbar^2} = 0$ (2-27b)	$v_o'' = 0$ (2-29b)
multiply (27a) by u_o, (27b) by u and subtract, getting	multiply (29a) by v_o, (29b) by v and subtract, getting
$\frac{d}{dr}(uu_o' - u_o u') = k^2 uu_o$ (2-28)	$\frac{d}{dr}(vv_o' - v_o v') = k^2 v_o v$ (2-30)

Subtract and integrate the above equations. Then

$$(uu_o' - u_o u' - vv_o' + v_o v')\Big|_{r=0}^{r=\infty} = k^2 \int_0^\infty (uu_o - vv_o)dr. \quad (2\text{-}31)$$

Because $u = v$, $u_o = v_o$ for $r > r_o$, the expression on the left hand side contributes nothing at the upper limit. Furthermore $u(0) = u_o(0) = 0$, hence (2-31) is

$$(vv_o' - v_o v')\Big|_{r=0} = k^2 \int_0^\infty (uu_o - vv_o)dr. \quad (2\text{-}32)$$

In analogy with (2-20) the solutions u and v can be written

$$u(r) \xrightarrow[r \to \infty]{} v(r) = C \sin(kr + \delta_o) = \frac{\sin(kr+\delta_o)}{\sin \delta_o}$$

where C is a normalization constant. Now (2-32) becomes

$$-\frac{1}{a} - k \cot \delta_o = k^2 \int_0^\infty (uu_o - vv_o)dr$$

and in the limit of zero energy neutrons $u \simeq u_o$, $v \simeq v_o$ so that

$$k \cot \delta = \frac{-1}{a} + \rho \frac{k^2}{2}$$

where

$$\rho \equiv 2\int_0^\infty (v_o^2 - u_o^2)dr$$

is the effective range.

Hence the cross section is given by

$$\sigma_T = \frac{4\pi}{k^2 + (\frac{1}{a} - \frac{\rho k^2}{2})^2} \qquad (2\text{-}33)$$

Besides being a function of $k^2 = 2mE/\hbar^2$, the cross section is expressed in terms of the two parameters, effective range ρ and scattering length a. The cross section is independent of the form and shape of the potential. Both ρ and a can be determined by measuring the cross section at different low energies of the incident neutron.

The theoretical estimate of the value of the scattering cross section for $\ell = 0$ is far below the experimentally observed value. In fact for a square well of reasonable width and depth

$$\sigma_T \simeq 4.5 \times 10^{-24} \text{ cm}^2$$

while

$$\sigma_{\text{experimental}} \simeq 20.4 \times 10^{-24} \text{ cm}^2.$$

This conflict was removed when Wigner realized that the theory for σ_T is based on a potential whose "strength" is calculated from the deuteron, where the spin is 1, i.e. neutron and proton are parallel, while scattering experiments are done using randomly oriented nuclei. The

scattering experiments then represent an average over parallel (triplet) and anti-parallel (singlet) states. The weight factor for the singlet and triplet cases are 1/4 and 3/4 respectively, hence the total cross section for scattering is

$$\sigma_T = \frac{3}{4}\sigma_t + \frac{1}{4}\sigma_s$$

where σ_t and σ_s are the triplet and singlet cross sections. Using (2-33) and working backwards assuming $\sigma_t = 20.4$ barns, $1/\gamma_t = 4.3$ F, and $r_t \simeq r_s \simeq 2$ F it can be determined that $W_s = 0.066$ MeV with $1/\gamma_s = 25$ F, where the scattering length a_s is negative. Hence the singlet state is not a bound deuteron state.

3. Pheonomenological Two-Nucleon Potentials

On the evidence presented so far it can be concluded that: (1) The deuteron is predominantly in a $^3S_1$ state since the solutions to the Schroedinger equation for a central potential are quite good; (2) since $\mu_d \neq \mu_p + \mu_n$, and $Q_d \neq 0$, there is reason to guess that noncentral forces are acting (the inequality of magnetic moments in a complex problem and could well have other interpretations); (3) the forces between neutron and proton are different in the singlet and triplet states, implying that nuclear forces are spin-dependent. There is a point of confusion on (3). Spin-dependent does not imply that this contribution is not central in nature. It means that the usual central scalar potential is different according to the relative orientation

of spins, a situation that has no direct analogy either in electromagnetism or atomic physics.

A realistic deuteron potential must incorporate these ideas and more. The potential must be symmetric in the coordinates of the two nucleons and invariant under rotations and reflection of their space coordinates. This means the potential is a scalar.

Some of the more detailed features of the nuclear potential can be directly related to the spin and isospin dependence of the nucleon interaction. An important contribution for the nuclear symmetry potential comes from the exchange character of the nuclear forces. Thus a Serber exchange potential, P^r, for the central interaction would be

$$V_c = \frac{1}{2}(1 + P^r)\, V(r) \quad \text{or}$$

$$V_c = \frac{1}{2}\left[1 - \frac{1}{4}(1 + \vec{\tau}_1 \cdot \vec{\tau}_2)(1 + \vec{\sigma}_1 \cdot \vec{\sigma}_2)\right] V(r) \qquad (2\text{-}34)$$

where $\vec{\tau}_1$, $\vec{\tau}_2$ and $\vec{\sigma}_1$, $\vec{\sigma}_2$ are the isospin and Pauli spin matrices respectively.

The occurrence of a rather strong spin-orbit force in the nuclear interaction gives rise to a spin-orbit coupling in the two body force;

$$V_{LS} = \frac{1}{h} V_{LS}(r)(\vec{r}_1 - \vec{r}_2) \times (\vec{p}_1 - \vec{p}_2) \cdot (\vec{s}_1 + \vec{s}_2). \qquad (2\text{-}35)$$

This V_{LS} contribution is based on Wigner's idea that velocity-dependent forces are acceptable when they depend only on the relative momentum $\vec{p}$ of the two nucleons.

All these facts taken together yield a general potential

$$V = V_C(r) + V_\sigma(r)\ \vec{\sigma}_1\cdot\vec{\sigma}_2 + V_T(r)S_{12} + V_{LS}(r)\vec{L}\cdot\vec{S} \quad (2\text{-}36)$$

where $\vec{\sigma}_1\cdot\vec{\sigma}_2$ represents the spin-spin interaction and S_{12} is the tensor operator

$$S_{12} = 3(\vec{\sigma}_1\cdot\hat{r})(\vec{\sigma}_2\cdot\hat{r}) - (\vec{\sigma}_1\cdot\vec{\sigma}_2). \quad (2\text{-}37)$$

The form of the tensor operator can be inferred by analogy with the classical problem of the potential energy of an electric dipole d_1 in the field of another dipole d_2 at a distance r.* Here

$$V_{dd} \sim r^{-3}\left[3(\vec{d}_1\cdot\hat{r})(\vec{d}_2\cdot\hat{r}) - \vec{d}_1\cdot\vec{d}_2\right]. \quad (2\text{-}38)$$

The r^{-3} comes from the fact that the electric charges interact with a potential proportional to r^{-1}. But the r-dependence of "mesic charges" which are thought to be the source of nuclear fields is unknown. Hence the r^{-3} dependence must be replaced by an arbitrary function of r, $V_T(r)$.

The structure of the nuclear force is closely related to the properties and interactions of the whole family of strongly interacting particles. It has not been possible so far to derive the forces between these particles, or their masses, from simple assumptions regarding the basic structure of the strong interaction. Nevertheless, certain relations between the interactions and masses of the

---

*See Appendix B for properties of the tensor operator S_{12}.

strongly interacting particles can be established. Of particular significance is the relationship between the nuclear force at large distances and the pion-nucleon interaction.

The force at large distances can be described in terms of an exchange of mesons, in a similar manner as the electromagnetic interaction can be analyzed in terms of photon exchange. The special role of pion exchange is due to the smallness of the pion mass as compared with that of other strongly interacting particles. The interaction associated with the exchange of a particle of mass m_π is limited to a range of the order of the compton wave length $\lambda_c = \hbar/m_\pi c$. In fact, the intermediate states involved in such an exchange have an energy of at least $m_\pi c^2$ and so are limited to a duration of order $\hbar/m_\pi c^2$. During this time, the emitted particle cannot travel farther than $\hbar/m_\pi c$ and thus, the interaction is expected to decrease strongly for distances greater than λ_c. If n particles are exchanged simultaneously, the corresponding intermediate energies are n x $m_\pi c^2$ and the range is λ_c/n. The interaction at the largest distances is thus determined by the exchange of single mesons.

The asymptotic form of the one-pion exchange potential (OPEP) is uniquely given by the mass and symmetry properties of the pion ($J^\pi = 0^-$, $T = 1$)

$$V_{OPEP} = \frac{1}{3}\frac{f^2}{hc} m_\pi c^2 (\vec{\tau}_1 \cdot \vec{\tau}_2)\left[(\vec{\sigma}_1 \cdot \vec{\sigma}_2) + S_{12}(1 + \frac{3}{x} + \frac{3}{x^2})\right]\frac{e^{-x}}{x} \qquad (2\text{-}39)$$

where $x = m_\pi c/\hbar = 0.70\ F^{-1}$, $f^2/hc = 0.081 \pm 0.002$.

The strength of the potential is determined by the coupling constant f for the process $N \rightarrow N + \pi$. The meson field is pseudoscalar since $J^\pi = 0^-$, and isovector since T = 1. Equation (2-39) reduces to (2-36) for the deuteron.

Early definitive work on the phenomenological nucleon-nucleon potential in the OPEP approximation was carried out by Glendenning and Kramer [18]. They attempted to construct triplet (spin) - even (parity) potentials that are asymptotic to the OPEP and are modified in the inner regions so that the deuteron properties are obtained. The results of an 8-parameter fit to an equation similar to (2-39) are found in Table III, entries 1-9. Coefficients in their potential are varied such that the empirical values of $Q_d = 28.2\ F^2$ and $a_t = 5.44 \pm 0.02$ F are reproduced. A hard core radius r_c was chosen so that the potential has a bound state at W = 2.226 MeV. (The hard core is discussed on page 38).

Many other authors have contributed to the data [19, 20, 21]. One of the most useful has been the Hamada-Johnston (HJ) [22] potential given by

$$V = V_C(r) + V_T(r)S_{12} + V_{LS}\vec{L}\cdot\vec{S} + V_{LL}(r)L_{12} \qquad (2\text{-}40)$$

TABLE III

Potential Identification	$r_c(f)$	$a_t(F^{-1})$	$\rho(F)$	$Q_d(F^2)$	$P_D(\%)$	λ
GK1	0.4815	5.376	1.717	28.79	7.415	0.02714
2	0.2466	5.368	1.709	28.21	6.281	0.02693
3	0.4747	5.456	1.812	28.17	5.970	0.02595
4	0.4425	5.364	1.703	28.22	7.103	0.02677
5	0.3632	5.366	1.705	28.02	6.710	0.02663
6	0.3924	5.384	1.726	28.12	5.957	0.02676
7	0.5369	5.477	1.836	28.14	6.029	0.02564
8*	0.5007	5.413	1.760	28.18	5.622	0.02654
9*	0.4329	5.373	1.715	28.29	7.425	0.02670
HJ	0.485	-	1.77	28.50	6.97	0.02656
FL	0.735	-	-	-	4.60	-
Experiment	-	5.40†	-	28.20††	-	-

λ is the asymptotic D state/S state ratio

* GK8 and 9 include the spin-orbit term in (2-34) while GK1-7 are without it.

† N. K. Glendenning and G. Kramer, Phys. Rev. 126, 2159, 1962.

†† G. P. Auffray, Phys. Rev. Letters 6, 120, 1961.

where

$$L_{12} = (\vec{\sigma}_1 \cdot \vec{\sigma}_2)\ \vec{L}^2 - \frac{1}{2}\left[(\vec{\sigma}_1 \cdot \vec{L})(\vec{\sigma}_2 \cdot \vec{L}) + (\vec{\sigma}_2 \cdot \vec{L})(\vec{\sigma}_1 \cdot \vec{L})\right]$$

$$= (\delta_{LJ} + \vec{\sigma}_1 \cdot \vec{\sigma}_2)\ \vec{L}^2 - (\vec{L} \cdot \vec{S})^2$$

and contains central V_c, tensor V_T, spin-orbit V_{LS}, and second-order spin-orbit V_{LL} components. It is from this potential that the later used Partovi wavefunctions have been derived. The radial functions are restricted by the condition that at large distance the central and tensor potentials should be described by the OPEP. The radial forms are:

$$V_c = v_o(\vec{\tau}_1 \cdot \vec{\tau}_2)(\vec{\sigma}_1 \cdot \vec{\sigma}_2)\ Y(x)[1 + a_c Y(x) + b_c Y^2(x)]$$

$$V_T = v_o(\vec{\tau}_1 \cdot \vec{\tau}_2)(\vec{\sigma}_1 \cdot \vec{\sigma}_2)\ Z(x)[1 + a_T Y(x) + b_T Y^2(x)]$$

$$V_{LS} = g_{LS}\ v_o Y^2(x)[1 + b_{LS}\ Y(x)]$$

$$V_{LL} = g_{LL}\ v_o\ \frac{Z(x)}{x^2}\ [1 + a_{LL} Y(x) + b_{LL} Y^2(x)]$$

$$v_o = \frac{1}{3}\frac{f^2}{hc}\, m_\pi c^2 = 3.65\ \text{MeV}$$

$$x = \frac{m_\pi c}{h}\, r = \frac{r}{1.43F}\ , \quad Y(x) = \frac{e^{-x}}{x}$$

$$Z(x) = 1 + \frac{3}{x} + \frac{3}{x^2}\ .$$

In addition the potential has been assumed to have a component giving rise to an infinite repulsion at radius

$$x_c = 0.343\ (r_c = 0.485\ \text{F}).$$

The values of the quantities V_c, V_T, etc. have been calculated for four different types of potentials. The results are shown in Table IV.

TABLE IV

	V_c(MeV)	V_T(MeV)	V_{LS}(MeV)	V_{LL}(MeV)
Singlet even	-1460	-	-	-42
Triplet even	- 207	-642	34	668
Singlet odd	2371	-	-	-6688
Triplet odd	- 23	173	-1570	-1087

Values of HJ potential at r_c = 0.485 F.

The "hard core" mentioned above is a phenomena that cannot be investigated through low energy nucleon-nucleon scattering. In the neighborhood near and above 200 MeV repulsive components in the nucleon-nucleon interaction are seen. One way of introducing a repulsive interaction (which might account for nucleon saturation) is in terms of a very strong repulsive potential of very short range - "the hard core." The infinite short ranged repulsion is only one, rather extreme, way of accounting for the observed effects. Finite repulsive potentials, "soft cores," as well as interactions depending explicitly on relative velocity can account for some experimental results.

A fairly recent idea by Feshbach and Lomon (FL) [23] in 1967, is to replace the interior region by appropriate boundary conditions at some finite radius. As long as the interactions responsible for these boundary conditions involve energies much greater than the bombarding energy, it may be expected that the boundary conditions will be approximately energy independent. The FL model also employs the (TPEP) two pion exchange potential.

4. Solutions of the Non-Central Force Deuteron Problem

Solutions to the non-central force deuteron problem are obtained by substituting the potential V_{OPEP} into the Schroedinger equation and solving for the wave functions. Angular momentum and parity arguments can determine the deuteron ground state angular wave function.

The total angular momentum of the deuteron is J = 1 and it is in a definite parity state. The value J = 1 can be obtained from different combinations of the orbital angular momentum ℓ, and the spin s such as:

$$\ell = 0 \quad s = 1 \longrightarrow {}^3S_1$$

$$\ell = 1 \begin{cases} s = 0 \longrightarrow {}^1P_1 \\ s = 1 \longrightarrow {}^3P_1 \end{cases}$$

$$\ell = 2 \quad s = 1 \longrightarrow {}^3D_1$$

and no others. If the deuteron is a mixture of these it can only be ${}^3S_1 + {}^3D_1$ or ${}^1P_1 + {}^3P_1$ since the combination must have a definite parity. Since an almost spherically

symmetric ground state exists, the obvious choice is the S state combination. It is not difficult to show that the odd parity states ($^1P_1 + {}^3P_1$) yield the wrong values for Q_d and μ_d.

The angular momentum wave function $\mathcal{Y}^{M}_{\ell SJ}$ for a two particle system in the orbital angular momentum state ℓ and spin state S, forming the total angular momentum J, with Z-component M is given by

$$\mathcal{Y}^{M}_{\ell SJ} = \sum_{M_s, m_\ell} \langle \ell S m_\ell M_s | JM \rangle \; Y_\ell^{m_\ell} \; \chi_s^{M_s} \tag{2-41}$$

where the $Y_\ell^{M_\ell}$ are the spherical harmonics, $\chi_s^{M_s}$ are the spin wave functions and $\langle \ell \; S m_\ell \; M_s | JM \rangle$ are the Clebsch-Gordon coefficients. Two spin ½ particles have the following spin states:

Triplet (s = 1)

$$\chi_1^1 = \langle \tfrac{1}{2}\tfrac{1}{2}\tfrac{1}{2}\tfrac{1}{2} | 11 \rangle \alpha(1)\alpha(2) = \alpha(1)\alpha(2) \tag{2-42a}$$

$$\chi_1^0 = \langle \tfrac{1}{2}\tfrac{1}{2}-\tfrac{1}{2}\tfrac{1}{2} | 10 \rangle \alpha(1)\beta(2) + \langle \tfrac{1}{2}\tfrac{1}{2}\tfrac{1}{2}-\tfrac{1}{2} | 10 \rangle \alpha(2)\beta(1)$$

$$= \frac{1}{\sqrt{2}} \left[\alpha(1)\beta(2) + \alpha(2)\,\beta(1) \right] \tag{2-42b}$$

$$\chi_1^{-1} = \langle \tfrac{1}{2}\tfrac{1}{2}-\tfrac{1}{2}-\tfrac{1}{2} | 1\text{-}1 \rangle \beta(1)\beta(2) = \beta(1)\beta(2) \tag{2-42c}$$

Singlet (S = 0)

$$\chi_0^0 = \langle \tfrac{1}{2}\tfrac{1}{2}\tfrac{1}{2}-\tfrac{1}{2} | 00 \rangle \alpha(1)\beta(2) + \langle \tfrac{1}{2}\tfrac{1}{2}-\tfrac{1}{2}\tfrac{1}{2} | 00 \rangle \beta(1)\alpha(2)$$

$$\chi_0^0 = \frac{1}{\sqrt{2}} \left[\alpha(1)\beta(2) - \beta(1)\alpha(2) \right] \tag{2-43}$$

where $\alpha = \binom{1}{0}$ and $\beta = \binom{0}{1}$ are "spin up" (proton) and "spin down" (neutron) states of the nucleon. The arguments of the α's and β's stand for particle number one or two. The angular momentum wave functions $\mathcal{Y}^{M}_{\ell SJ}$ for the two states under consideration are

$$^3S_1: \quad J = 1, \quad M = 1, \quad \ell = 0, \quad s = 1$$

$$\mathcal{Y}^{1}_{011} = \langle 0101|11\rangle\, Y^0_0\alpha(1)\alpha(2) = Y^0_0\alpha(1)\alpha(2) \qquad (2\text{-}44)$$

$$^3D_1: \quad J = 1, \quad M = 1, \quad \ell = 2, \quad s = 1$$

$$\mathcal{Y}^{1}_{211} = \sum_{M_s} \langle 21(1-M_s)M_s|11\rangle\, Y_2^{1-M_s}\,\chi_1^{M_s}$$

$$= \sqrt{\frac{3}{5}}\, Y^2_2\, \beta(1)\beta(2) - \sqrt{\frac{3}{10}}\, Y^1_2\, \frac{1}{\sqrt{2}}\left[\alpha(1)\beta(2)+\beta(1)\alpha(2)\right]$$

$$+ \sqrt{\frac{1}{10}}\, Y^0_2\, \alpha(1)\alpha(2). \qquad (2\text{-}45)$$

The Schroedinger equation in the center-of-mass system is

$$\left[\frac{-\hbar^2}{2m}\nabla^2 + V_c + V_T S_{12}\right]\phi = E\phi \qquad (2\text{-}46)$$

where

$$\phi = \phi_s + \phi_D = \frac{u(r)}{r}\mathcal{Y}^{1}_{011} + \frac{w(r)}{r}\mathcal{Y}^{1}_{211} \qquad (2\text{-}47)$$

is the ground state deuteron wave function. For ease the linear spin-orbit and quadratic spin-orbit parts of the potential (2-40) have been ignored. Rearranging (2-46)

$$\left(\frac{-\hbar^2}{2m}\nabla^2 + V_c - E\right)\left(\frac{u(r)}{r}\mathcal{Y}_{011}^{1} + \frac{w(r)}{r}\mathcal{Y}_{211}^{1}\right)$$

$$+ V_T\left(\frac{u}{r}\sqrt{8}\,\mathcal{Y}_{211}^{1} + \frac{w}{r}\left[\sqrt{8}\,\mathcal{Y}_{011}^{1} - 2\mathcal{Y}_{211}^{1}\right]\right) = 0. \qquad (2\text{-}48)$$

In writing (2-48) the following properties of S_{12} have been used:

$$S_{12}\mathcal{Y}_{011}^{1} = \sqrt{8}\,\mathcal{Y}_{211}^{1} \qquad (2\text{-}49a)$$

and

$$S_{12}\mathcal{Y}_{211}^{1} = \sqrt{8}\,\mathcal{Y}_{011}^{1} - 2\mathcal{Y}_{211}^{1}. \qquad (2\text{-}49b)$$

Note that

$$\nabla^2 = \frac{1}{r^2}\frac{\partial}{\partial r}\left(r^2\frac{\partial}{\partial r}\right) - \frac{L^2}{\hbar^2 r^2} \qquad (2\text{-}50)$$

where

$$L^2 = \frac{-\hbar^2}{\sin^2\theta}\left[\sin\theta\frac{\partial}{\partial\theta}\left(\sin\theta\frac{\partial}{\partial\theta}\right) + \frac{\partial^2}{\partial\phi^2}\right] \qquad (2\text{-}51)$$

and

$$L^2 Y_\ell^{m_\ell}(\theta,\phi) = \ell(\ell+1)\hbar^2\, Y_\ell^{m_\ell}(\theta,\phi). \qquad (2\text{-}52)$$

Hence

$$\nabla^2\left(\frac{u}{r}\mathcal{Y}_{011}^{1}\right) = \frac{1}{r}\frac{d^2u}{dr^2}\mathcal{Y}_{011}^{1} \qquad (2\text{-}53)$$

and

$$\nabla^2\left(\frac{w}{r}\mathcal{Y}_{211}^{1}\right) = \left(\frac{1}{r}\frac{d^2w}{dr^2} - \frac{1}{r}\frac{2(2+1)}{r^2}w\right)\mathcal{Y}_{211}^{1}. \qquad (2\text{-}54)$$

Multiply (2-48) by $\mathcal{Y}^{*1}_{011}$, integrate over the solid angle, and make use of the orthonormality property of the $\mathcal{Y}^{M}_{\ell SJ}$ to get

$$\frac{-\hbar^2}{2m} u''(r) + (V_c - E)u(r) = -\sqrt{8}\, V_T\, w(r). \qquad (2\text{-}55)$$

Similarly, multiply (2-48) by $\mathcal{Y}^{*1}_{211}$ and integrate to get

$$\frac{-\hbar^2}{2m}\left[w''(r) - 6\,\frac{w(r)}{r^2}\right] + \left[V_c - 2V_T - E\right] w(r)$$

$$= -\sqrt{8}\, V_T u(r). \qquad (2\text{-}56)$$

These coupled differential equations were first obtained by Rarita and Schwinger [24].

A method for solving these equations has been described by Hamada [21], who states that (2-55) and (2-56) have two sets of linearly independent solutions. Thus choose (u_1, w_1) and (u_2, w_2) with the asymptotic requirements that the first solution behave as an S wave function and the other as a D wave function:

$$\begin{pmatrix} u_1 \\ w_1 \end{pmatrix} \longrightarrow \begin{pmatrix} e^{-\alpha r} \\ 0 \end{pmatrix} \qquad (2\text{-}57a)$$

and

$$\begin{pmatrix} u_2 \\ w_2 \end{pmatrix} \longrightarrow \begin{pmatrix} 0 \\ e^{-\alpha r}\left[1 + 3/\alpha r + 3/(\alpha r)^2\right] \end{pmatrix}. \qquad (2\text{-}57b)$$

Starting with the behavior at large r, integrate (2-48) inward to get the two solutions for arbitrary r. Then u(r) and w(r) are obtained as a linear combination of these two solutions:

$$\begin{pmatrix} u(r) \\ w(r) \end{pmatrix} = \frac{1}{(1+\lambda^2)^{\frac{1}{2}}} \left[\begin{pmatrix} u_1(r) \\ w_1(r) \end{pmatrix} + \lambda \begin{pmatrix} u_2(r) \\ w_2(r) \end{pmatrix} \right]. \tag{2-58}$$

The requirement that u and w in (2-58) vanish at the core radius r_c gives an equation for r_c which is solved by an interpolation procedure. The asymptotic D state/S state ratio λ is then determined from

$$\lambda = - \frac{u_1(r_c)}{u_2(r_c)} = - \frac{w_1(r_c)}{w_2(r_c)} . \tag{2-59}$$

The solutions (2-58) are found in practice by numerical methods. Now having the wave functions in hand the magnetic moment and quadrupole moment can be predicted by taking the expectation values

$$\langle \mu_z \rangle = \int \phi^* \, \hat{\mu}_z \, \phi \, d\vec{r}, \tag{2-60}$$

$$\hat{\mu}_z = \frac{1}{2} \ell_z + g_p s_{pz} + g_n s_{nz} \tag{2-61}$$

and

$$\langle Q_d \rangle = \int \phi^* \, \hat{Q}_d \, \phi \, d\vec{r}, \tag{2-62}$$

$$\hat{Q}_d = 3Z^2 - r^2. \tag{2-63}$$

Typical results are listed in Table III for various potentials. (See Appendix C for example calculations of $\langle \mu_z \rangle$ and $\langle Q_d \rangle$.)

B. THE SCATTERING OF ELECTRONS FROM PROTONS AND DEUTERONS

Traditionally electron scattering cross sections have been handled through the techniques of first order

time-dependent perturbation theory, the main result of which is the Fermi Golden Rule No. 2. This rule relates the transition probability per unit time, Γ, to the square of the matrix element for the transition. Specifically,

$$\Gamma = \frac{2\pi}{h} |\langle f|H_I|i\rangle|^2 \frac{dN}{dE} \tag{2-64}$$

where dN/dE is the density of states like $|f\rangle$ around the energy E, and H_I is the interaction Hamiltonian. The cross section is then defined as

$$\sigma = \frac{\Gamma}{\text{incident particle flux}}. \tag{2-65}$$

Quantum electrodynamics (QED), which is the interaction of the Dirac spinor field with the electromagnetic field, provides the mechanism for computing the cross section via S-matrix theory. In general terms the S-matrix is a unitary operator that transforms the initial state $|i\rangle$ into the final state $|f\rangle$, i.e., $S|i\rangle = |f\rangle$, where

$$S_{fi} = \sum_{n=0}^{\infty} \frac{1}{n!} (-i)^n \int d^4x_1 \ldots \int d^4x_n \tau \left[H_I(x_1) \ldots H_I(x_n)\right] \tag{2-66}$$

and τ is the chronological operator that orders the interaction with respect to causality. The expression (2-66) is integrated over all four space and hence is not physically measurable. If S_{fi} is normalized to unit space-time volume then it can be written

$$\frac{|S_{fi}|}{VT} \sim \delta^4 (p_f - p_i)|M_{fi}| \tag{2-67}$$

where δ^4 is a four dimensional delta function expressing the conservation of four momentum in the transition from $|i\rangle$ to $|f\rangle$. The cross section for a transition from a two-particle initial state $|i\rangle$ into some group of final states is in the center-of-mass

$$\sigma = \frac{(2\pi)^2}{h} \frac{1}{|\vec{p}|} \frac{1}{\frac{1}{E(\vec{p}_1)} + \frac{1}{E(\vec{p}_2)}} \sum_{\substack{\text{final} \\ \text{spins}}} \int_{\substack{\text{final} \\ \text{momenta}}} \delta^4(p_f - p_i) |M_{fi}|^2 d\vec{p}_1 \ldots d\vec{p}_n . \tag{2-68}$$

Integration over suitable variables yields the desired differential cross section $d\sigma/d\Omega$.

At the heart of (2-68) is the matrix element $|M_{fi}|$. It is here the character of the interaction is found while the other factors represent kinematical quantities. The form of M_{fi} can be surmised by examination of the Feynman diagrams for the process under consideration.

Much of QED is conveniently described by Feynman diagrams. Here the diagrams will be mainly used to supplement the understanding of the electromagnetic interaction, but their use is certainly not limited to this role. If the diagram can be drawn, then there exist specific rules for constructing the S-matrix therefrom.

Electron scattering is graphically represented by Figure 2. Both graphs are equivalent, but (a) is most often seen since it is just a little more suggestive of the scattering process in the center-of-mass frame.

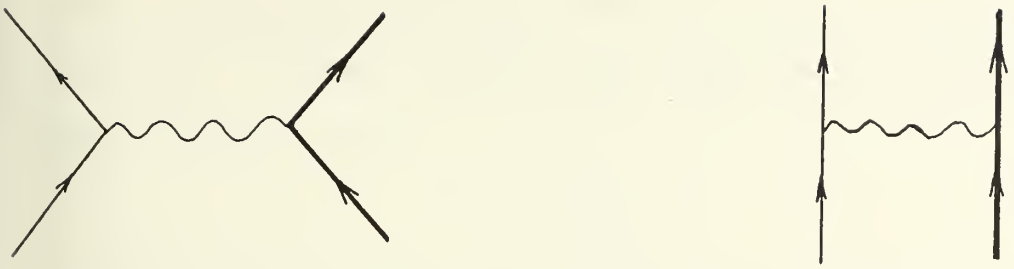

(a) (b)

Figure 2

The time axis is directed upwards unless otherwise noted. The horizontal axis can represent a space or momentum interval, the distinction between the two being of no importance here. The arrows on the lines point in the direction of increasing time for a particle. If the arrows were reversed the particle then represented would be the antiparticle of the original one. Figure 3 sometimes is said to represent particles in the "scattering channel" while the "crossed or annihilation channel" is represented by the same diagram rotated by $\pi/2$.

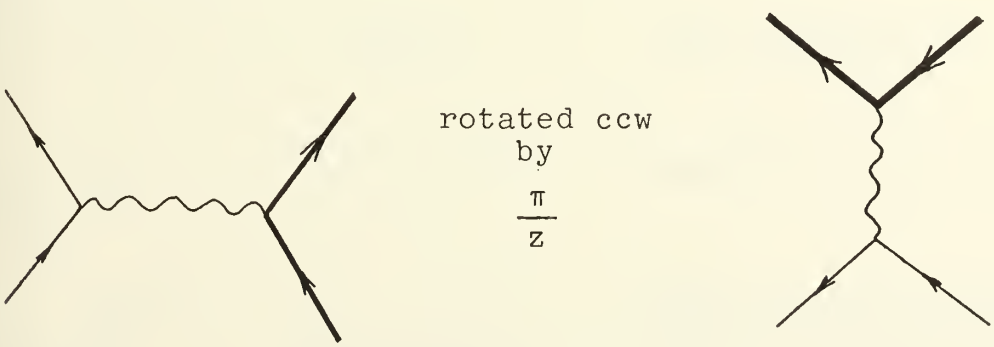

scattering channel

annihilation channel

Figure 3

Lines beginning and ending within a graph represent "virtual particles." Table V below lists some of the more important graph elements seen.

TABLE V

Graph Element	Factor in the S-Matrix	Interaction
	$\sqrt{\frac{m}{E_p}}\, u(p),\ \sqrt{\frac{m}{E_p}}\, \bar{u}(p)$	annihilation (creation) of an electron
	$\sqrt{\frac{m}{E_p}}\, v(p),\ \sqrt{\frac{m}{E_p}}\, \bar{v}_p$	annihilation (creation) of an antielectron
	$\frac{e_\mu(\vec{k})}{\sqrt{2\omega_k}}$	annihilation (creation) of a photon
	$\frac{i\gamma p - m}{p^2 + m^2}$	electron progator
	$\frac{1}{q^2}$	photon progator
	$\frac{1}{k^2 + m^2}$	meson progator
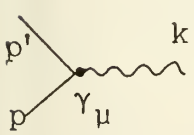	$\gamma_\mu \delta(p-p'-k)$	photon-electron vertex
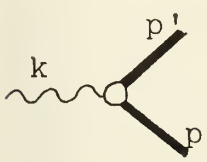	$\gamma^\mu 0^\mu \delta(p-p'-k)$	photon-nucleon vertex. Bubble or cross hatched circle represents ignorance of the true interaction; mathematically this ignorance is represented by form factors

1. Elastic Electron-Proton Scattering from Point Protons

To calculate the elastic electron-proton (e-p) scattering cross section from point (Dirac) protons in the first Born approximation it is assumed that (1) the electron is a physical point, and (2) the one photon exchange process describes elastic scattering. The graph of Figure 2 is then valid.

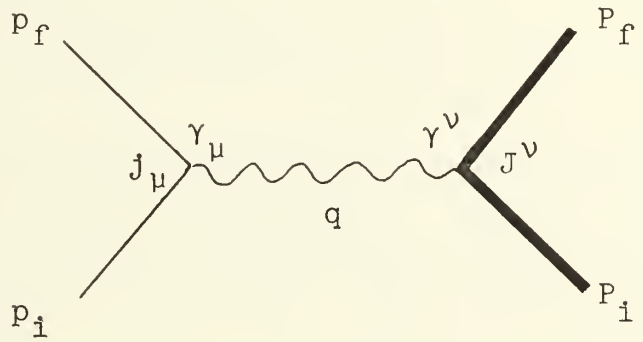

Figure 4

From the figure define the kinematical quantities p_i, p_f, P_i, P_f as the four-momentum of the incident and final electron and proton respectively; q is then the four-momentum transfer

$$q^2 \equiv (p_i - p_f)^2 \equiv (P_i - P_f)^2. \qquad (2\text{-}69)$$

Choose the convention that $q^2 < 0$ for electron scattering.* By looking at Figure 4 it can be seen that

*The metric used is $q^2 = q_0^2 - \vec{q}^2$. In the lab frame the recoil energy given the struck particle is small with respect to the total incident electron energy thus $q^2 \simeq -\vec{q}^2 < 0$. The four vector q^2 is then said to be spacelike. In the annihilation channel $q^2 \geq 4M^2 > 0$ and is timelike. Another metric commonly used is $\vec{q}^2 = q^2 - q_0^2$. The different metrics yield cross sections and form factors with some sign differences. This possible ambiguity is being remedied by use of the variable t for $\pm\vec{q}^2$ in many newer papers.

$$S_{fi} \sim M_{fi} = j_\mu \frac{1}{q^2} J^\mu \tag{2-70}$$

which represents the interaction of the electron four-current j_μ with the four-current of the proton J^μ via virtual photon progator $\frac{1}{q}2$.

Equation (2-70) is the equivalent of taking the interaction Hamiltonian to be

$$H_I(x) = j_\mu(x)\ A^\mu(x) \tag{2-71}$$

where $A^\mu(x)$ is the electromagnetic field of the proton, which in turn depends on the proton current $J^\mu(x)$. Regardless of the point of view the cross section (2-68) becomes

$$\sigma \sim \delta^4(p_f - p_i + P_f - P_i)\left|j_\mu \frac{e^2}{q^2} J^\mu\right|^2. \tag{2-72}$$

QED predicts the form of the current for the electron,

$$j_\mu \longrightarrow \bar{u}(p_f)\gamma_\mu u(p_i) \tag{2-73}$$

and by analogy for the proton

$$J^\mu \longrightarrow \bar{U}(P_f)\gamma^\mu U(P_i) \tag{2-74}$$

where u,U and $\bar{u},\bar{U}$ are the incident and final electron and proton spinors, respectively; and γ is a 4×4 matrix. Substitution of the currents into (2-72) and carrying out the trace calculation of $|M_{fi}|^2$ followed by a sum over final spins and an integration over final momenta will finally yield the result

$$\left(\frac{d\sigma}{d\Omega}\right)_{\substack{\text{Dirac}\\ \text{Proton}}} = \left(\frac{e^2}{2E}\right)^2 \frac{\cos^2\frac{\theta}{2}}{\sin^4\frac{\theta}{2}} \left(1 + \frac{2E}{MC^2}\sin^2\frac{\theta}{2}\right)^{-1} \left(1 - \frac{\hbar^2 q^2}{2m^2}\tan^2\frac{\theta}{2}\right) \tag{2-75}$$

where

$$\left(\frac{e^2}{2E}\right)^2 \frac{\cos^2\frac{\theta}{2}}{\sin^4\frac{\theta}{2}} = \text{Mott cross section} = \left(\frac{d\sigma}{d\Omega}\right)_{\text{Mott}} \tag{2-76}$$

$$\text{and } \left(1 + \frac{2E}{MC^2}\sin^2\frac{\theta}{2}\right)^{-1} = \text{recoil factor} = \xi \tag{2-77}$$

are the results of the kinematical quantities in (2-68). The square of the invariant matrix element $|M_{fi}|$ yields for a Dirac proton

$$|M_{fi}|^2 = 1 - \frac{\hbar^2 q^2}{2m^2}\tan^2\frac{\theta}{2} \, . \tag{2-78}$$

In obtaining (2-75) the approximation $m_e \to 0$ since $m_e \ll E$ has been used. Equation (2-75) is correct for scattering from a point proton with no anomalous magnetic moment.

But the proton is known to have an anomalous moment so the structure of M_{fi} must be changed to reflect this fact. In addition, the possibility of nucleon structure should be taken into account in M_{fi} (the electron remains a point). Figure 4 is redrawn to schematically illustrate the change in M_{fi}.

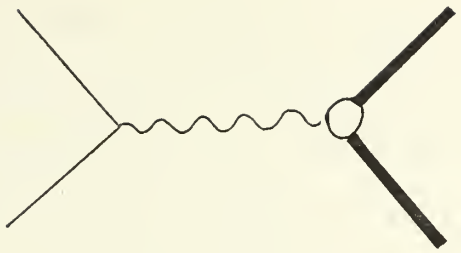

Figure 5

The bubble at the photon-nucleon vertex represents the non-locality of the photon-nucleon interaction and the anomalous moment of the proton. The matrix element is now

$$M_{fi} \sim j_\mu \frac{1}{q^2} J^\mu$$

where

$$J^\mu \longrightarrow \bar{U}(P_f) O^\mu U(P_i) \tag{2-79}$$

and

$$O^\mu = F_1(q^2)\gamma^\mu + F_2(q^2)\sigma^{\mu\nu}q. \tag{2-80}$$

The quantities F_1 and F_2 are undetermined real functions of q^2, while $\sigma^\mu \equiv \frac{i}{2}\{\gamma^\mu,\gamma^\nu\}$. Foldy [25] has shown that while (2-80) is not unique it has the proper general form.

With the above changes (2-75) becomes

$$\left(\frac{d\sigma}{d\Omega}\right)_R = \left(\frac{d\sigma}{d\Omega}\right)_{Mott} x\, \xi\, x \left[F_1^2 - \frac{\hbar^2 q^2}{4m_p^2 c^2}\left\{2(F_1 + \kappa_p F_2)^2 \tan^2\frac{\theta}{2} + \kappa_p^2 F_2^2\right\}\right] \tag{2-81}$$

where the final bracket is the invariant matrix element $|M_{fi}|^2$, and where $\kappa_p = 1.79$ is the protons anomalous (Pauli)

moment. Equation (2-81) is known as the Rosenbluth cross section. The factor $F_1(q^2)$ is found to represent the proton's charge distribution and its normal magnetic moment, while $F_2(q^2)$ represents the anomalous part of the magnetic moment. F_1 and F_2 are called the Dirac and Pauli form factors respectively. Yennie [26], and later Hand, Miller and Wilson [27] pointed out that F_1 and F_2 should not be considered to be electric or magnetic form factors. More properly certain linear combinations of F_1 and F_2 defined to be

$$G_E = F_1 + \frac{\hbar^2 q^2}{4m^2c^2} \kappa_p F_2 \xrightarrow[q^2 \to 0]{} 1 \tag{2-82}$$

and

$$G_M = F_1 + \kappa_p F_2 \xrightarrow[q^2 \to 0]{} 1 + \kappa_p = \mu_p \tag{2-83}$$

are termed electric and magnetic form factors. The major advantage of (2-82) and (2-83) is that in the Rosenbluth cross section (2-81) the cross term $(F_1 + \kappa_p F_2)^2$ is removed,

$$\frac{d\sigma}{d\Omega} = \left(\frac{d\sigma}{d\Omega}\right)_{\text{Mott}} \xi \left[\frac{G_E^2 - \frac{\hbar^2 q^2}{4m^2c^2} G_M^2}{1 - \frac{\hbar^2 q^2}{4m^2c^2}} - \frac{\hbar^2 q^2}{4m^2c^2} 2 \tan^2 \frac{\theta}{2} G_m^2 \right]. \tag{2-84}$$

In both the cross section formulas the form of the quantity in braces is $A(q^2) + B(q^2) \tan^2 \frac{\theta}{2}$. It can be shown that this is the most general form for the one photon exchange process, regardless of the structure of the

electron and the proton. The interpretation of A and B in terms of G_E and G_m or F_1 and F_2 depends of course on the structure assumed.

2. Nucleon Form Factors

In the text above no real attempt has been made to coherently explain the form factor concept. So far they have been characterized mainly as correction factors that when multiplied by the scattering cross section for point (structureless) particles yield the cross section for scattering from physical particles. Thus, as introduced, these dimensionless quantities are meaningless unless some predictions can be made from a basic theory of matter about the structure and behavior of the form factors.

While the simple idea of the form factor representing some physical extension in space can be illustrated by non-relativistic examples, a more comprehensive discussion of their meaning needs the help of the so-called dispersion relations. Both viewpoints are investigated below.

In Section II, part A2, the scattering amplitude $f(\theta)$ was found in a partial wave solution of the Schroedinger equation for the scattering of neutrons from protons. Of interest here is the solution of the Schroedinger equation for the scattering of electrons from two potentials V(r), one with a point charge source, the other with a smeared out charge distribution.

With all assumptions as in Section II part A2, the Schroedinger equation for scattering is again

$$(\nabla^2 + k^2)\psi(r) = \frac{2m}{\hbar^2} V(r)\psi(r). \qquad (2\text{-}85)$$

This differential Schroedinger equation is solved formally for ψ making (2-85) into an integral equation. The inverse of the linear differential operator $(\nabla^2 + k^2)$ is an integral, hence

$$\psi'(r) = \int G(r,r') \frac{2m}{\hbar^2} V(r')\psi(r')dr' \qquad (2\text{-}86)$$

where r' is a dummy variable of integration and G(r,r') is a function characteristic of the form of the differential operator. G(r,r') is known as a Green Function. The general solution to (2-85) is the sum of the solution to the homogenous problem (in this case it would be the unscattered plane wave $e^{i\vec{k}\cdot\vec{r}}$ since $\frac{2m}{\hbar^2} V(r) = 0$) and some particular solution to the inhomogenous problem which is given by (2-86). Hence

$$\psi(r) = e^{i\vec{k}\cdot\vec{r}} + \int G(r,r') \frac{2m}{\hbar^2} V(r')\psi(r')dr'. \qquad (2\text{-}87)$$

This is called the integral equation for scattering, and the solution is found by iteration. The first iterated form is called the Born or plane-wave approximation

$$\psi = e^{i\vec{k}\cdot\vec{r}} + \frac{2m}{\hbar^2}\int G(r,r') e^{i\vec{k}\cdot\vec{r}} dr'. \qquad (2\text{-}88)$$

Comparing (2-88) and (2-16) yields the scattering amplitide*

*In order that the comparison be made the correct form of G(r,r') must be determined.

$$f(\theta) = \frac{2m}{\hbar^2}\int e^{i\vec{q}\cdot\vec{r}}\, V(r')dr' \qquad (2\text{-}89)$$

where $\vec{q} = \vec{k}_i - \vec{k}_f$. For a spherically symmetric potential V, (2-89) is

$$f(\theta) = \frac{2m}{\hbar^2 q^2}\int_0^\infty r'\sin qr'\, V(r')\, dr'. \qquad (2\text{-}90)$$

For a point charge of Ze, the potential V is Ze^2/r, thus

$$f_{pt.}(\theta) = \frac{2mZe^2}{\hbar^2 q^2} \qquad (2\text{-}91)$$

while for a distributed charge of Ze of the form

$V_D = \frac{Ze^2}{r}(1 - e^{-\alpha r})$, $\alpha \neq 0$,

$$f_D(\theta) = \frac{2mZe^2}{\hbar^2 q^2}\frac{\alpha^2}{q^2+\alpha^2} = f_{pt.}(\theta)\frac{\alpha^2}{q^2+\alpha^2}. \qquad (2\text{-}92)$$

Hence the structure of the distributed charge shows up as a factor times the point charge scattering amplitude. It can be shown that the form factor here is the Fourier transform of the charge distribution. Figure 6 illustrates the behavior of (2-91) and (2-92) as a function of q^2. The slope of $f(\theta)$ at $q^2 = 0$ is proportional to the radius of the structure under consideration. Before continuing it must be stressed that all that has been said so far of form factors refers to the non-relativistic case. In a relativistic example difficulties are immediately apparent. A charge distribution, spherical in one reference frame is elongated in another frame so that the meaning of the radius

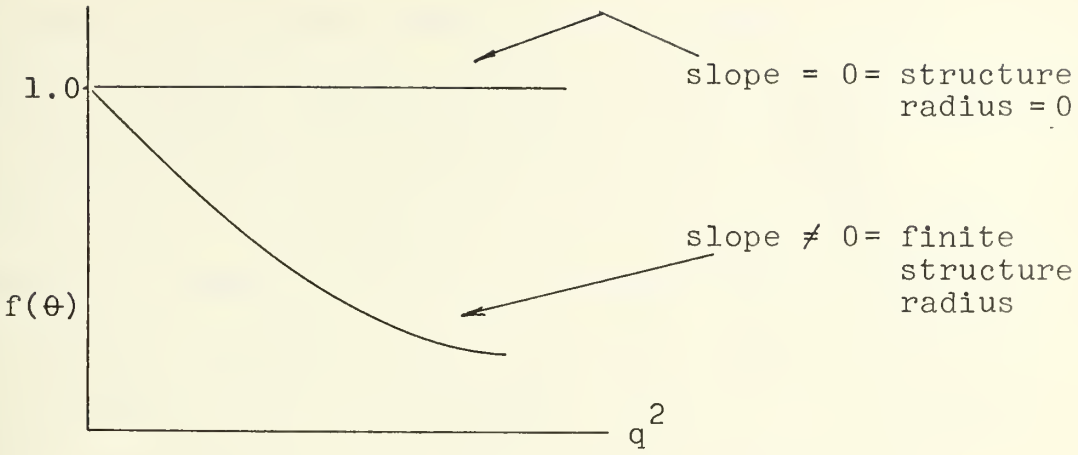

Figure 6

of a charge distribution is not clear. No longer can a form factor be thought of properly as the Fourier transform of the distribution. One has to be concerned with the form factors themselves and not their three-dimensional Fourier transforms in a particular reference frame.

The Meson theory of nuclear forces mentioned briefly in Sections I part D and II part A3 states that virtual pions are constantly being emitted and reabsorbed by a nucleon. Further, two nucleons are stuck together through an exchange of pions. Now, since nucleons are surrounded by a cloud of pions, the virtual photon emitted by an electron scattered from the nucleon might have in fact, interacted with the nucleon meson cloud. So the simple electromagnetic interaction of a photon and a nucleon may be quite a bit more complex and depend on the dynamics of the strong interaction of the pion and the nucleon. Dispersion relations then attempt to understand form factor behavior as a function of

q^2 in terms of the strong interaction dynamics. What follows is a simple minded attempt to make plausible the form of the equations put forth for the form factor.

The basic idea of dispersion relations (spectral representations, or S-matrix theory of strong interactions) is that a quantum mechanical amplitude for a physical process is the boundary value of an analytic function of a complex variable. For electron scattering $F(q^2)$ would be the boundary value along the real line of the analytic function $F(z)$ where $z \to q^2 + i\varepsilon$. A dispersion relation is an integral equation that relates a dispersive process to an absorptive process. The best known example is that of the dispersion of light in a dielectric, where the complex index of refraction $n(\omega) = n_r(\omega) + i \frac{c}{2\omega} \alpha(\omega)$ is expressed as an integral over all frequencies involving the absorption coefficient $\alpha(\omega)$:

$$n_r(\omega) - 1 = \frac{2}{\pi} P \int_0^\infty \frac{\omega' \, \mathrm{Im}\, n(\omega)}{\omega'^2 - \omega^2} \, d\omega' = \frac{c}{\pi} \int_0^\infty \frac{\alpha(\omega') d\omega'}{\omega'^2 - \omega^2} \qquad (2\text{-}93)$$

(P represents the Cauchy principal value of the integral)

A classical optical example of (2-93) is Sellmiers equation for the anomalous dispersion of light,

$$n^2 - 1 = \sum_{i=1}^{N} \frac{A_i \lambda^2}{\lambda^2 - \lambda_i^2} \qquad (2\text{-}94)$$

where λ is the incident light wave length, λ_i the i^{th} resonant wavelength, A_i a constant, and N the number of natural frequencies of the medium.

In electron scattering

$$F(q^2) = \frac{1}{\pi} \int_{4m_\pi^2}^{\infty} \frac{\mathrm{Im}F(q^2)}{q'^2 - q^2} \, dq'^2 \qquad (2\text{-}95)$$

is a direct analog of (2-93). Now three mesons, the ρ, ϕ, and the ω-meson have been found experimentally to have the correct properties so that they may couple to the nucleon and to the virtual photon. They correspond to the N natural frequencies above. Hence it is plausible to write keeping (2-94) in mind

$$F(q^2) = \sum_{i=1}^{3} \frac{g_{ij}}{1 - \frac{q^2}{m_i^2}} \qquad j = p, n. \qquad (2\text{-}96)$$

In terms of the physical form factors G, (2-96) might be written

$$G_{E_p}(q^2) = \frac{g_{\omega p}}{1 - \frac{q^2}{m_\omega^2}} + \frac{g_{\phi p}}{1 - \frac{q^2}{m_\phi^2}} + \frac{g_{\rho p}}{1 - \frac{q^2}{m_\rho^2}} + 1 - g_{\omega p} - g_{\phi p} - g_{\rho p}$$

and

$$G_{M_p}(q^2) = \frac{\mu_{\omega p}}{1 - \frac{q^2}{m_\omega^2}} + \frac{\mu_{\phi p}}{1 - \frac{q^2}{m_\phi^2}} + \frac{\mu_{\rho p}}{1 - \frac{q^2}{m_\rho^2}} + 1 - \mu_{\omega p} - \mu_{\phi p} - \mu_{\rho p} \qquad (2\text{-}97)$$

where the g's and μ's are coupling constants to be fitted to experimental data. The twelve coupling constants in (2-97) are not all independent and their number can be significantly reduced. The best fit available for the proton was used here to predict G_{E_p} for use in (2-84). De Vries [28] adjusted

the free parameters appearing in (2-97) so that a minimum is obtained in a χ^2 fit to experimental data. The following values were determined: $g_{\omega p} = 2.628$, $g_{\phi p} = 1.853$, $g_{\rho p} = 1.191$, where $m_\omega^2 = 15.6\ F^{-2}$, $m_\phi^2 = 26.6\ F^{-2}$ are experimentally confirmed resonances of fairly narrow width. Since the ρ resonance appears as a rather broad peak (750 ± 100) MeV and since some observers [29] have shown that the effective position of the ρ mass can be at about 600 MeV, the mass of the ρ resonance has been taken as a free parameter, determined to be $m_\rho^2 = 8.463\ F^{-2}$. Before continuing it should be noted that both (2-94) and (2-97) are approximations of (2-93) and (2-95) respectively in the sense that the resonances considered are taken to be delta functions in the integrands of the more accurate form factor expression (2-93) and (2-95)

It is interesting to note that the theory outlined above actually preceded the discovery of the mesons that it requires. Dispersion relations as applied to the strong interaction was developed in 1957 by Chew [30] et al on the basis of a two-pion exchange approximation. This theory was not able to explain form factor behavior, and it later showed (1959) that a three pion resonance must exist in order that theory and experiment agree.

A multiplicity of form factor notations exist today. Coupled with their often misleading names and differently defined static limits, they present a baffling array.

Commonly, the starting place is with the two functions $F_1(\vec{q}^2)$ and $F_2(\vec{q}^2)$, called the Dirac and Pauli form factors (really there are four form factors, two for the proton, two for the neutron). They describe the structure of the normal Dirac coupling and the anomalous Pauli coupling between the nucleon and the electromagnetic field. F_1 and F_2 are not directly related to the electric and magnetic moment distributions of the nucleon, but in older papers they are often erroneously called electric and magnetic form factors. Still another general name for F_1 and F_2 are vertex form factors referring obviously to their use in the current operator J^μ. The Dirac and Pauli form factors have the following static limits:

$$F_{1_p}(0) = 1 \qquad F_{1_n}(0) = 0$$

$$F_{2_p}(0) = 1.79 = \kappa_p \qquad F_{2_n}(0) = -1.91 = \kappa_n \qquad (2\text{-}98)$$

Hand, Miller and Wilson [27] popularized the use of the physical form factors G. They were introduced to simplify the Rosenbluth cross section by removing the cross product terms in F_1 and F_2 and are in no way more fundamental than the vertex form factors. They are defined

$$G_E \equiv F_1 + \eta\kappa F_2 \equiv F_{CH}$$

$$G_m \equiv F_1 + \kappa F_2 \equiv (1+k)F_{MAG} \qquad (2\text{-}99)$$

where $\eta = -\vec{q}^2/4m^2$, m the neutron or proton mass, κ the anomalous proton or neutron moment. F_{ch} and F_{mag} were used

briefly before the G factors became popular. The form factors G_E and G_m do merit the names, electric and magnetic form factor, and they have static limits

$$G_{E_p}(0) = 1 \qquad G_{E_n}(0) = 0$$

$$G_{m_p}(0) = 2.793 \qquad G_{m_n}(0) = -1.91 \tag{2-100}$$

It is often found that still another type of form factor is convenient to work with. In isotopic spin notation where $\tau_z = 1$ for the proton and $\tau_z = -1$ for the neutron, the charge and magnetic form factors can be written succinctly for both the neutron and proton as

$$G_E = \tfrac{1}{2}(1 + \tau_z)\, G_{E_p} + \tfrac{1}{2}(1 - \tau_z)\, G_{E_n}$$

$$G_m = \tfrac{1}{2}(1 + \ _z)\, G_{M_p} + \tfrac{1}{2}(1 - \ _z)\, G_{m_n}$$

or as,

$$G_E = \tfrac{1}{2}(G_{E_p} + G_{E_n}) + \tfrac{1}{2}\gamma_z(G_{E_p} - G_{E_n})$$

$$G_m = \tfrac{1}{2}(G_{m_p} + G_{m_n}) + \tfrac{1}{2}\gamma_z(G_{m_p} - G_{m_n})$$

Now define the isoscalar form factors as,

$$G_E^s \equiv \tfrac{1}{2}(G_{E_p} + G_{E_n}) \xrightarrow[q^2 \to 0]{} \tfrac{1}{2}$$

$$G_m^s \equiv \tfrac{1}{2}(G_{m_p} - G_{m_n}) \xrightarrow[q^2 \to 0]{} \tfrac{1}{2}(\mu_p + \mu_n) \tag{2-101}$$

and the isovector form factors as,

$$G_E^V \equiv \frac{1}{2}(G_{E_p} - G_{E_n}) \xrightarrow[q^2 \to 0]{} \frac{1}{2}$$

$$G_m^V \equiv \frac{1}{2}(G_{m_p} - G_{m_n}) \xrightarrow[q^2 \to 0]{} 2.35 \qquad (2\text{-}102)$$

These (iso) form factors are convenient for use in theoretical work because the electromagnetic current J_μ may be split into isoscalar and isovector parts, i.e. $J_\mu = J_\mu^S + J_\mu^V$. The intermediate states in the photon-nucleon vertex can be characterized by this isoscalar-isovector idea in that the two pion resonances with (T=0, J=1) ω and ϕ manifest themselves in the isoscalar form factors G_E^S and G_m^S, whereas the third resonance (T=1, J=1)ρ contributes to the isovector form factors G_E^V and G_M^V. It is interesting to note that only the isoscalar form factor $2G_E^S = (G_{E_p} + G_{E_n})$ appears in the deuteron cross section, which might be expected since the deuteron current is an isoscalar.

There is an important relationship between the physical form factors that was discovered in 1961 at Orsay by Lehmann, Taylor, and Wilson [31]. In low q^2 measurements (actually the work was at $q^2 = 2.98\ F^{-2}$) of the e-p cross section the following was noted:

$$G_{E_p} \simeq \frac{G_{m_p}}{\mu_p} \qquad (2\text{-}103)$$

Later data verified this up to approximately 100 F^{-2}, and (2-103) came to be known and called the "scaling rule." There is some suggestion of (2-103) when the vertex form

factors are expressed in terms of the physical form factors, for example inverting (2-99) yields

$$F_1 = \frac{G_E - \eta G_m}{1-\eta}, \quad \kappa F_2 = \frac{G_m - G_E}{1-\eta}.$$

The above have poles at $\eta=1$ unless (2-103) is true. Drickey and Hand have experimentally verified (2-103) to include the deuteron with

$$G_{E_d} \simeq \frac{G_{m_d}}{\mu'_d}, \quad \mu_d' = 1.71 = \frac{M_d}{M_p}\mu_d. \tag{2-104}$$

A further relationship of this type has been noted,

$$\frac{G_{m_p}}{\mu_p} = \frac{G_{m_n}}{\mu_n}. \tag{2-105}$$

Figure 7 shows that the scaling rules can be used as an established empirical fact (to at least 20 F^{-2}) without introducing appreciable error.

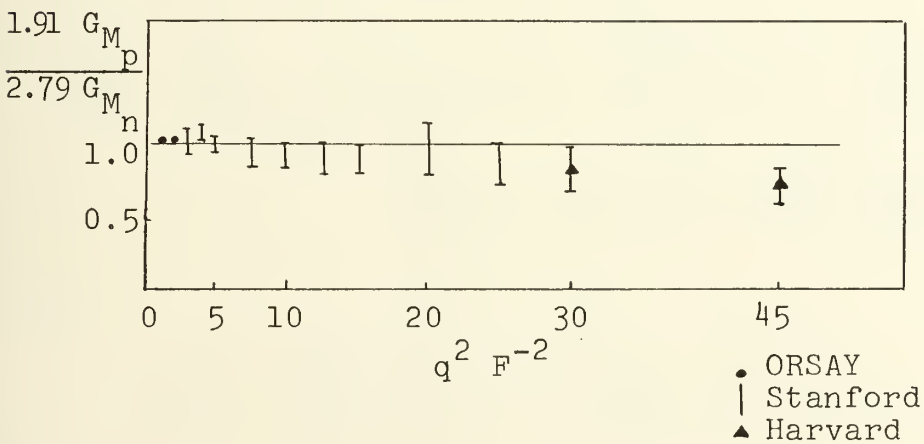

Figure 7

3. Elastic Electron Deuteron Scattering

Following the same general procedure as Rosenbluth did with the proton, Jankus (1956) derived [3] the cross section for elastic electron-deuteron (e-d) scattering from a point deuteron in the first Born approximation. His results differ qualitatively from the proton cross section in one important way, i.e., there are three form factors characterizing the deuteron while two suffice for the proton. This is in agreement with the work of Glaser and Jaksic [32]. Their study showed that the cross section for scattering a relativistic electron from a potential with spin J, contains 2J + 1 form factors. The three deuteron form factors are found to correspond to the charge, quadrupole, and magnetic moments in the static limit $q^2 \to 0$. The general form of the cross section is as it should be for the one photon exchange process, $A(q^2) + B(q^2) \tan^2 \frac{\theta}{2}$.

Specifically Jankus found that

$$\frac{d\sigma}{d\Omega} = \left(\frac{d\sigma}{d\Omega}\right)_{\text{Mott}} \left(1 + \frac{2E}{M_d c^2} \sin^2 \frac{\theta}{2}\right)^{-1} \left[D_c^2(\vec{q}^2) + \frac{8}{9} \eta^2 D_Q^2(\vec{q}^2) + \frac{2}{3}\eta \left\{ 1 + 2(1-\eta) \tan^2 \frac{\theta}{2} \right\} D_M^2(\vec{q}^2) \right] \qquad (2\text{-}106)$$

where

$$D_c(\vec{q}) = \int_0^\infty \left[u^2(r) + w^2(r) \right] j_o(\tau) dr \longrightarrow 1 \qquad (2\text{-}107)$$

is the charge structure factor,

$$D_Q(\vec{q}^2) = \frac{6\sqrt{2}}{q^2} M_d^2 \int_0^\infty \left[u(r)w(r) - \frac{w^2(r)}{\sqrt{8}}\right] j_2(\tau)dr \longrightarrow M_d^2 Q \quad (2\text{-}108)$$

is the quadrupole moment structure factor.

$$D_M^M(\vec{q}^2) = \int_0^\infty \left[u^2(r) - \tfrac{1}{2}w^2(r)\right] j_o(\tau)dr + \frac{1}{\sqrt{2}} \int_0^\infty \left[u(r)w(r) + \frac{w^2(r)}{\sqrt{2}}\right] j_2(\tau)dr \longrightarrow 1 - \tfrac{3}{2}P_D \quad (2\text{-}109a)$$

accounts for the contribution of the intrinsic magnetic moments of the proton and the neutron to the scattering process and

$$D_M^E(\vec{q}^2) = \tfrac{3}{2} \int_0^\infty w^2(r)\left[j_o(\tau) + j_2(\tau)\right] dr \longrightarrow \tfrac{3}{2} P_D \quad (2\text{-}109b)$$

is the magnetic contribution to the scattering process arising from the convection of charge in the deuteron. Together (2-109a,b) are

$$D_M(\vec{q}^2) = \frac{1}{2}\left[(\mu_p + \mu_n)2D_M^M + D_M^E\right] \quad (2\text{-}110)$$

Also given are the static limits ($q^2 \to 0$). The j_o and j_2 are spherical Bessel functions, $\tau = |\vec{q}|r/2$, Q is the quadrupole moment and P_D the percentage D-state (see page 127).

While the currents in e-p scattering were easily found, the deuteron current presents somewhat more of a problem. The virtual photon is expected to interact with one nucleon only. But the interaction amplitude of an electron with a bound nucleon is unknown. The natural thing to do is to

assume that since the deuteron is a loosely bound system, the photon interacts with a nearly free nucleon, while the other nucleon participates just as a spectator. This is called the impulse approximation and is described graphically by Figure 8.

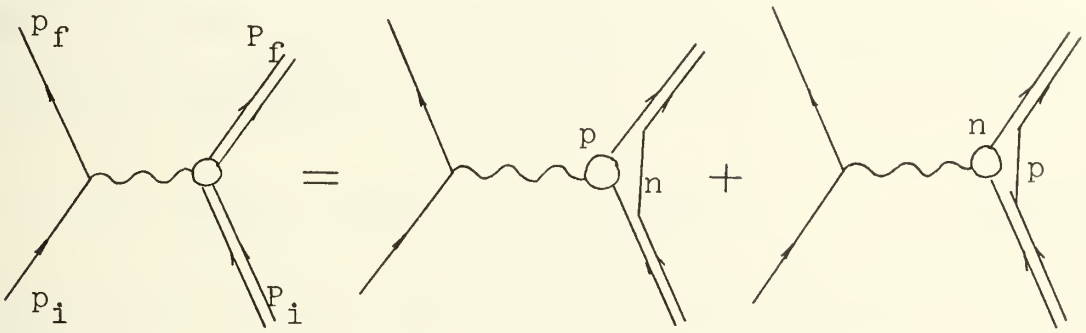

Figure 8

Here the bubbles represent the photon - free nucleon vertex. Distortion of the free electromagnetic form factor (vertex) due to binding, i.e., the difference between bound and free form factors, is thought to be less than 5% [33]. Now that the impulse approximation has freed the nucleons, the nucleon participating with the photon in the interaction is described by the free field Dirac Equation.

Since the impulse approximation involves the interaction of a photon with an individual "free" nucleon, the current is again of the form $\bar{U}O^{\mu}U$, where O^{μ} is given by

$$O_p^\mu = F_{1p}(q^2)\gamma^\mu + F_{2p}(q^2)\sigma^{\mu\nu}q_\nu,$$

$$O_n^\mu = F_{1n}(q^2)\gamma^\mu + F_{2n}(q^2)\sigma^{\mu\nu}q_\nu. \qquad (2\text{-}111)$$

The deuteron current is then

$$J_d^\mu \longrightarrow \bar{U}O_p^\mu U + \bar{V}O_n^\mu V. \qquad (2\text{-}112)$$

Adler [45] writes the relevant part of the S-matrix form in the impulse approximation as

$$\sigma \sim |S_{fi}|^2 \sim |M_{fi}|^2 = |j_\mu \frac{e^2}{q^2} J_d^\mu|^2. \qquad (2\text{-}113)$$

Just as in the proton case, $|M_{fi}|^2$ is evaluated and found to be

$$|M_{fi}|^2 = G_c^2 + \frac{8}{9}\eta^2 G_Q^2 + \frac{2}{3}\eta G_M^2 \left[1 + 2(1-\eta)\tan^2\frac{\theta}{2}\right] \qquad (2\text{-}114)$$

where $\eta = -\vec{q}^2/4M_d^2$, and G_c, G_Q and G_M are the charge, quadrupole and magnetic form factors given by (including their static limits).

$$G_c \equiv (G_{E_p} + G_{E_n})\, D_c \xrightarrow[q^2 = 0]{} 1 \qquad (2\text{-}115)$$

and

$$G_Q = (G_{E_p} + G_{E_n})\, D_Q \longrightarrow M_d^2 Q \qquad (2\text{-}116)$$

and

$$G_M = (G_{E_p} + G_{E_n})D_M^E + (G_{M_p} + G_{M_n})2D_M^M \longrightarrow \frac{M_d}{M_p}\mu_d, \qquad (2\text{-}117)$$

where the D's are given in equations (107) through (110). The steps from a point deuteron to a finite size deuteron is thus carried out by the introduction of the free nucleon form factors. This step is justified by the impulse approximation.

The contributions of G_C^2 (charge), G_Q^2 (quadrupole) and G_M^2 (magnetic) to

$$A(Q^2) = G_C^2(q^2) + \frac{8}{9}\eta^2 G_Q^2(q^2) + \frac{2}{3}\eta G_M^2(q^2) \qquad (2\text{-}118)$$

are shown in Figure 9.

4. Neutron Charge Form Factor from e-d Scattering

Equation (2-117) can be simplified considerably by scaling, i.e.,

$$G_{M_d} = \mu_d' G_{C_d} \quad , \quad \mu_d' = 1.71$$

and

$$\frac{G_{M_p}}{\mu_p} = \frac{G_{M_n}}{\mu_n} = G_{E_p} \; .$$

For the case of the deuteron

$$G_{M_d} \equiv (G_{E_p} + G_{E_n})\, \mu_d'\, D_C \qquad (2\text{-}119)$$

so that with $1 - \eta \to 1$,

$$G_d^2 = (G_{E_p} + G_{E_n})^2 \left[D_C^2(1 + \frac{2}{3}\eta\mu_d'^2 + \frac{4}{3}\eta\mu_d'^2 \tan^2\frac{\theta}{2}) + \frac{8}{9}\eta^2 D_Q^2\right]$$

$$G_d^2 = (G_{E_p} + G_{E_n})^2 \, F_d'^2 \qquad (2\text{-}120)$$

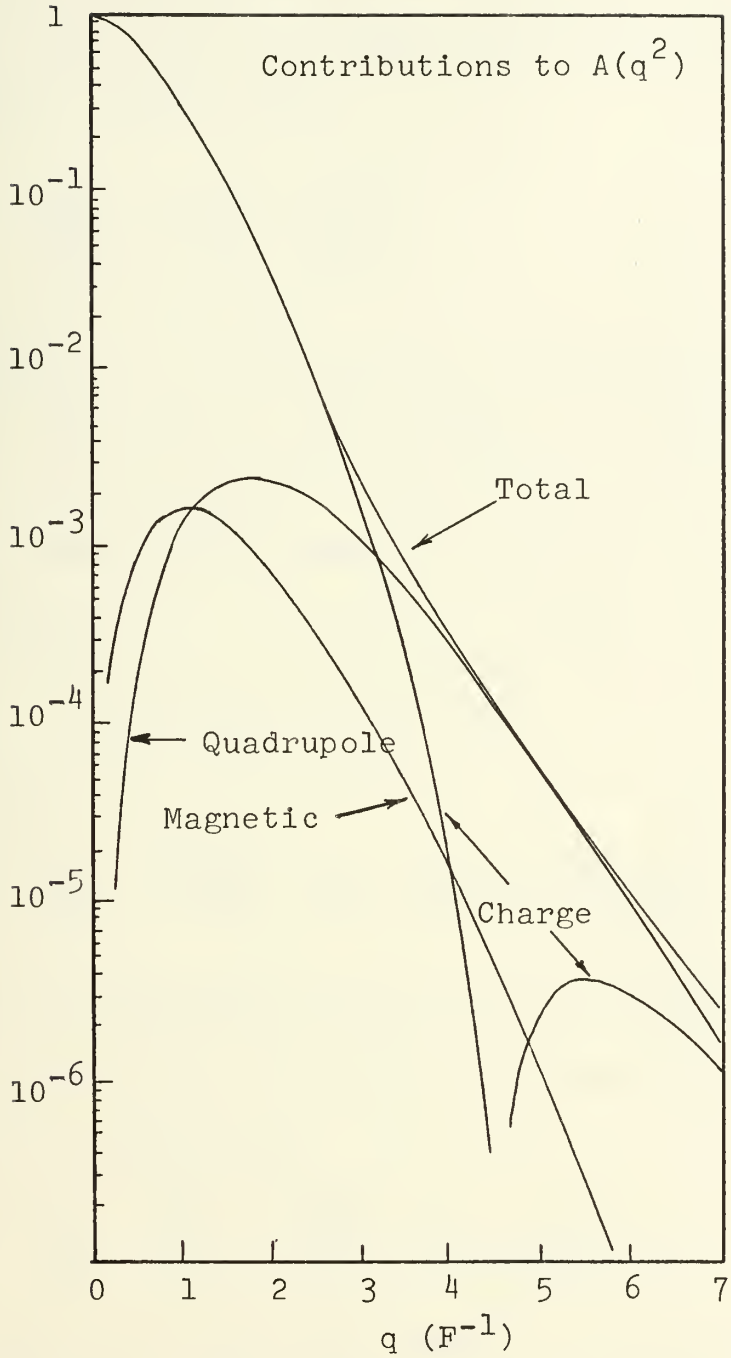

Figure 9

The functions G_c^2 (charge), $\frac{8}{9}\eta^2 G_Q^2$ (quadrupole) and $\frac{2}{3}\eta G_M^2$ (magnetic). The smooth curve is the sum of these three terms (taken from Ref. 46).

where F_d^2 is called the deuteron structure factor and is the same as the result of Jankus for a point (nucleons) in the deuteron. From (2-120)

$$\frac{G_d}{G_{E_p}} = F_d' \left(1 + \frac{G_{E_n}}{G_{E_p}}\right). \tag{2-121}$$

The aim of the experiment is the evaluation of the charge form factor of the neutron. The magnetic contribution to G_d^2 and G_p^2 must therefore be eliminated. In the case of the deuteron the magnetic contribution is given by (2-120) as

$$C = \frac{2}{3}\eta\mu_d'^2 \left(1 + 2\tan^2\frac{\theta}{2}\right) \tag{2-122}$$

so that

$$G_{E_d}^2 = \frac{G_{EXP}^2}{1+C}, \text{ with } G_{EXP}^2 \equiv \left[\frac{\sigma_{exp}}{\sigma_{mott}}\right]_d \tag{2-123}$$

where the quadrupole term has been neglected.

In the case of the proton the magnetic contribution is found by considering

$$G_p^2 = \frac{G_{E_p}^2}{1-\eta} + \eta\frac{G_{M_p}^2}{1-\eta}\left(1 + 2\tan^2\frac{\theta}{2}\right) \tag{2-124}$$

Scaling assumes $G_M = \mu G_E$ where $\mu = 2.79$ so,

$$G_p^2 = \frac{G_{E_p}^2}{1-\eta}\left\{1 - \eta\mu^2\left(1 + 2\tan^2\frac{\theta}{2}\right)\right\}. \tag{2-125}$$

The term

$$C = \eta\mu^2\left(1 + 2\tan^2\frac{\theta}{2}\right) \tag{2-126}$$

is then the magnetic correction term. Thus

$$G_p^2 = \frac{G_{E_p}^2}{1-\eta}(1 + C)$$

so that

$$G_{E_p}^2 = \frac{G_p^2(1-\eta)}{1 + C} \tag{2-127}$$

where

$$G_p^2 = \frac{\sigma_{exp}}{\sigma_{mott}} .$$

Finally, for experimental comparisons

$$\frac{G_{E_d}}{G_{E_p}} = F_d \left(1 + \frac{G_{E_n}}{G_{E_p}}\right)$$

or

$$\frac{G_{E_n}}{G_{E_p}} = \frac{1}{F_d}\frac{G_{E_d}}{G_{E_p}} - 1. \tag{2-128}$$

The value of G_{E_n} from (2-128) is very sensitive to the uncertainty in F_d and G_{E_n}/G_{E_p}. For example a 1% error in F_d translates into about a 10% error in G_{E_n}/G_{E_p}.

The only reliable data in the range of q^2 considered here have been presented by Drickey and Hand [1]. Their results were in complete disagreement with the neutron-electron interaction slope. Their data will be presented after reanalysis of the theory in part B5.

5. Review of Relativistic Deuteron Theories

Essentially, all the material above is based upon the solutions to a nonrelativistic Schroedinger equation for the two-nucleon problem. The results produced using the nonrelativistic S and D state wave functions are, at times, surprisingly good. Still, there are problems as the nagging difficulty in the determination of the percentage D state, and the theoretical determination of the deuteron magnetic moment, not to mention the conflict that is the point of this work, i.e., $G_{E_n} \simeq 0$ while $dG_{E_n}/d(q^2)\Big|_{q^2 = 0} \neq 0$. Hence sufficient reason exists for improving the theory, as well as the experiment.

The Jankus theory on which the cross section (2-106) was derived is itself one of the major limitations in the development of better answers for the deuteron. Gross states that the theory gives no indication of what has been left out, or how to calculate corrections, which might include the effects of off-the-mass-shell contributions arising from the fact that the nucleons are bound and not free. Intermediate states, i.e., pion exchange currents, could cause further corrections. Thus to isolate possible corrections a fully relativistic theory should be developed, one that would reduce to Jankus theory at low q^2. Corrections then could be localized and more carefully defined. This is a difficult order to fill, and to date no entirely satisfactory solution has been proposed, though many authors have tried. The most interesting attempts are briefly discussed below.

Van [34] has calculated, using deuteron wave functions derived from a Bethe-Salpeter equation, relativistic corrections to the deuteron form factor. These wave functions, which are relativistic generalizations of Hulthen wave functions (no hard core) tend to make the functional D of Equation (2-106) larger at high momentum transfers than do models having a hard core. The essential part of Van's results is a comparison between his predictions of D_C (F_{ch}^{ch} in Van's notation) calculated with the (relativistic) Hulthen wave functions and the corresponding $D_C(F_{ch}^{N}$, Van) of the nonrelativistic case. The comparison showed $F_{ch}^{ch}(q^2) > F_{ch}^{NR}$ in a range of q^2 from 0 to 9 F^{-2}, which results in F_d being larger than in the relativistic case. Recalling (2-128) quickly confirms the fact that the end result is to make G_{E_n}/G_{E_p} even smaller. The increase in F_{ch}^{ch} from F_{ch}^{NR} is attributed to the quadrupole contribution (+3.5% at $q^2 = 1\ F^{-2}$), and to final state wave function Lorentz contraction (-1.5% at $q^2 = 1\ F^{-2}$).

Adler [45] has obtained what amounts to first order relativistic corrections to the nonrelativistic impulse approximation deuteron form factors. His theory is intrinsically nonrelativistic and differs from that of Section II part B2 only by the use of Pauli spinors (for convenience) instead of Dirac spinors, and by retaining powers of deuteron moments such that the final cross sections are correct to order q^2/m^2. The extra terms now found in the

deuteron current are incorporated into additive corrections to G_C and G_Q. Specifically

$$G_C^{ADLER} = G_C - \frac{G_{RS}}{8M_d^2}\frac{9}{4}q^2\int_0^\infty w^2\left[\frac{j_1(\frac{qr}{2})}{|\vec{q}|r}\,dr\right] = G_C - \Delta G_C^R$$

and

$$G_Q^{ADLER} = \frac{2\sqrt{2}}{3}\eta G_Q - \frac{G_{RS}\,q^2}{8M_d^2}\Delta G_Q$$

where

$$\Delta G_Q = 24\int_0^\infty w(u'r-u)\,\frac{j_2(qr/2)}{\vec{q}^2r^2}\,dr + \frac{6}{5\sqrt{2}}\int_0^\infty w^2\,\frac{j_1(qr/2)-4j_3(qr/2)}{|\vec{q}|r}\,dr$$

and where

$$G_{RS} \equiv G_{R_p} + G_{R_n}\,, \quad G_R = F_1(q^2) + 2\kappa F_2(q^2).$$

At $q^2 = 1.0\ F^{-2}$ where $G_C = 0.55$, $\Delta G_C^R \simeq 8 \times 10^{-5}$ and where $G_Q = 0.03$, $G_Q^R = 2 \times 10^{-4}$, hence the corrections are rather too small to effect F_d greatly but go in the right direction. Further, these corrections to F_d do not alter the value of μ_d since it depends only on P_D, and the value of Q_d is changed by a bare 1%. In summary then, it is doubtful that these corrections are very meaningful in a theory using nonrelativistic wave functions.

Adler glossed over at least one sticky problem in the above work. He admits the need for a "fudge factor" in resolving the kinematical difficulty in the lab frame of an energy transfer (recoil) to only one of the nucleons by

the virtual photon. Gourdin [35] has made what amounts to the same calculation but in the Breit frame where the momentum transfer is entirely spacelike, i.e., $q^2 = -\vec{q}^2$, $q_0^2 = 0$. His difficulty was in the transformation of the nonrelativistic deuteron wave functions into the Breit frame. His solution to this was to assume that the wave function were unchanged. Gourdin's results were approximately the inverse of Adler's, i.e., of the same magnitude but opposite in sign. Unlike Adler, Gourdin did derive a very small correction to the magnetic form factor but it is so small that it is not observed for $q^2 \leq 6\ F^{-2}$. The value then of these works lies in the fact that it almost certainly seals the fate of any straightforward attempt to determine (quasi) relativistic corrections.

The strictly relativistic approaches (a covariant dispersion relation representation) are more basic and more difficult than the quasi-relativistic work above. Success with this technique is limited to the low momentum transfer region where it is now believed that the theory is more accurate than experiment. The early papers of Jones [4] and Cutkosky [36] are interesting when applied to the G_{E_n} problem. Using the triangle impulse approximation diagram (page 67) Cutkosky calculated the simplest absorptive amplitude which yields a deuteron structure factor of (all spins ignored)

$$F_d^{\Delta}(q^2) = \frac{1}{1+\eta}\left[\frac{\sqrt{1+\eta}}{\sqrt{\eta}\ \cot\ \frac{\alpha}{M}}\ \tan^{-1}\ \frac{\sqrt{\eta}\ \cot\ \frac{\alpha}{M}}{\sqrt{1+\eta}}\right], \alpha = \sqrt{wM}. \quad (2\text{-}129)$$

The relativistic analog using the tail approximation is

$$F_d^T(q^2) = \int_0^\infty u(r) j_o(qr/2) dr = \frac{4\alpha}{|\vec{q}|} \tan^{-1} \frac{|\vec{q}|}{4\alpha} \qquad (2\text{-}130)$$

where

$$\sigma = \sigma_{Mott} \; G_E^{S2} \; F_d^T. \qquad (2\text{-}131)$$

Comparison of the two F_d^T and F_d^Δ yield the relativistic corrections

$$F_d^T \longrightarrow \frac{F_d^T}{1+\eta} \qquad (2\text{-}132)$$

and

$$|\vec{q}| \longrightarrow \frac{\sqrt{q^2}}{\sqrt{1+\eta}} \qquad (2\text{-}133)$$

These imply that a surprisingly rapid curvature is needed at small q^2 for G_{E_n} in order that the n-e interaction be in consonance with $G_{E_n} \simeq 0$ at 0.3 - 0.6 F^{-2}.

Gross has done the most extensive work in the area of the purely relativistic approach [2, 8, 9, 10, 11]. He ambitiously set out to construct a complete theory fully relativistic and fundamental in the sense that very few phenomenological parameters occur and based on single-variable unsubtracted dispersion relations and coupled unitarity equations. He had partial success but numerical predictions of the ratio of relativistic to nonrelativistic form factors seems much too large at high q^2. In the range of low q^2 ($\simeq$ 0.25 - 1.0 F^{-2}) agreement is reasonable, and his predictions for μ_d and Q_d are within 2% of the

experimental value. In work on relativistic corrections to the impulse approximation in elastic e-d scattering Gross realized that the purely dispersion technique tended to mix up the internal structure of the interacting particles, i.e., the deuteron wave function and the nucleon form factors with the deuteron current. This leads him to eventually express his theory in a formulation closer to that of potential theory.

Specifically he obtained a modified Bethe-Salpeter type wave function retaining terms up to the order of M^{-2}, and then used the relativistic nucleon current to derive the deuteron form factor. An estimate of the size of the correction to the charge form factor is obtained by taking the slope of the correction term at $q^2 = 0$. Gross found that the correction is proportional to $-1/8M^2$ which is of right sign so as to make the neutron charge form factor more positive (towards agreement with thermal n-e slope data).

The relativistic correction mentioned above came mainly from relativistic modifications of the deuteron wave functions and the nucleon current. Adler had previously looked into the nucleon current modifications but his analysis had been based on nonrelativistic deuteron wave functions. Gross states that the wave function modifications have the largest effect and hence Adler's corrections are insufficient. Van did use relativistic wave functions from a Bethe-Salpeter equation in his study of corrections to the impulse

approximation. His difficulty was in using a separable potential* which was equivalent to using a Hulthen wave function which has no hard core, and thus gives values of F_d too large. The trouble is that here relativistic corrections to e-d scattering and the model dependence question have been intermixed. Van did not avoid this by comparison of his relativistic corrections to corresponding nonrelativistic models since the two were not in the same reference frame. That is to say the relativistic model (in the Breit frame for example) when Lorentz transformed into the deuteron rest frame was not compared to a corresponding nonrelativistic model, which if it is a good model already, simulates all relativistic effects as seen in the rest frame.

The principal contribution to the correction of the charge form factor of the deuteron comes from taking into account the recoil motion of the deuteron, which in turn distorts the wave function. Lorentz contraction also adds to the wave function distortion, though not as much as in Van's case. Ignoring the correction for the quadrupole and magnetic terms, the result of Gross' calculation for the charge form factor is

$$G_C = (G_{E_p} + G_{E_n})\, D_C^R \qquad (2\text{-}134)$$

---

*Van did this in order to improve on Jones and Cutkosky's asymptotic "tail" wave function approximation $\psi_d = \frac{e^{-\alpha r}}{r}$.

where

$$D_C^R = (1 + \frac{\eta}{8}) \int_0^\infty (u^2 + w^2)\, j_o\, dr + \Delta D_C \qquad (2\text{-}135)$$

and

$$\Delta D_C = \frac{-\eta}{6} \int_0^\infty (u^2 - uru' - u\kappa u + 7w^2 - wrw' - w\kappa w)(j_0 + j_2)\, dr$$

$$+ \frac{\eta}{4} \int_0^\infty (uru' + wrw')\, j_o\, dr. \qquad (2\text{-}136)$$

In this expression prime refers to differentiation with respect to r, and

$$\kappa \equiv r^2 \left[\frac{d^2}{dr^2} - \alpha^2\right]. \qquad (2\text{-}137)$$

The arguments of the Bessel functions are of course qr/2, and q is $|q^\mu|$. Now in terms of Gross's corrections, $A(q^2)$ is

$$A(Q^2) = (G_{E_p} + G_{E_n})^2 D_C^{R2} = (G_{E_p} + G_{E_n})^2 (F_d^2 + \Delta F_d) \qquad (2\text{-}138)$$

where the quadrupole contribution to the charge form factor, $8/9\eta^2 G_Q^2$, is small. Thus, since A is an experimental quantity and does not change due to corrections, a change is forced in G_{E_n}. To see this write

$$G_C = (G_{E_p} + G_{E_n}^{NR}) D_C^{NR} = (G_{E_p} + G_{E_n}^{NR}) D_C \qquad (2\text{-}139)$$

(no corrections).

But

$$G_C = (G_{E_p} + G_{E_n}^R)D_C^R = (G_{E_p} + [G_{E_n}^{NR} + \Delta G_{E_n}])(D_C^{NR} + \Delta D_C) \quad (2\text{-}140)$$

(with relativistic corrections).

Equating the right hand sides of (2-139) and (2-140) yields

$$-\Delta G_{E_n} D_C^{NR} \simeq (G_{E_p} + G_{E_n}^{NR})\,\Delta D_C \simeq G_{E_p}\Delta D_C$$

or

$$\Delta G_{E_n} \simeq -G_{E_p}\frac{\Delta D_C}{D_C^{NR}} \simeq -G_{E_p}\frac{\Delta F_d}{F_d} \quad (2\text{-}141)$$

where F_d is the deuteron's charge structure function. Gross wrote (2-141) leaving out the F_d. Since $F_d \lesssim 1$ for very low q^2, $\Delta G_{E_n} \simeq G_{E_p}\Delta F_d$ gives an upper limit to the correction as $q^2 \to 0$ in the n-e interaction. Figure 10 summarizes the corrections. In the range of q^2 considered here, Gross' correction ΔG_{E_n} is proportional to $-\frac{q^2}{8M_p^2}$ and practically model independent.

Using this correction to the charge form factor of the neutron plus Feshbach-Lomon wave functions for the deuteron, Gross reanalyzed the $G_{E_n} \simeq 0$ data of Drickey and Hand. Figure 11 shows a comparison of results with Partovi (i.e. HJ) and Feshbach-Lomon wave functions. Gross' correction coupled with FL wave functions seems to remove the discrepancy between the electron scattering and n-e interaction results.

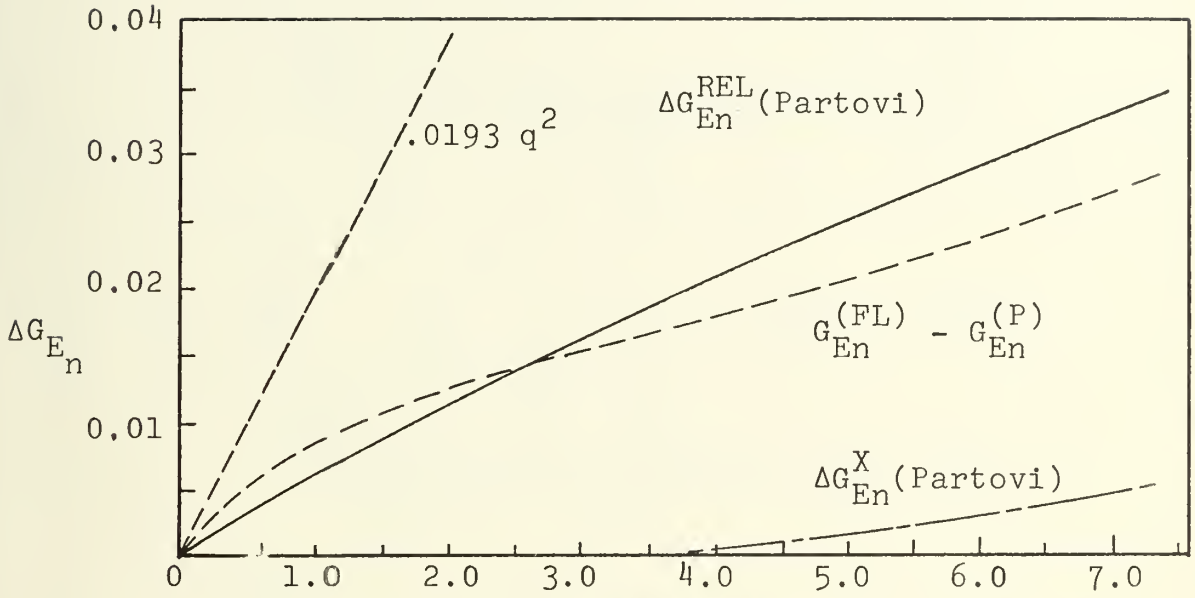

Figure 10

The relativistic correction is labeled by $\Delta G^{REL}_{E_n}$, the difference between the Feshbach-Lomon model and the Partovi model is labeled $G^{(FL)}_{E_n} - G^{(P)}_{E_n}$ and the meson exchange contributions are labeled $\Delta G^{X}_{E_n}$. The thermal neutron slope is given for reference (taken from Ref. 2).

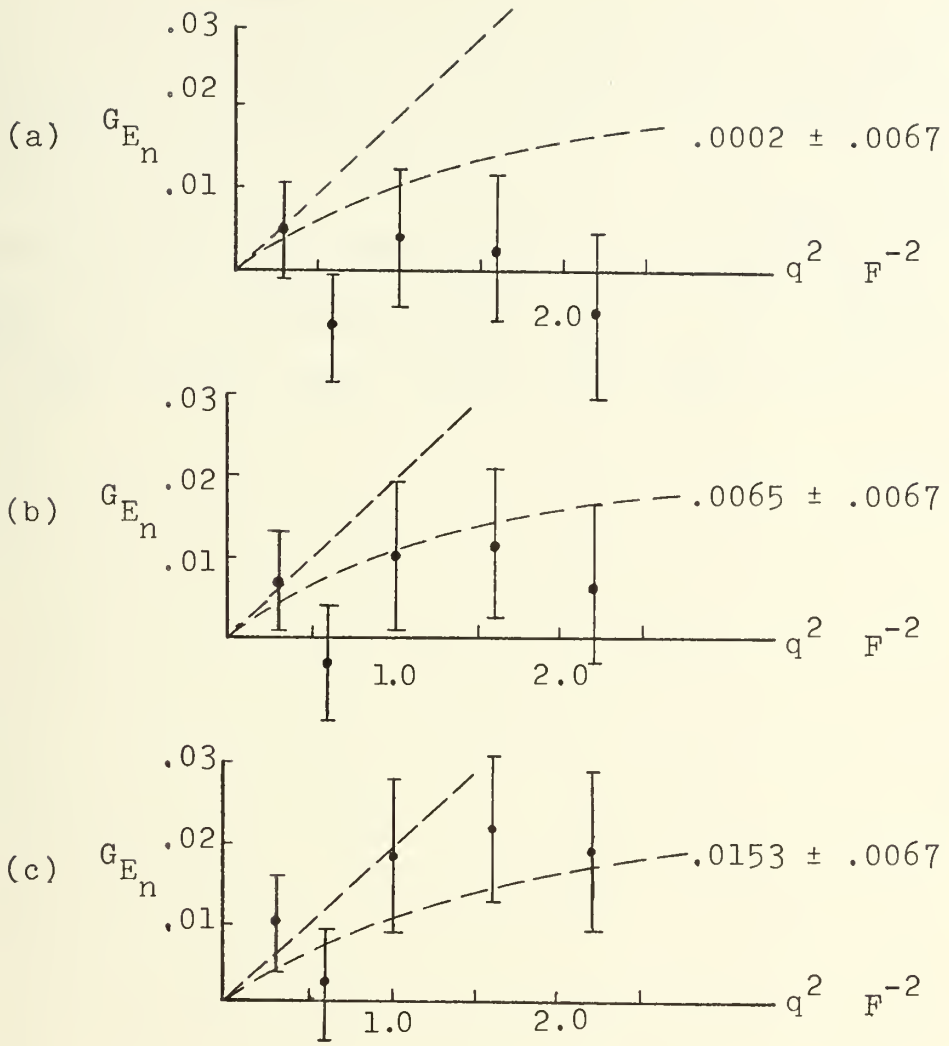

Figure 11

The data of Drickey and Hand. The dashed lines are the thermal neutron slope, +0.0193 ± 0.0004 and the fit of Chilton and Urhane (unpublished). The number on the right of each figure is the slope determined from the first three data points of each graph. (a) The data analyzed with Partovi wave function, (b) the data analyzed with Partovi wave function including relativistic corrections, and (c) the data analyzed with the Feshbach-Lomon wave function including relativistic corrections (taken from Ref. 2).

A recent attempt by Chilton and Urhane [37] to explain $G_{E_n} \simeq 0$ for $q^2 \simeq 0.3 - 1.0\ F^{-2}$ with $G'_{E_n}(0) \neq 0$, was made by fitting the nucleon form factors with rational functions of the variables $1 + q^2/m_\pi{}^2$. They found G_{E_n} is never far from zero and bends over rapidly with increasing q^2 (see Figure 10). Nevertheless with Chilton and Urhane's fit, G_{E_n} does not get back to zero till beyond $12\ F^{-2}$.

III. APPARATUS AND EXPERIMENTAL PROCEDURES

A. THE NPS LINAC

The Naval Postgraduate School linear accelerator (LINAC) is a low intensity (20 μamp maximum average current), 100 MeV, three section, 30 foot long electron linear accelerator. While its construction and general operation have been described elsewhere [38], several important modifications have been accomplished and will be mentioned briefly.

A supplementary cooling water system with a steam heat exchange was added for the accelerating sections. This was done so that the water temperature could be precisely controlled (±1°C) throughout a run lasting for an extended length of time. In the present experiment, runs of up to 38 hours were made, and since the machine's energy stability is strongly dependent on the accelerator's changes in temperature, this is a critical point.

Until recently the target chamber vacuum had been isolated from the accelerator sections by a three mil aluminum window 32 inches upstream from the target. This window caused considerable beam spread and by the time the target was illuminated by electrons, the beam spot was approximately 3/16 - 1/4 inch in diameter. Now, with the addition of a fore-diffusion vacuum pump combination in the target area, the entire accelerator, from electron gun (source) to target, is open. In fact with the spectrometer

coupled to the target chamber, electrons pass only through the target itself and a five mil aluminum exit window from the spectrometer before striking the detectors. Upstream secondary emission monitors (SEM) have been moved to locations downstream of the target. The accelerator - target chamber - spectrometer combination is maintained at a pressure of 10^{-5} mm of Hg. The removal of the SEM and window has significantly reduced the beam spot size, and it is now estimated from beam appearance on a zinc-sulfide (ZnS) screen that 2/3 of the electrons are confined to a spot 1.0 mm in diameter.

Past nuclear structure experiments [39] have experienced severe problems in background radiation levels. Major shielding modifications were made to correct this situation. More paraffin and borated paraffin in the form of a floor to ceiling wall was added to the existing shielding in the beam deflection area. In the target area, a platform loaded with paraffin four feet above the floor and extending 30 inches out from the wall was suspended from the overhead. Its purpose was to shield the counter house from line-of-sight radiation from the beam dump. Wax was placed in the spaces between the I-beams in the overhead in order to reduce reflection of neutrons into the counting system. The primary shielding effort was on the counting house itself. Concrete blocks were replaced by boxes of paraffin and much lead was replaced by special bricks composed of 5% boron, 80% lead by weight and polyethylene. A cross

section of the counter house is shown in Figure 12. This shielding arrangement reduced the background to quite an acceptable ratio of 2000 to 1.

B. THE TEN-CHANNEL COUNTING SYSTEM

1. The Ten-Channel System

In general there are two main categories of detectors: slit-defined momentum acceptance, and counter-geometry defined acceptance detectors. A single counter, slit defined detector was replaced by a ten counter geometry defined system. The ten counters, which span a portion of the focal plane of the spectrometer and define adjacent momentum intervals, are known as a "ladder." The advantages of this arrangement over the single channel system is obvious; for one spectrometer momentum setting, ten pieces of information instead of one are gathered.

The ladder is composed to ten 7/16 inch high, 1/16 inch thick NE102 plastic scintillators placed approximately 1/2 inch behind the focal plane of the spectrometer as shown in Figure 12.* A large one-piece scintillator used in coincidence with the front counters and called the backing counter, is placed 3 inches behind the 10 singles counters. The choice of 7/16 inch high (in the dispersion direction) counters produce a momentum acceptance $\Delta p/p$ of about 0.3%

---

*The ten scintillators (counters or channels) are numbered in ascending order 1 to 10, where channel 1 represents the lowest momentum accepted.

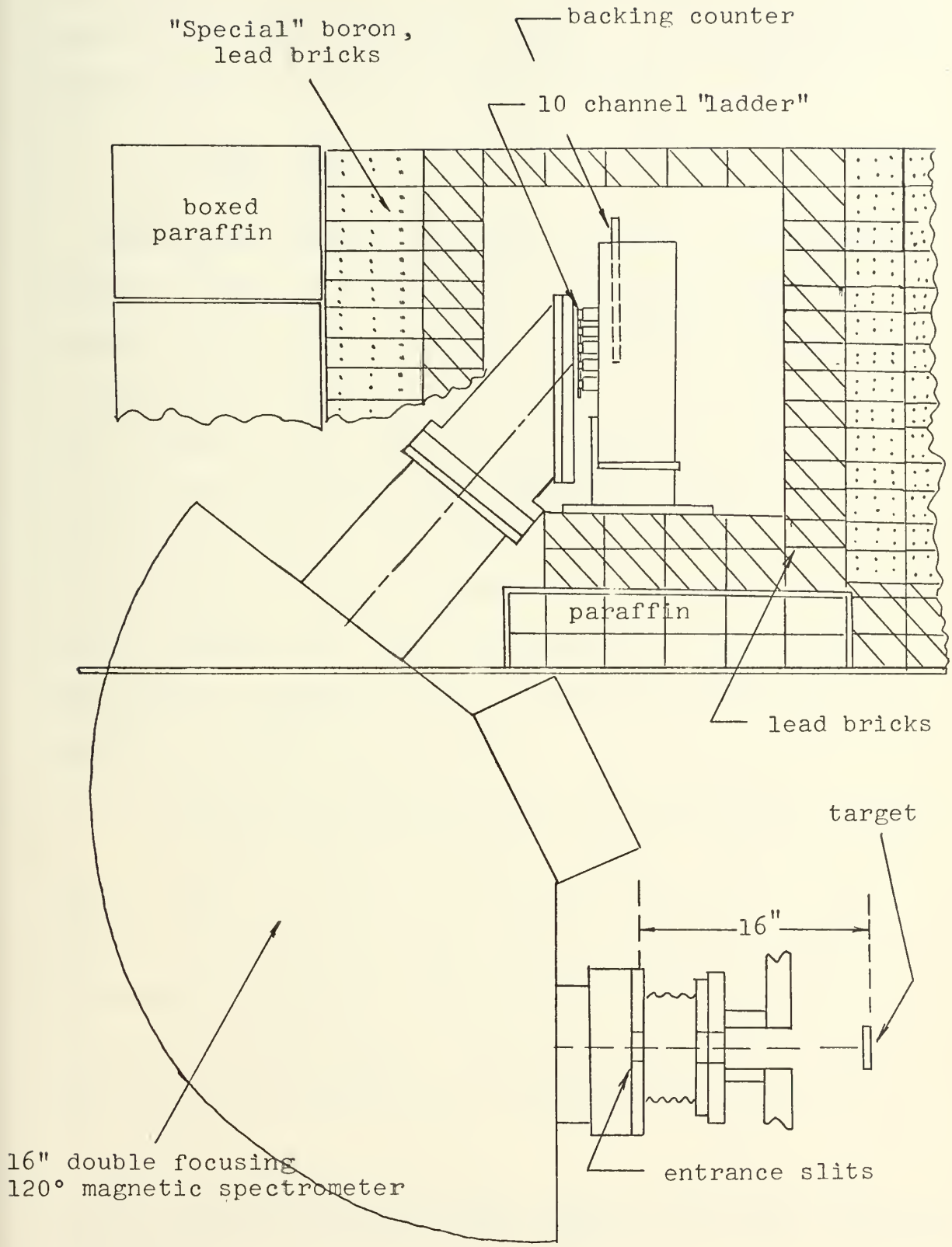
"Special" boron, lead bricks
backing counter
10 channel "ladder"
boxed paraffin
paraffin
lead bricks
target
16"
16" double focusing 120° magnetic spectrometer
entrance slits

Figure 12

per channel or about 3% for the entire ladder. An electron scattered from the target and subject to the spectrometer's magnetic field B, follows a path of radius r, given by

$$r = \frac{p}{Be} = \frac{E}{Bec} . \qquad (3\text{-}1)$$

Thus higher momentum electrons are seen by the higher numbered channels. Further the momentum resolution is greatest for the higher channels. An electron traversing the spectrometer and passing through a particular scintillator produces a pulse that is collected by an Amperex XP 1110 photomultiplier tube, amplified, transmitted, discriminated, fanned out, and finally registered on one of ten scalers. A block diagram of the counting system is shown in Figure 13.* With the exception of the scalers, which allow a counting speed of 20 MHz, the electronics is capable of 100 MHz counting rates.

2. Resolution and Efficiency of the Ten-Channel System

In order that the system be useful, two quantities must be known: The relative counting efficiency of each channel and the momentum separation of adjacent channels. The momentum separation (resolution) of the channels was obtained by taking elastic scattering peaks from a thin carbon foil and detecting the electrons scattered as a

*The Chronetics and EG and G counting equipment was loaned to NPS by the High Energy Physics Laboratory, Stanford University.

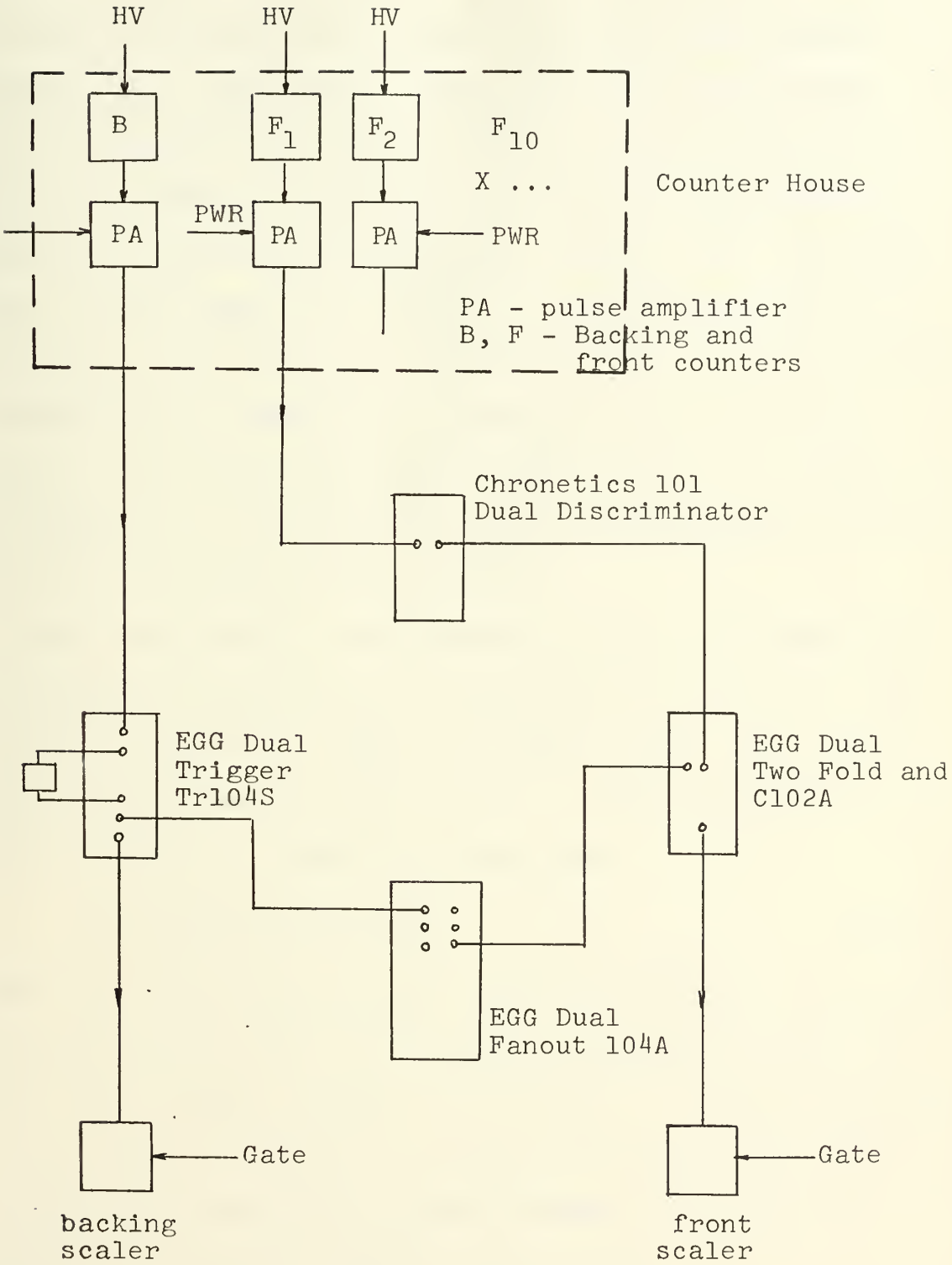
HV
HV
HV
B
F1
F2
F10
X ...
Counter House
PA
PWR
PA
PA
PWR
PA - pulse amplifier
B, F - Backing and
front counters
Chronetics 101
Dual Discriminator
EGG Dual
Trigger
Tr104S
EGG Dual
Two Fold and
C102A
EGG Dual
Fanout 104A
Gate
Gate
backing
scaler
front
scaler

Figure 13

function of spectrometer momentum in each channel. That is, the 10 counters were treated as if they were single counters while the sharp elastic peak was moved through them by changing the momentum setting of the spectrometer. A plot of counts in the scalers vs. spectrometer momentum yields 10 elastic scattering peaks (Figure 14). The separation of the peaks as a function of electron momentum p is a measure of the channel's resolution. The 10 elastic peaks produced are not identical in height or area, but since they all "see" the same elastic carbon peak, the differences are ascribed to the differing relative efficiencies in detection and recording of the electrons.

Now specifically, the resolution of the 10 channels was determmined by taking 21 - ten peak sets at incident electron momentums from 27 $\frac{MeV}{c}$ to 94 $\frac{MeV}{c}$ and with scattering angles varying between 45° and 105°. These experimental data were fit to a quadratic expression

$$p = p_s(\alpha + \beta N + \gamma N^2) \qquad (3\text{-}2)$$

where N is the channel number, p_s is the momentum setting of the spectrometer, and p is the mean momentum of channel N. A best fit produced values for α, β and γ. If p_s is defined as the momentum setting for which a particle of momentum p_s entering the spectrometer passes through the center of channel 6, then (3-2) can be rewritten as

$$\frac{}{p_N(p_s)} = p_s[1 + A(N-6) + B(N-6)^2]$$

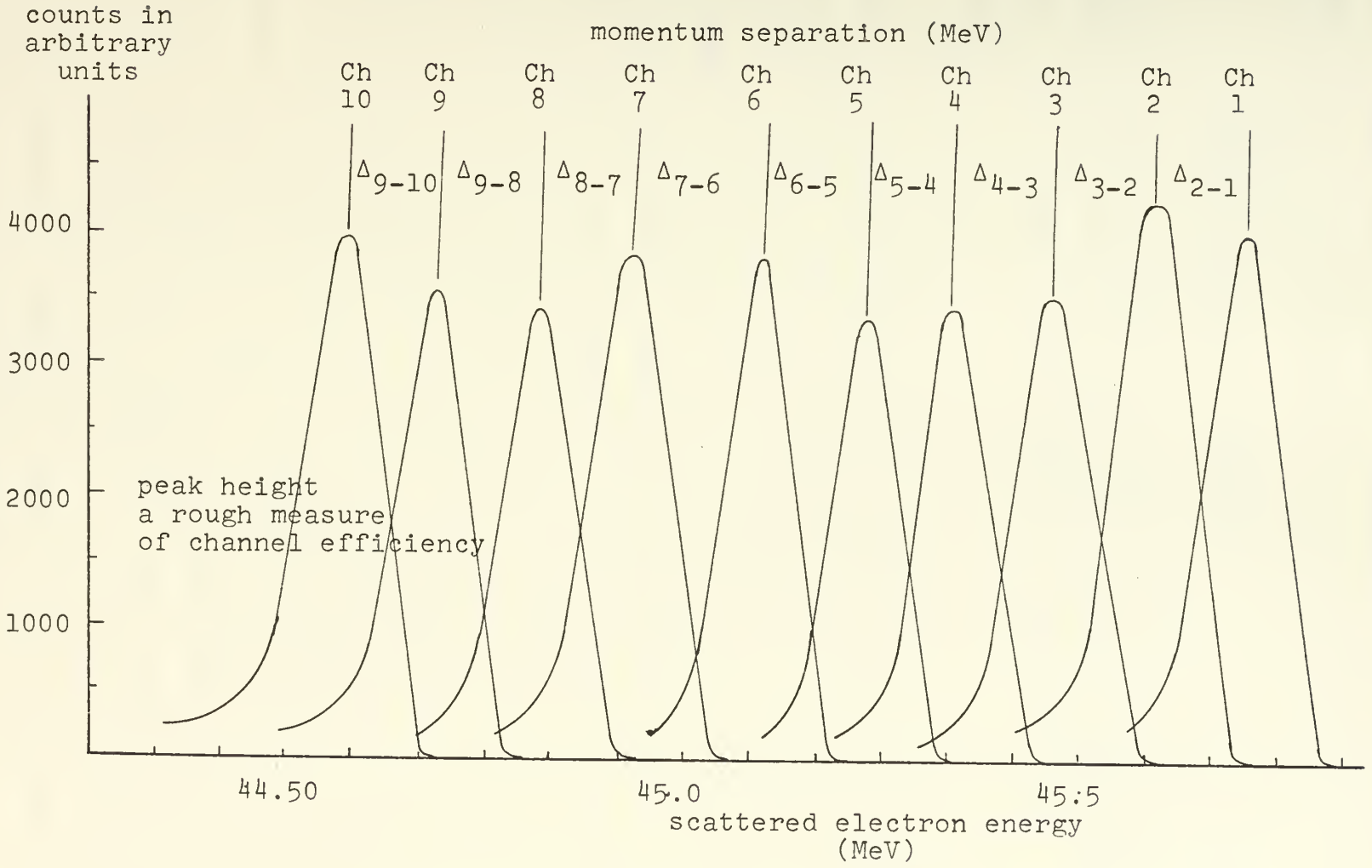
counts in arbitrary units
momentum separation (MeV)
Ch 10
Ch 9
Ch 8
Ch 7
Ch 6
Ch 5
Ch 4
Ch 3
Ch 2
Ch 1
Δ9-10
Δ9-8
Δ8-7
Δ7-6
Δ6-5
Δ5-4
Δ4-3
Δ3-2
Δ2-1
4000
3000
2000
1000
peak height
a rough measure
of channel efficiency
44.50
45.0
45.5
scattered electron energy
(MeV)

Figure 14

A and B again are constants independent of p. The channel momentum acceptance is then

$$\frac{d(\overline{p_N(p_s)})}{d(N-6)} \Big/ p_s = A + 2B(N-6). \qquad (3\text{-}4)$$

Typical values of A and B are 3.0×10^{-3} and -1.3×10^{-5} respectively and it is clearly seen that the higher channels (i.e., $N > 5$) have a higher resolution than the lower channels.

So that the energy spectrum of the scattered electrons can be determined properly the relative efficiencies need to be measured. The efficiencies can vary for several reasons, some of which are: Differences in detection thresholds and physical properties of the plastic scintillators; spectrometer transmission characteristics; and solid angle. The determination of the relative efficiencies was based on the method of Crannel and Suelzle [40], and essentially involved measuring the shape of an inelastic continuum of scattered electrons. The shape was found by observing the spectrum with all ten channels at several different momentum settings assuming initially that each channel has efficiency one. Then the counts from individual channels are compared to the calculated shape and corrected channel efficiencies are obtained. Next, a more accurate shape is predicted on the basis of the corrected efficiencies and the process is repeated. Three or four iterations will normally produce constant efficiencies.

Typically, five different momentum settings over a total momentum range of 6% (twice the 10 channel span) with at least 1000 counts per channel per setting were taken. It is important that the efficiency data be taken in the energy range in which the experiment is to be performed. Hence if an elastic deuteron peak is located at 50 MeV, then the machine energy should be adjusted so that a smooth part of some inelastic continuum lies at that point. In carbon 12, the radiation tail of the elastic peak is sufficiently smooth at 30 MeV below the peak, thus for the above situation a machine energy of 80 MeV would be set, and the five momentum (energy) settings could be taken at 52, 51, 50, 49, and 48 MeV for example. Carbon is obviously not suited for the NPS machine because then a practical limit of 65 MeV would be imposed on the incident energy for the proton and deuteron peaks (i.e., 65 + 30 MeV = 95 MeV needed for efficiency and any more would exceed machine capability). Aluminum was substituted; its inelastic tail contains peaks only at 2.2 and 3.0 MeV. Arbitrarily a value of 6 MeV down from the aluminum-elastic peak was chosen as the experimental area from which to obtain the relative counting efficiencies. Normally it is best to exactly duplicate in the efficiency measurement the conditions of the particular experiment, but this was found to be impossible in some cases. On the high energy runs, 94 MeV (location of elastic peaks under consideration), 94 + 6 = 100 MeV was an impractical energy to obtain and maintain. Thus the

efficiency data were taken at a somewhat lower energy. Also aluminum not CH_2 or CD_2 was always used for efficiencies since it was desirable not to take the risk of burning or destroying the experimental targets during the long high beam strength used in efficiency runs.

To calculate the relative efficiency of channel k it is necessary to predict the total number of counts channel k receives in the L spectrometer momentum settings. Thus

$$\sum_{s=1}^{L} C_k(p_s) = \sum_{s=1}^{L} \int_{p_\ell(k,p_s)}^{p_h(k,p_s)} E_k(p,p_s)T(p_s)dp \qquad (3\text{-}5)$$

where p is the particle momentum, $T(p_s)dp$ is the number of electrons with momentum between p and p + dp which enter the spectrometer, $E_k(p,p_s)$ is the efficiency of channel k for particles of momentum p, and $p_h(k,p_s)$ and $p_\ell(k,p_s)$ the highest and lowest momentum accepted by channel k. Assume that

$$T(p_s) = \sum_{n=0}^{2} R_n p_s^{n+1} \qquad (3\text{-}6)$$

where R_n can be determined (needs to be done only once) by a least squares fit to the points $T_c(p_s) = \sum_{k=1}^{10} C_k(p_s)$ as a function of p_s. Hence the efficiency of channel k is given by the ratio

$$E_k = \left[\sum_{s=1}^{L} C_k(p_s) \Big/ \sum_{s=1}^{L} \sum_{n=0}^{2} R_n p_s^{n+1} \right] \qquad (3\text{-}7)$$

which is the total number of counts observed vs. the predicted total number of counts.

C. THE TARGETS

Solid polyethylene $(CH_2)_n$ and deuterized polyethylene $(CD_2)_n$ were chosen as the sources of protons and deuterons. The immediate difficulty is that these plastic targets would be destroyed by heat (melted) in the concentrated electron beam. Hence the CH_2 and CD_2 targets were made to move in the horizontal direction so that the beam sampled a width of about one inch over the target face. The carbon in CH_2 and CD_2 has much greater atomic weight (12 umu) than does either isotope of hydrogen (H = 1.00783 umu and D = 2.01410 umu) and hence suffers much less recoil when struck by an electron. Thus both the elastic proton and deuteron peaks ride well down on the inelastic tail of their respective carbon peaks. In order to isolate the proton and deuteron peaks it is necessary to subtract out the carbon content. A carbon target is needed then for standardization. Hence arrayed down the target ladder were movable CD_2 and CH_2 targets, a stationary carbon standardization target, aluminum target for efficiencies and a ZnS screen for machine tuning and beam observation.

The CD_2 target was 3 cm x 10 cm x 0.10122 cm and specified to be 99.9% enriched. The thickness of the CH_2 and C targets were governed by the desire to make the number of C atoms in each of the three targets as nearly the same

as possible. With the material available a CH_2 target 0.10434 ± 0.00070 cm thick and a 0.09398 ± 0.00061 cm thick carbon target were constructed. The carbon target was produced by laminating 7 thin (5 mils) graphite foils. The densities of the samples were determined to be: $\rho(CD_2)$ = 1.081 ± .006 gm cm^{-3}, $\rho(CH_2)$ = 0.925 ± 0.005 gm cm^{-3}, and $\rho(C)$ = 1.028 ± 0.005 gm cm^{-3}.

In the course of a run the electron beam illuminated the CH_2 and CD_2 targets for as long as 8 hours apiece. After these long runs considerable browning of the material was evident, and the possibility of damage to the target because of a change in the composition of the material was considered. Subsequent runs on the undarkened area versus the darkened area gave no indication of any decomposition. Further the darkened areas tended to fade in time so no permanent damage could be supposed. The browning of the target is assumed to be an atomic electron dislocation phenomena.

D. COLLECTION OF DATA

After deciding upon the momentum transfer to investigate, the appropriate incident energy-scattering angle combination was chosen. The basic measurement desired was the ratio of the electron-proton to the electron-deutron scattering cross section. Forward scattering angles were chosen where possible in order to emphasize the electric interaction. With this angular restriction the momentum transfers ranged

for the proton and deuteron from about $0.1 \leq q^2 \leq 0.5\ F^{-2}$ for the available machine energies.

The machine was tuned for maximum beam and current stability. The energy defining slits were set for $\Delta E/E \simeq 0.5\%$, and the beam spot was carefully steered to the target center line. Collection of raw data consists of recording the number of counts shown in scalers 1 through 10, the backing scaler counts, the time elapsed while counting, the spectrometer setting in MeV, and the number of electrons passing through the target. All the scaler data are fed directly to a teletype machine that both punches an 8 track paper tape, and prints out a hard copy. The paper tape is then interpreted and IBM cards produced for use in computer data analysis.

For this experiment data were taken in the following way. The machine was tuned to an energy approximately 6 MeV higher than the energy at which the elastic proton peak would occur. Efficiency data using a 20 mil aluminum target were taken. The machine energy was then lowered to the value selected for the proton run. Comparison elastic carbon peaks in CH_2 and C were taken to provide normalization data used in scaling the carbon for subtraction. Then the elastic proton peak from CH_2 and the underlying carbon tail for subtraction were obtained. Machine energy was again lowered to the proper value and the deuteron runs were completed in a manner similar to that for the proton. On all peaks the counting rates in the front channels were

limited to 75 counts per second, while the backing channel was limited to 100 counts per sec. Tests showed that the counting system (presumably the scalers themselves, not the counting electronics) could digest counting rates of up to 200 counts per second before any appreciable loss was detected. Since the deuteron is twice as heavy as the proton, less incident energy is required to achieve the same momentum transfer as that of the proton. In all experiments a peak was determined by three spectrometer settings, hence 30 points define a scattering peak. The small energy steps taken depended on the machine energy and the relative energy (momentum) separation of the various channels. The aim was to achieve a uniform distribution of points over the area investigated.

Where the peak is located on the ladder is important. The end channels, 1, 2, 9, and 10 tend to have more widely varying efficiencies than the center channels and they experience edge effects, so they are unsuitable for the peak determination. It was found that placing the peak initially between channels 6 and 7 gave the best results. Then the top of the peak was defined by a single counter reducing a potential problem of matching the counts of different channels at a critical point. The peak height was chosen on the basis of time versus statistical accuracy. That is, a total of 4×10^4 counts are needed under a peak to insure 0.5% counting statistics, but the time needed to accumulate that many counts is often prohibitive,

particularly at the higher values of q^2. It was decided that no more than three hours per spectrometer setting would be allotted for counting.

In order to extend the range of momentum transfers, another set of data was taken by the author at the Mark III accelerator at Stanford University. Where possible, overlapping sets of data were taken to check for any systematic errors in the equipment. The range covered at Stanford was $0.20 \leq q^2 \leq 0.80\ F^{-2}$. No systematic deviations between the two sets of measurements were found and the data reduction was performed independent of the source.

The experimental equipment at Stanford is basically the same as that at the Naval Postgraduate School with the exception that a 100 channel ladder is used and that part of the data reduction is performed on an IBM 7700 on-line computer.

IV. DATA REDUCTION

A. ANALYSIS OF RAW DATA

Raw data are accumulated in the form of counts in ten channels for a single spectrometer setting, and are analyzed or "unfolded" by matching the counts in a particular channel to the appropriate energy. The assignment of energy values to channels is determined by (3-3). The raw counts are first corrected for background, then counting rate corrections are applied. Finally the efficiency determined by (3-7) is used to predict a corrected count for the particular channel. In practice all the above calculations are carried out by computer. Typical unfolded energy spectra for both proton and deuteron runs are shown in Figures 15, 16, 17, and 18.

B. CALCULATION OF EXPERIMENTAL CROSS SECTIONS AND FORM FACTORS

The experimental cross sections for e-p and e-d scattering were determined from

$$\sigma_{Exp}^{p,d} = \frac{N_{sc}}{N_{in}\, n_t\, \Delta\Omega} K_s K_b \text{ cm}^2 \text{ ster}^{-1} \qquad (4\text{-}1)$$

where N_{sc} is the number of scattered electrons detected by the spectrometer, N_{in} is the number of incident electrons, n_t is the number of target atoms per cm^2, $\Delta\Omega$ is the solid angle subtended by the spectrometer entrance port, and

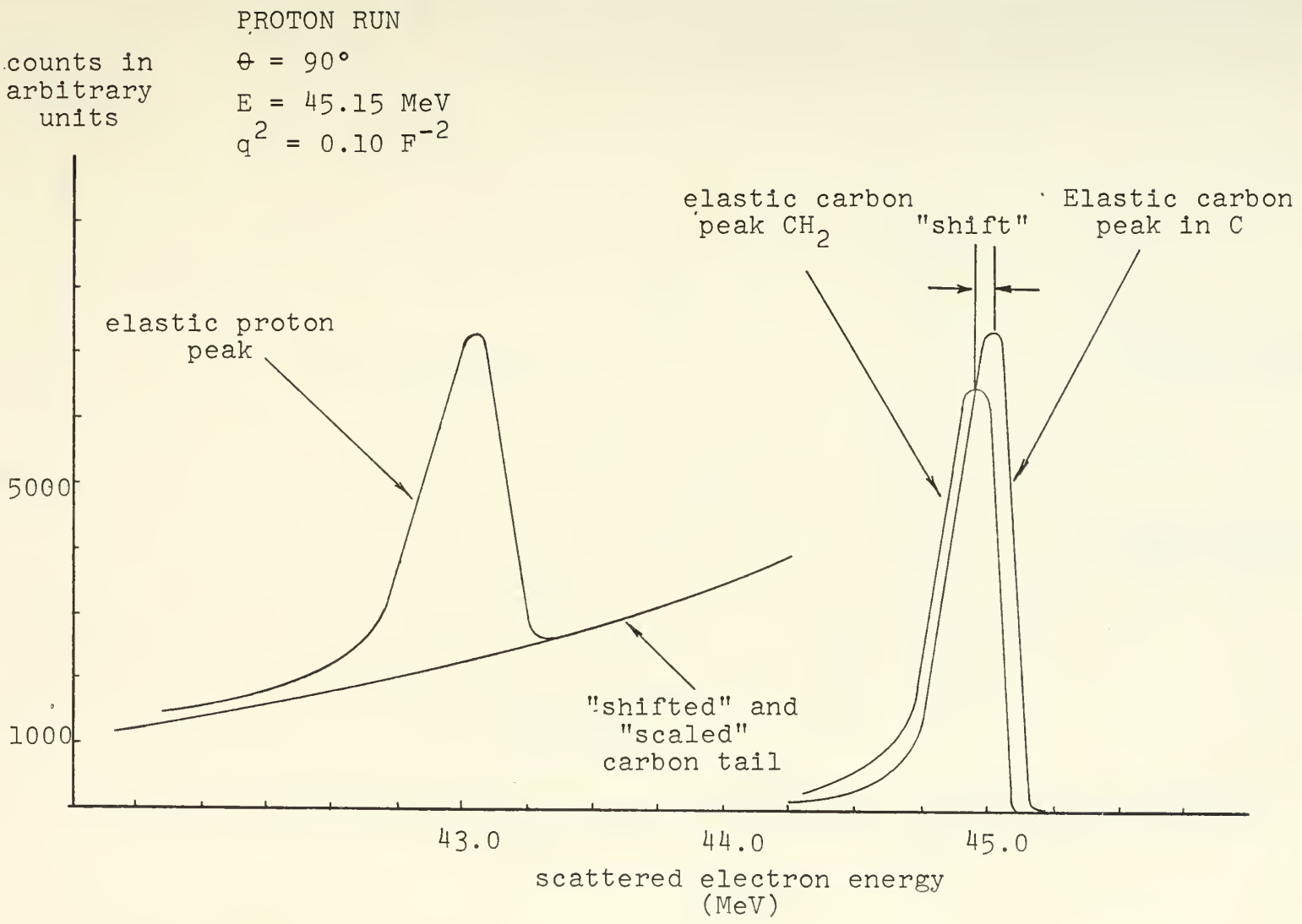
PROTON RUN
θ = 90°
E = 45.15 MeV
q² = 0.10 F⁻²
counts in arbitrary units
elastic carbon peak CH2
"shift"
Elastic carbon peak in C
elastic proton peak
5000
1000
"shifted" and "scaled" carbon tail
43.0
44.0
45.0
scattered electron energy (MeV)

Figure 15

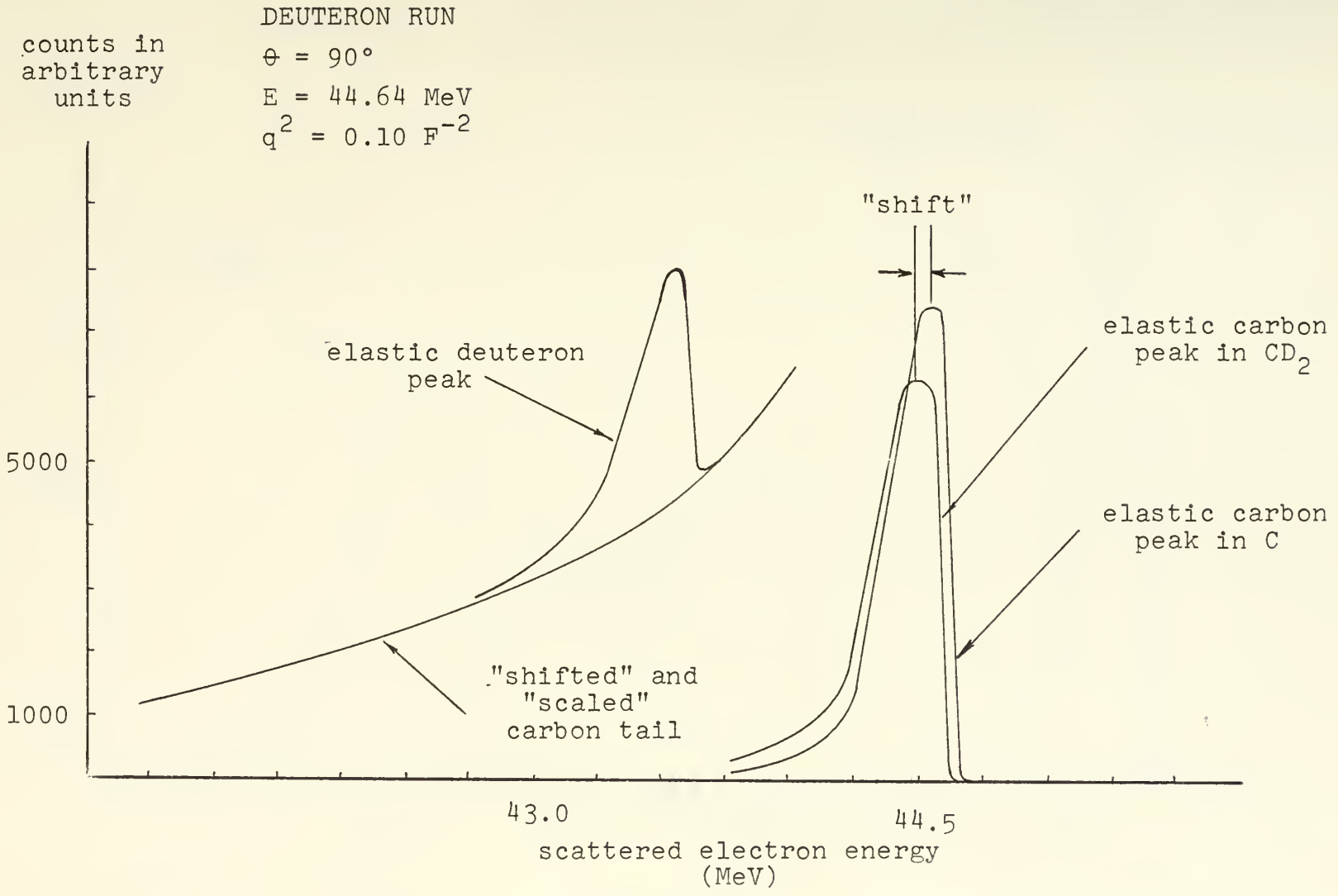
DEUTERON RUN
θ = 90°
E = 44.64 MeV
q² = 0.10 F⁻²
counts in arbitrary units
5000
1000
"shift"
elastic deuteron peak
elastic carbon peak in CD₂
elastic carbon peak in C
"shifted" and "scaled" carbon tail
43.0
44.5
scattered electron energy (MeV)

Figure 16

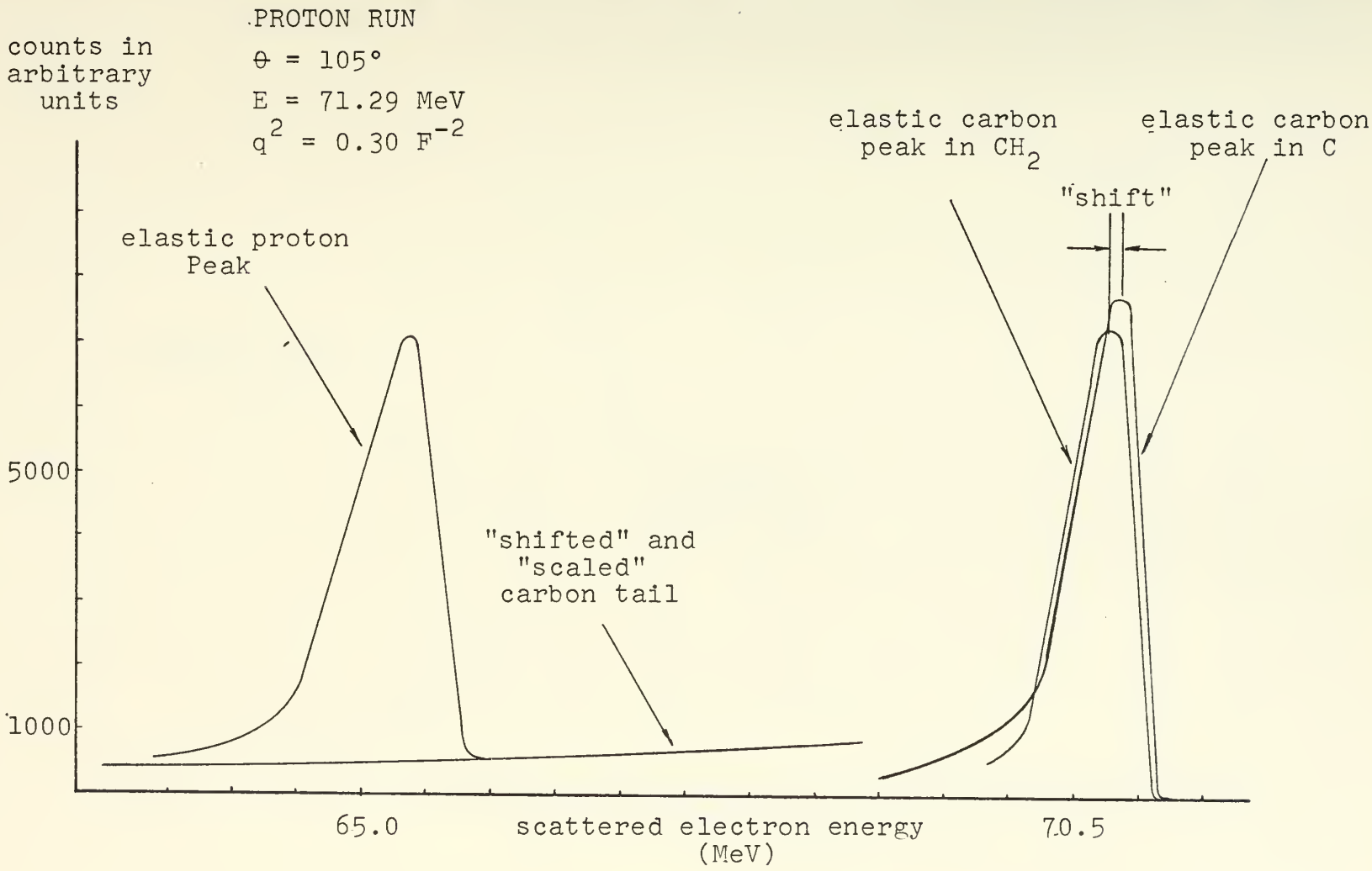
PROTON RUN
θ = 105°
E = 71.29 MeV
q² = 0.30 F⁻²
counts in arbitrary units
elastic carbon peak in CH2
elastic carbon peak in C
"shift"
elastic proton Peak
"shifted" and "scaled" carbon tail
5000
1000
65.0
scattered electron energy (MeV)
70.5

Figure 17

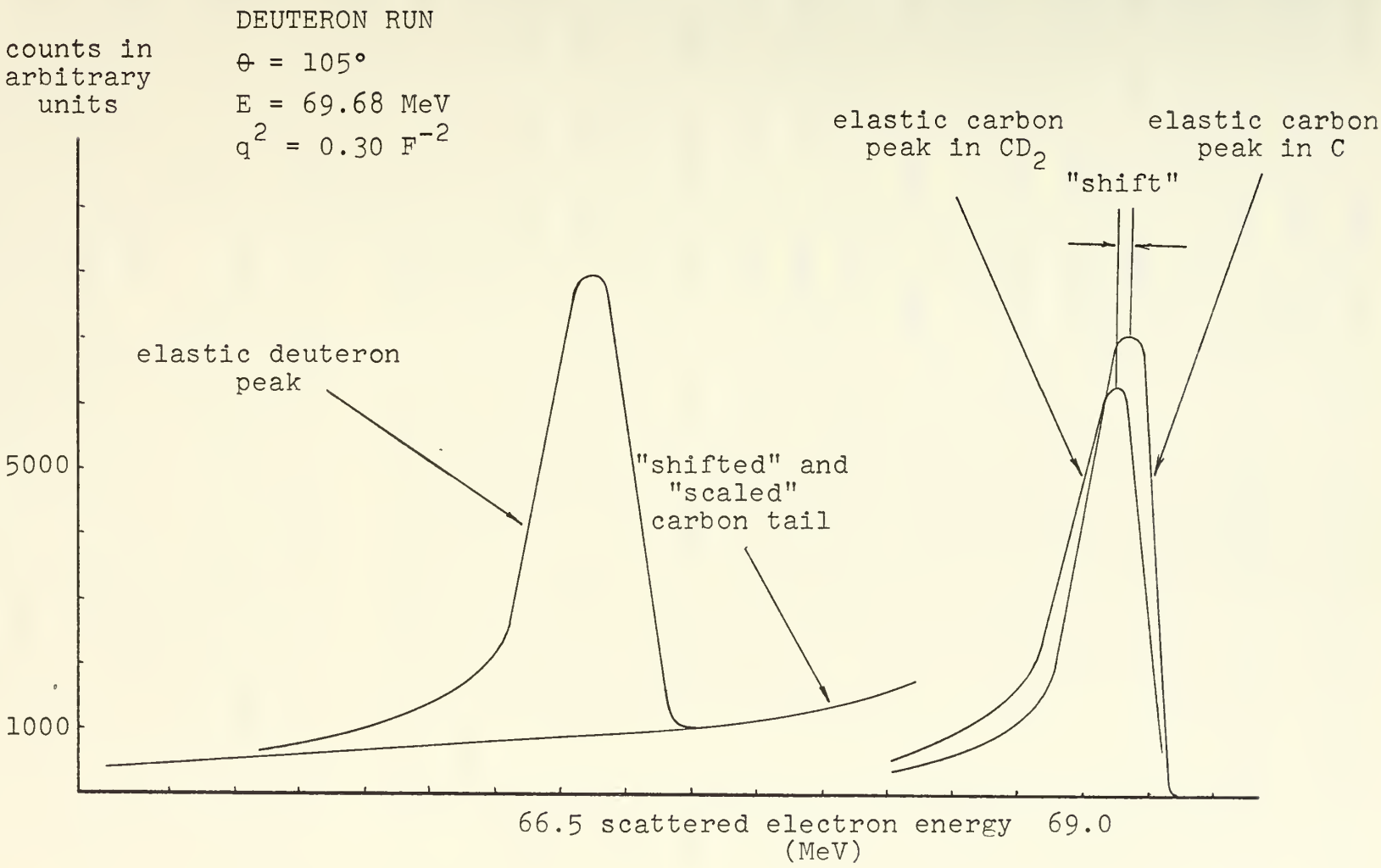
DEUTERON RUN
θ = 105°
E = 69.68 MeV
q² = 0.30 F⁻²
counts in arbitrary units
5000
1000
elastic deuteron peak
"shifted" and "scaled" carbon tail
elastic carbon peak in CD₂
"shift"
elastic carbon peak in C
66.5
scattered electron energy
69.0
(MeV)

Figure 18

finally K_s and K_b are the radiative corrections of Tsai [41] and Bethe-Ashkin [42].

At the heart of the calculation of (4-1) is N_{sc} which is the integrated area under the scattering peak in counts-MeV per MeV. The scattering peak is produced by drawing a smooth curve through the data points in the counts vs. energy plot.

Both the elastic proton and deuteron peaks ride on the radiation tail of the elastic carbon peak (see Figure 15, etc.). Thus, in order to obtain the relevant areas for the cross section, the underlying carbon tail must be subtracted out. Comparison of the elastic carbon peaks in CH_2 and CD_2 to that of the pure carbon target provided the target normalization factors. These factors consisted of (1) "shifts" of the elastic carbon peak from the carbon target such that its peak energy coincided with that of the carbon peak from CH_2 or CD_2; and (2) vertical "scaling" of the carbon tail through a comparison of the areas of the elastic carbon peaks. The area remaining after the subtraction is N_{sc}.

The number of electrons incident upon the target is measured by a Secondary Emission Monitor (SEM) downstream from the target. The SEM is not an absolute device to measure the charge. In a ratio experiment, the only requirement is that it be stable during a set of runs. This stability has been frequently checked against a Faraday cup. Obviously the number measured is wrong by at

least the number of electrons scattered by the target, but this is so small compared to N_{in} as to be totally insignificant. n_t is a static parameter; it depends only on target composition and target angle ϕ,

$$n_t = \frac{\rho t \, N_a}{A \cos \phi} \tag{4-2}$$

where ρ is the target density in gm cm^{-3}, t thickness in cm, N_a Avogadro's number, A the atomic weight, and ϕ the angle between the beam line and the downstream target normal. The solid angle $\Delta\Omega$ is defined by 1 inch thick tungsten slits on the spectrometer entrance port, 16 inches from target center.

It can be seen by comparison of two experimental cross sections that the only remaining quantities that enter a ratio experiment are N_{sc} and n_t.

As mentioned above, we have used an expression due to Tsai to account for the radiative correction K_s. This correction is a significant improvement over that given by Schwinger [43]. Presented here is Schwinger's much simpler expression (4-3) as an illustration of the parameters entering the correction.

$$K_s = e^{\delta_s}, \quad \delta_s = \frac{2\alpha}{\pi}\left\{\left[\ln\frac{E}{\Delta E\,\xi^{3/2}} - \frac{13}{12}\right]\left[\ln\frac{2EM_c^2}{(mc^2)^2}\left(1 - \frac{1}{\xi}\right)\right] + \frac{17}{36}\right\} \tag{4-3}$$

The Bethe-Ashkin correction is given by

$$K_b = e^{\delta_b}, \quad \delta_b = \frac{\rho t}{X_o \cos\phi \ln 2} \ln\frac{E}{\Delta E\,\xi^{3/2}} \tag{4-4}$$

Briefly, K_s is a multiplicative correction to the cross section which accounts for radiation emitted during a large-angle scattering event (nuclear bremsstrahlung). K_b corrects for the radiation that occurs before or after the large-angle event and is sometimes known as thick target bremsstrahlung. For a discussion of the terms in (4-3) and (4-4) see Gordon [44]. The ξ used above corresponds to the nucleon recoil factor in (2-77).

The ratio of the experimental cross section to the cross section predicted for a point nucleon (Mott cross section) Equation (2-76), yields the experimental form factors G_p^2 or G_d^2. To these quantities, the magnetic corrections as outlined by equations (2-122) and (2-126) are then applied.

This yields the square of the electric form factor of the proton, $G_{E_p}^2$, and the sum of the squares of the electric and quadrupole form factors of the deuteron, $G_{E_d}^2 + \frac{8}{9}\eta^2 G_{Q_d}^2$. Because of the smallness of η in our range of momentum transfers ($\eta_{max} = 2.2 \times 10^{-3}$ at $q^2 = 0.80\ F^{-2}$) the quadrupole term contributes only about one part in 10^{-4} to the form factor and can be safely neglected.

The end result of the experiment is then the ratio $G_{E_d}^2 / G_{E_p}^2$ from which the ratio G_{E_n} / G_{E_p} is extracted with the help of equation (2-128).

In summary, the quantity evaluated from the data is

$$\frac{G_{E_d}^2}{G_{E_p}^2} = \frac{N_{sc}^d \times n_t^p \times C^d \times \sigma_{Mott}^p \times K_s^d \times K_b^d}{N_{sc}^p \times n_t^d \times C^p \times \sigma_{Mott}^d \times K_s^p \times K_b^p} \qquad (4\text{-}5)$$

where C represents the magnetic correction, σ_{Mott} the Mott cross section, and the indices p,d refer to proton or deuteron, respectively.

C. EXPERIMENTAL ERRORS

Errors encountered in the measurements are of both statistical and systematic nature. Systematic errors, such as the value of the solid angle, counting rate correction, target angle, scattering angle, and SEM efficiency cancelled out since they were measured under the same experimental conditions. The absolute error in the energy of the incoming electrons is about 0.2%. Since the Mott cross section for the deuteron and the proton are evaluated at nearly the same energy, this error becomes insignificant. The same is true for the errors in the radiative corrections if they are evaluated over roughly the same energy cut off ΔE (Equation 4-3).

The only significant error of a systematic nature is the error in the target thickness and density, ρt. Because of the thinness of the targets, it could be established to only 0.5%.

The statistical error consists of two parts, the actual counting error and the error in the efficiency correction. It is in principle possible to keep these errors arbitrarily small by taking a very high number of counts. Restrictions in counting speed as posed by the electronic equipment and time limitation in the use of the accelerator pose a

practical limit. All but two peaks contain 40,000 counts, which would make their statistical error to be 0.5%. The required carbon subtraction introduces an additional error, depending on the number of carbon counts under the peak area.

The error in the efficiency corrections is quite iniformly 0.5% for the Naval Postgraduate School runs, where roughly the same number of counts have been taken to establish the relative efficiencies. In the Stanford runs the error varies from 0.27% to 0.65%.

For each measurement of $G^2_{E_d}/G^2_{E_p}$, the error is then the square root of the quadratic sum of the counting, efficiency, and target error.

One half of this percentage error enters the ratio G_{E_d}/G_{E_p} and, therefore, the calculation of G_{E_n}/G_{E_p}. This is the error quoted in Table VII.

V. COMPARISON TO THEORY AND DISCUSSION

A. EXPERIMENTAL RESULTS

The experimental data are presented in Table VI. The error quoted consists of counting errors (including the carbon subtractions and efficiency corrections) and an error of 0.5% in the target thickness.

Table VII shows four sets of values of G_{E_n}/G_{E_p} as obtained by: (a) the Feshbach-Lomon wave function with relativistic corrections; (b) the Feshbach-Lomon wave function without relativistic corrections; (c) the Partovi wave function with relativistic corrections, and; (d) the Partovi wave function without relativistic corrections. Values for the relativistic correction ΔG_{E_n} and, as an example, the structure factor F_d for the Feshbach-Lomon wave function are also given. In each of the columns are shown the slopes $(dG_{E_n}/G_{E_p})/dq^2$ to illustrate the rapid decrease in slope when going from a relativistically corrected Feshbach-Lomon wave function to an uncorrected Partovi wave function.

The b' fit of de Vries [28] for the absolute proton charge form factor was used to extract G_{E_n} from the G_{E_n}/G_{E_p} ratio. This fit is in very good agreement with the absolute measurements of G_{E_p} by Drickey and Hand [1]. Table VIII shows the results of the b' fit for the two extreme cases presented in Table VII. The slopes as determined by the

the two sets of data are also given for comparison with the neutron-electron interaction slope.

B. DISCUSSION

The Figures 19 and 20 illustrate the results tabulated in Tables VII and VIII respectively. It can be seen from the slope of Figure 20 that the Partovi wave function without relativistic corrections does not significantly differ from the data of Drickey and Hand pictured in Figure 10(a). That is, they both essentially agree that the slope is very small or zero. On the other hand the slope for the Feshbach-Lomon wave function with relativistic corrections approaches closely the value of the slope for the neutron-electron interaction.

Barring unexpected fluctuations in the proton form factor G_{E_p} in the range of momentum transfers of interest here it can be concluded that:

(a) The Feshbach-Lomon wave function together with the relativistic corrections ΔG_{E_n}, removes the apparent discrepancy between the neutron-electron slope at $q^2 \simeq 0$ and the slope given from values of G_{E_n} (obtained by electron scattering) in the range $0.10 \leq q^2 \leq 0.80\ F^{-2}$.

(b) Even within the relatively large errors propagated into G_{E_n}, the Partovi wave function with relativistic corrections applied, is in disagreement with the neutron-electron interaction slope.

(c) With the present small experimental uncertainties, it is reasonable to state that this experiment should be added to the group of experiments which must be explained by any deuteron theory. That is, a proper model for the deuteron must be found that will predict the slope as determined by the neutron-electron scattering experiments.

The important qualitative conclusion from these experimental results is that the neutron has a non-zero charge form factor. This implies that there is a charge distribution within the neutron. The neutron thus must have a layered charge structure with the outermost part of the charge distribution being negative in sign.

TABLE VI

MEASURED RATIO OF G_{E_d}/G_{E_p}

q^2 (F^{-2})	θ	E_{i_p} (MeV)	E_{i_d} (MeV)	Magnetic Correction[a] proton	Magnetic Correction[a] deuteron	G_{E_d}/G_{E_p}	Percent error	Weighted Average G_{E_d}/G_{E_p}	
	75°	52.30	51.77	0.9828	0.9988	0.9499	1.14		
0.10	90°	45.15	44.64	0.9760	0.9984	0.9459	0.86	0.9374	0.0052
	45°	82.58	82.04	0.9897	0.9993	0.9200	0.91		
	75°	74.59	73.52	0.9661	0.9976	0.8734	0.71		
	120°	53.06	51.99	0.8948	0.9925	0.9030	0.59		
	45°	117.40	116.30	0.9796	0.9985	0.8931	1.54		
0.20	45°	117.40	116.30	0.9796	0.9985	0.9284	1.06	0.8903	0.0028
	45°	117.40	116.30	0.9796	0.9986	0.9144	1.06		
	45°	117.40	116.30	0.9796	0.9985	0.8677	0.81		
	45°	117.40	116.30	0.9796	0.9985	0.8737	0.81		
	45°	144.30	142.80	0.9697	0.9978	0.8275	0.79		
	75°	91.93	90.33	0.9500	0.9965	0.8317	0.99		
0.30	90°	79.59	77.99	0.9313	0.9951	0.8462	0.61	0.8392	0.0030
	105°	71.29	69.68	0.9014	0.9929	0.8424	0.64		
	90°	92.48	90.34	0.9106	0.9935	0.7984	0.62		
	45°	167.20	165.10	0.9601	0.9971	0.8153	0.88		
0.40	45°	167.20	165.10	0.9601	0.9971	0.7945	0.89	0.8041	0.0031
	45°	167.20	165.10	0.9601	0.9971	0.8114	0.75		
0.50	60°	144.80	142.10	0.9383	0.9955	0.7626	0.79	0.7626	0.0060
0.60	60°	159.20	156.00	0.9270	0.9946	0.7260	0.71	0.7260	0.0052
0.80	75°	153.50	149.20	0.8772	0.9906	0.6707	0.97		
	75°	153.50	149.20	0.8772	0.9906	0.6773	0.85	0.6744	0.0043

a: The magnetic correction gives the number by which the experimental G_p^2 or G_d^2 is to be multiplied to remove the magnetic contributions and yield $G_{E_p}^2$ or $G_{E_d}^2$.

TABLE VII

VALUES FOR G_{E_n}/G_{E_p}

q^2 (F^{-2})	ΔG_{E_n}	F_d^{FL}	$\left(\frac{G_{E_n}}{G_{E_p}}\right)^{FL} + \Delta G_{E_n}$	$\left(\frac{G_{E_n}}{G_{E_p}}\right)^{FL}$ no ΔG_{E_n}	$\left(\frac{G_{E_n}}{G_{E_p}}\right)^{P} + \Delta G_{E_n}$	$\left(\frac{G_{E_n}}{G_{E_p}}\right)^{P}$ no ΔG_{E_n}
0.10	0.0006	0.9398	-0.0020 ± 0.0055	-0.0026 ± 0.0055	-0.0034 ± 0.0055	-0.0040 ± 0.0055
0.20	0.0012	0.8867	+0.0052 ± 0.0032	+0.0040 ± 0.0032	+0.0030 ± 0.0032	+0.0018 ± 0.0032
0.30	0.0018	0.8397	+0.0012 ± 0.0038	-0.0006 ± 0.0036	-0.0020 ± 0.0036	-0.0038 ± 0.0036
0.40	0.0024	0.7976	+0.0103 ± 0.0038	+0.0081 ± 0.0038	+0.0062 ± 0.0038	+0.0038 ± 0.0038
0.50	0.0030	0.7596	+0.0069 ± 0.0079	+0.0039 ± 0.0079	+0.0014 ± 0.0079	-0.0016 ± 0.0079
0.60	0.0036	0.7251	+0.0048 ± 0.0071	+0.0012 ± 0.0071	-0.0009 ± 0.0071	-0.0045 ± 0.0071
0.80	0.0048	0.6645	+0.0197 ± 0.0055	+0.0149 ± 0.0065	+0.0134 ± 0.0065	+0.0083 ± 0.0065
		Slope:	0.0185 ± 0.0038	0.0125 ± 0.0038	0.0087 ± 0.0040	0.0027 ± 0.0040

TABLE VIII

SLOPE OF THE CHARGE FORM FACTOR

dG_{E_n}/dq^2

q^2 (F^{-2})	G_{E_p} [a] de Vries b' fit	$G_{E_n}^{FL}$	$G_{E_n}^{FL}+\Delta G_{E_n}$	$G_{E_n}^{P}$
0.10	0.9881	-0.0027	-0.0020 ± 0.0054	-0.0038 ± 0.0054
0.20	0.9765	+0.0039	+0.0051 ± 0.0031	+0.0017 ± 0.0031
0.30	0.9652	-0.0006	+0.0012 ± 0.0035	-0.0037 ± 0.0035
0.40	0.9540	+0.0077	+0.0103 ± 0.0036	+0.0036 ± 0.0036
0.50	0.9431	+0.0037	+0.0067 ± 0.0074	-0.0015 ± 0.0074
0.60	0.9321	+0.0011	+0.0047 ± 0.0066	-0.0042 ± 0.0066
0.80	0.9115	+0.0138	+0.0184 ± 0.0059	+0.0076 ± 0.0059
		Slope:	0.0179 ± 0.0036	0.0026 ± 0.0036

Slope of n-e interaction = 0.0193 ± 0.0004

a: No error has been applied to G_{E_p}.

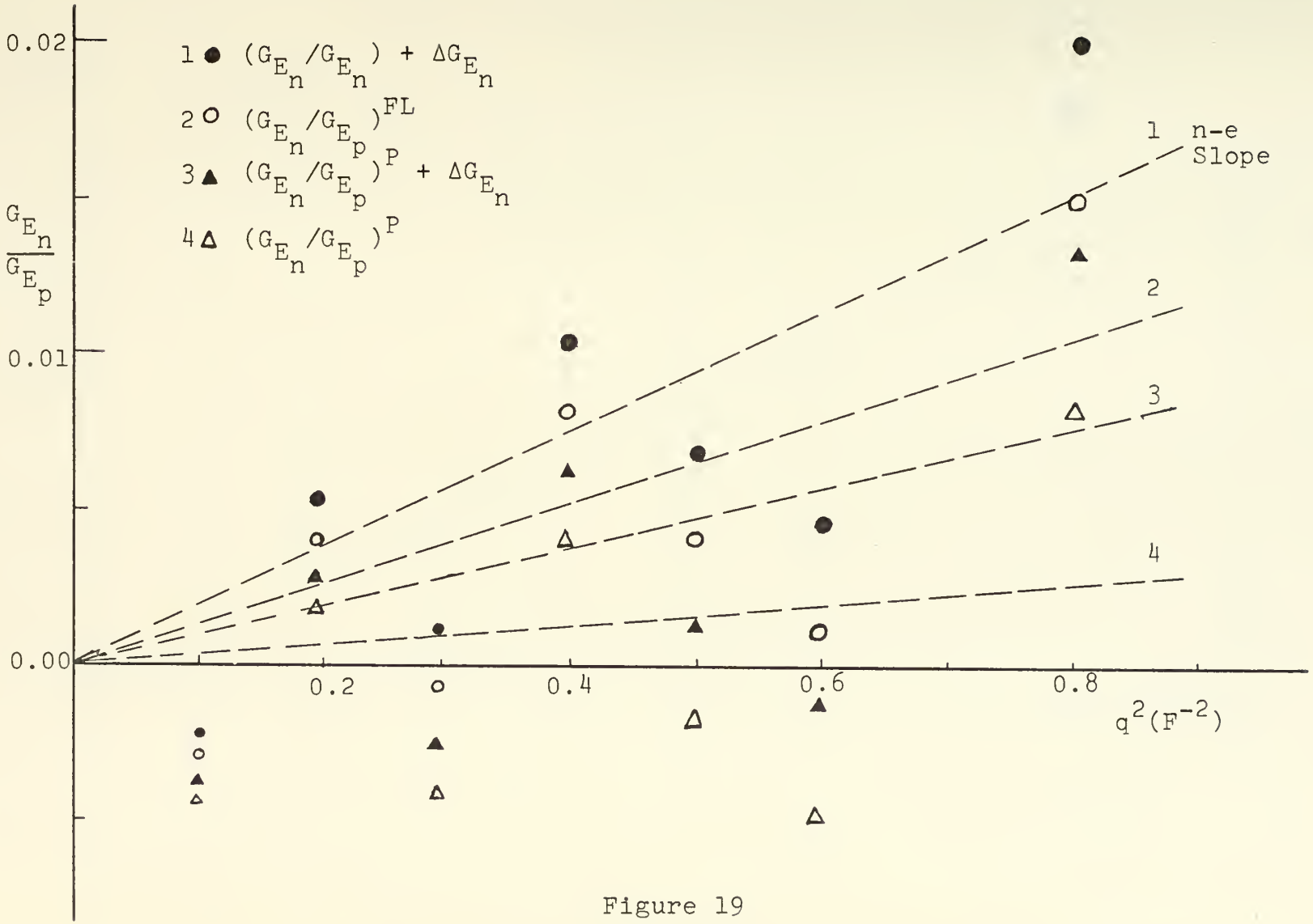
0.02
0.01
0.00
$\frac{G_{E_n}}{G_{E_p}}$
1 ● $(G_{E_n}/G_{E_n}) + \Delta G_{E_n}$
2 ○ $(G_{E_n}/G_{E_p})^{FL}$
3 ▲ $(G_{E_n}/G_{E_p})^{P} + \Delta G_{E_n}$
4 △ $(G_{E_n}/G_{E_p})^{P}$
1 n-e Slope
2
3
4
0.2
0.4
0.6
0.8
$q^2(F^{-2})$

Figure 19

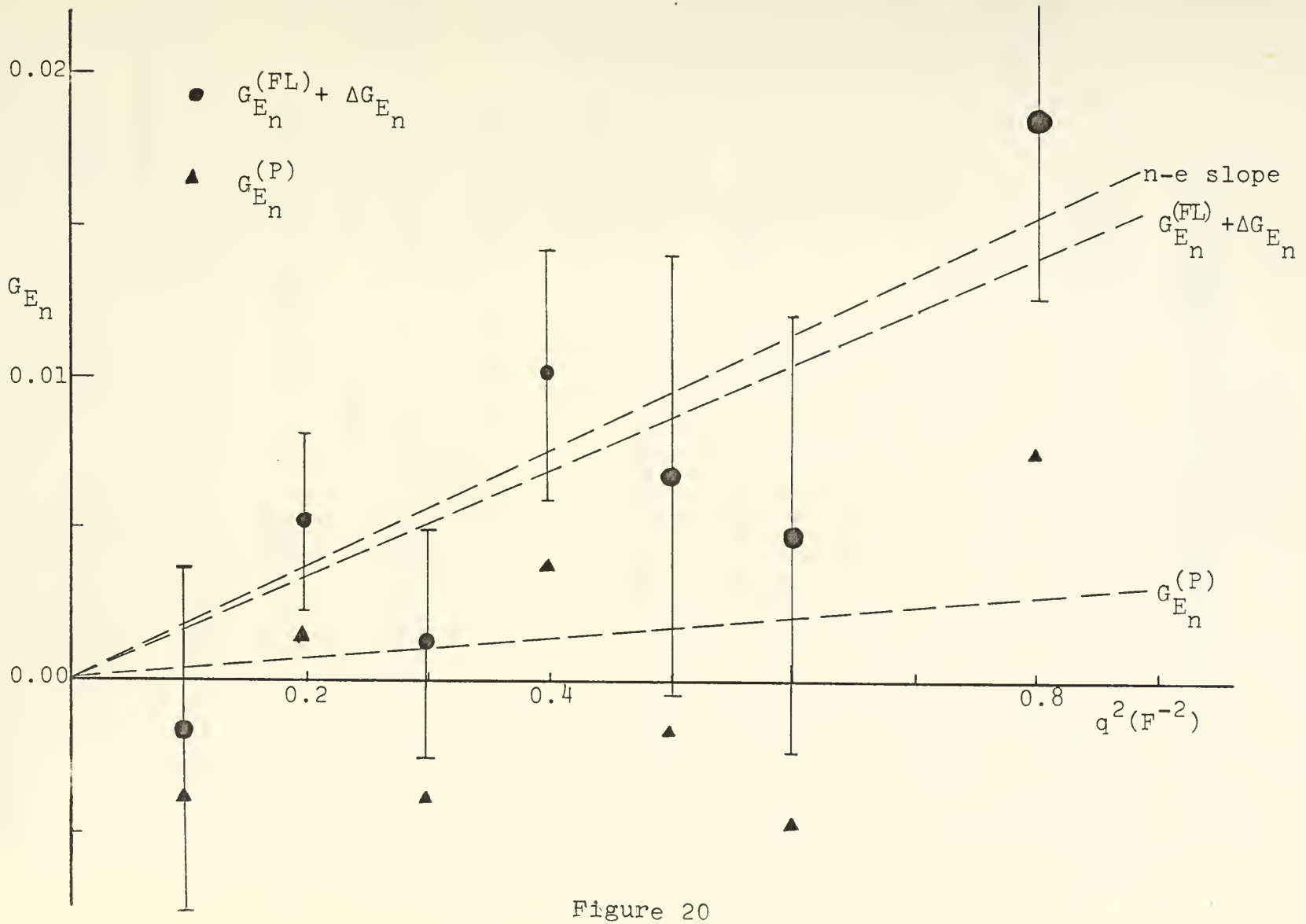
0.02
0.01
0.00
G_{E_n}
$G_{E_n}^{(FL)} + \Delta G_{E_n}$
$G_{E_n}^{(P)}$
n-e slope
$G_{E_n}^{(FL)} + \Delta G_{E_n}$
$G_{E_n}^{(P)}$
0.2
0.4
0.8
$q^2(F^{-2})$

Figure 20

APPENDIX A

THE NEUTRON CHARGE FORM FACTOR FROM THE NEUTRON-ELECTRON INTERACTION

In the n-e experiments what is measured is a scattering amplitude of a neutron by a bound electron. In the Born approximation for neutrons of very long wavelength this is related to the volume integral of V(r), the interaction potential [25]. The magnitude of the n-e interaction is expressed in the form of an equivalent potential V_0 over a sphere of radius $r_0 = \frac{e^2}{m_e c^2}$, the classical electron radius, so that the volume integral of V_0 is the experimental value of the potential. The potential V_0 is simply a convention since the classical electron radius plays no fundamental role in the problem. Thus,

$$\int V(\vec{r})d\vec{r} \xrightarrow[V(\vec{r}) = V_0 = \text{const.}]{} V_0 \int_0^{r_o} d\vec{r} = \frac{4\pi}{3} r_0^3 V_0 \quad \text{(A-1)}$$

Using Poisson's equation and the definition of r.m.s. radius $\langle r^2 \rangle \equiv \int r^2 \rho(r) d\vec{r}$, (A-1) becomes

$$\int V(\vec{r})d\vec{r} = \frac{2\pi e}{3} \int r^2 \rho(r) d\vec{r} = \frac{2\pi e^2}{3} \langle r^2 \rangle \quad \text{(A-2)}$$

Equating the right hand sides of (A-1) and (A-2) yields, in rationalized MKS units

$$\frac{2\pi e^2}{3 \times 4\pi\varepsilon_o} \langle r^2 \rangle = \frac{4\pi}{3} r_o V_o \text{ (eV) } 1.6 \times 10^{-19}$$

where ε_o is the permitivity of free space and in $(\text{Fermi})^2$

$$\langle r^2 \rangle = \frac{V_o(eV) \times r_o^3 \times 8\pi\varepsilon_o}{e \times 10^{-30}} F^2$$

$$\langle r^2 \rangle = 3.14 \times 10^{-5} V_o \text{ (eV) } F^2. \qquad \text{(A-3)}$$

From (2-90) the expression for the charge form factor is given by

$$G_{E_n} = 1 - \frac{q^2 \langle r^2 \rangle}{6} + \ldots \qquad \text{(A-4)}$$

so that the slope at the limit $q^2 \to 0$ gives

$$\left[\frac{dG_{E_n}}{dq^2}\right]_{q^2 \to 0} = \frac{-\langle r^2 \rangle}{6} = -5.23 \times 10^{-6} V_o(eV) F^2 \qquad \text{(A-5)}$$

Krohn and Ringo's [16] latest value is $V_o = -3720$ eV, hence,

$$\left[\frac{dG_{E_n}}{dq^2}\right]_{q^2 \to 0} = +0.0193 F^2.$$

APPENDIX B

PROPERTIES OF THE TENSOR OPERATOR S_{12}

Several experimental facts, like the nonadditivity of the magnetic moments (i.e., $\mu_p + \mu_n \neq \mu_d$) and the presence of the quadrupole moment Q_d in the deuteron, led to the suggestion that the nature of the nuclear force is partially noncentral, that is, it contains a partly "tensor" force.

Require that the tensor operator be symmetric in particles 1 and 2, and that it be invariant under the parity transformation (space reversal). Let $\vec{r} \equiv \vec{x}_1 - \vec{x}_2$ be the relative coordinates of particle 1 and 2. The particles have spins given by $\vec{\sigma}_1$ and $\vec{\sigma}_2$ where σ's are the Pauli spin matrices (an explicit representation)

$$\sigma_x = \begin{pmatrix} 0 & 1 \\ 1 & 0 \end{pmatrix} \quad \sigma_y = \begin{pmatrix} 0 & -i \\ i & 0 \end{pmatrix} \quad \sigma_z = \begin{pmatrix} 1 & 0 \\ 0 & -1 \end{pmatrix} \tag{B-1}$$

These matrices obey Pauli matrix algebra,

$$[\sigma_i, \sigma_j]_- = 2\delta_{ij} \qquad i,j = x,y,z \tag{B-2}$$

$$\vec{\sigma} \times \vec{\sigma} = 2i\vec{\sigma} \tag{B-3}$$

$$\sigma_x^2 = \sigma_y^2 = \sigma_z^2 = 1 \tag{B-4}$$

$$(\vec{\sigma}\cdot\vec{A})(\vec{\sigma}\cdot\vec{B}) = (\vec{A}\cdot\vec{B}) + i\vec{\sigma}\cdot(\vec{A}\times\vec{B}) \tag{B-5}$$

Application of the parity operator P to $\vec{r}$ and $\vec{\sigma}$ yields,

$$P\vec{r} \rightarrow -\vec{r}, \quad P\vec{\sigma} \rightarrow \vec{\sigma}.$$

Thus the vector $\vec{r}$ can appear only an even number of times in the tensor operator. Further, since the tensor operator is symmetric in 1 and 2, $\vec{\sigma}_1$ and $\vec{\sigma}_2$ should appear in some bilinear combination. With (B-2,3,4,5) in mind it is found that the only linearly independent quantities which can be made from $\vec{r}$, $\vec{\sigma}_1$ and $\vec{\sigma}_2$ are

$$(\vec{\sigma}_1 \cdot \vec{\sigma}_2) \qquad \text{and} \qquad (\vec{\sigma}_1 \cdot \vec{r})(\vec{\sigma}_2 \cdot \vec{r}) \tag{B-6}$$

The traditional definition then for the tensor operator S_{12} is

$$S_{12} = 3(\vec{\sigma}_1 \cdot \hat{r})(\vec{\sigma}_2 \cdot \hat{r}) - (\vec{\sigma}_1 \cdot \vec{\sigma}_2) \tag{B-7}$$

where $\hat{r} \equiv \vec{r}/|r|$.

The tensor operator (B-7) has some interesting properties, namely $\langle S_{12} \rangle$ over all directions vanishes. Consider

$$\langle (\vec{\sigma}_1 \cdot \hat{r})(\vec{\sigma}_2 \cdot \hat{r}) \rangle = \frac{1}{4\pi} \int (\vec{\sigma}_1 \cdot \hat{r})(\vec{\sigma}_2 \cdot \hat{r}) \sin\theta \, d\theta \, d\phi \tag{B-8}$$

Take $\vec{\sigma}_1$ along z-axis, $\vec{\sigma}_2$ in the x-z plane making angle α with the z axis, and $\vec{r}$ a vector making angles θ, and ϕ. Then

$$\vec{\sigma}_1 = \sigma_1 \hat{z} \tag{B-9}$$

$$\vec{\sigma}_2 = \sigma_2(\sin\alpha \, \hat{x} + \cos\alpha \, \hat{z}) \tag{B-10}$$

$$\hat{r} = \sin\theta \cos\phi \, \hat{x} + \sin\theta \sin\phi \, \hat{y} + \cos\theta \, \hat{z} \tag{B-11}$$

Putting (B-9,10,11) in (B-8) and integrating over θ and ϕ yields

$$\langle(\vec{\sigma}_1\cdot\hat{r})(\vec{\sigma}_2\cdot\hat{r})\rangle = \frac{1}{3}\,\sigma_1\sigma_2\cos\alpha = \frac{1}{3}\,(\vec{\sigma}_1\cdot\vec{\sigma}_2) \qquad \text{(B-12)}$$

Hence it follows that $\langle S_{12}\rangle = 0$.

APPENDIX C

CALCULATION OF DEUTERON MAGNETIC AND QUADRUPOLE MOMENTS

The neutron and proton magnetic moments μ_n, and μ_p have been quite accurately determined, as has the deuteron's magnetic moment μ_d. The difference $(\mu_p + \mu_n) - \mu_d = 0.0222$nm is small but not zero and much larger than the experimental error. A possible explanation is that the deuteron spends a small part of the time in some state other than the symmetric $^3S_1$ state. The task is to find the correct mixture of states that can account for the deuteron's moment.

Recall the angular wave functions for the $^3S_1$ and $^3D_1$ states

$$^3S_1: \mathcal{Y}_{011}^{1} = Y_o^o \chi_1^1 \tag{2-56}$$

$$^3D_1: \mathcal{Y}_{211}^{1} = \sqrt{\frac{3}{5}}\, Y_2^2 \chi_1^{-1} - \sqrt{\frac{3}{10}}\, Y_2^1 \chi_1^0 + \sqrt{\frac{1}{10}}\, Y_2^o \chi_1^1 \tag{2-57}$$

Using (2-56) and (2-57) construct the deuteron wave function $\phi_{\ell SJ}(\vec{r})$. Thus

$$^3S_1: \phi_{011}^{1}(\vec{r}) = \frac{u(r)}{r}\mathcal{Y}_{011}^{1} \tag{C-1}$$

$$^3D_1: \phi_{211}^{1}(\vec{r}) = \frac{w(r)}{r}\mathcal{Y}_{211}^{1} \tag{C-2}$$

The nuclear magnetic moment operator can be written

$$\hat{\mu}_z = \sum_{k=1}^{z} (\hat{\ell}_{zk} + g_p \hat{S}_{zk}) + g_n \sum_{k=z+1}^{A} \hat{S}_{zk} \tag{C-3}$$

where ℓ_k is the orbital angular momentum of the k^{th} proton, S_k the spin angular momentum of the k^{th} proton (or neutron) and where g_p and g_n are the gyromagnetic ratios of the proton and neutron, $g_p = 5.59$, $g_n = -3.83$. (The carot over μ_z denotes μ_z as an operator.) In the c-m system and for the deuteron (C-3) becomes

$$\hat{\mu}_z = \frac{1}{2}\ell_z + g_p S_{zp} + g_n S_{zn} \qquad \text{(C-4)}$$

where the orbital angular momentum associated with the proton is half of the relative orbital angular momentum. The magnetic moment is found by taking the expectation value of (C-4) between the state $\phi_{\ell SJ}^{m}$.

$$\langle \mu_z \rangle = \int d\vec{r}\ \phi_{\ell SJ}^{*m}\ \hat{\mu}_z\ \phi_{\ell SJ}^{m} = \langle \phi_{\ell SJ}^{m} | \hat{\mu}_z | \phi_{\ell SJ}^{m} \rangle \qquad \text{(C-5)}$$

The following formula are useful in evaluating (C-5)

$$\ell_z Y_\ell^m = mY_\ell^m \qquad g_{p,n} = 2\mu_{p,n} \qquad (S_{p,n})_z = \frac{1}{2}(\vec{\sigma}_{p,n})_z$$

$$S_{zp}\chi_1^1 = \frac{1}{2}\chi_1^1 \qquad S_{zn}\chi_1^1 = \frac{1}{2}\chi_1^1$$

$$S_{zp}\chi_1^0 = \frac{1}{2}\chi_0^0 \qquad S_{zn}\chi_1^0 = -\frac{1}{2}\chi_1^0 \qquad \text{(C-6)}$$

$$S_{zp}\chi_1^{-1} = -\frac{1}{2}\chi_1^{-1} \qquad S_{zn}\chi_1^{-1} = -\frac{1}{2}\chi_1^{-1}$$

$$S_{zp}\chi_0^0 = \frac{1}{2}\chi_1^0 \qquad S_{zn}\chi_1^0 = -\frac{1}{2}\chi_1^0$$

Hence

$$\hat{\mu}_z \mathcal{Y}_{011}^{1} = \tfrac{1}{2}(g_p + g_n)\mathcal{Y}_{011}^{1} = \tfrac{1}{2}(g_p + g_n) Y_0^0 \chi_1^1$$

$$\hat{\mu}_z \mathcal{Y}_{211}^{1} = \sqrt{\tfrac{3}{5}}\left(1 - \frac{g_p + g_n}{2}\right) Y_2^2 \chi_1^{-1} - \tfrac{1}{2}\sqrt{\tfrac{3}{10}}\, Y_2^1\left[\chi_1^0 + (g_p - g_n)\chi_0^0\right]$$

$$+\sqrt{\tfrac{1}{10}}\,\frac{g_p + g_n}{2}\, Y_2^0 \chi_1^1. \qquad \text{(C-7)}$$

The orthonormality of the spherical harmonics Y integrated over the solid angle, and the orthonormality of the spin-wave functions $\chi_s^{m_s}$ applied to (C-7) yields

$$^3S_1: \langle \phi_{011}^{1} | \hat{\mu}_z | \phi_{011}^{1} \rangle = \frac{g_p + g_n}{2} \int_0^\infty u^2(r)dr = \frac{g_p + g_n}{2} \qquad \text{(C-8)}$$

$$= 0.8797 \text{ nm}$$

$$^3D_1: \langle \phi_{211}^{1} | \hat{\mu}_z | \phi_{211}^{1} \rangle = \left[\tfrac{3}{4} - \tfrac{1}{4}(g_p + g_n)\right] \int_0^\infty w^2(r)dr = \qquad \text{(C-9)}$$

$$\left[\tfrac{3}{4} - \tfrac{1}{4}(g_p + g_n)\right] = 0.3101 \text{ nm}$$

In evaluating the radial integrals the assumption was made that the deuteron was in a definite state, either S or D but not both. But the deuteron magnetic moment is 0.8573 nm, that is, neither of the two values above. Thus consider a mixture of the two states.

The total wave function for a combination of states is

$$\phi = \phi_s + \phi_D = \phi_{011}^{1} + \phi_{211}^{1} \qquad \text{(C-10)}$$

Normalization gives

$$\langle\phi|\phi\rangle = P_s + P_D = 1 \qquad \text{(C-11)}$$

where $P_s \equiv \int_0^\infty u^2(r)dr$, $P_D = \int_0^\infty w^2(r)dr$ are the individual probabilities that the deuteron is in an S or D state. Thus

$$\mu_{^3S_1+^3D_1} = \frac{1}{2}(g_p + g_n)P_s + \left[\frac{3}{4} - \frac{1}{4}(g_p + g_n)\right]P_D \qquad \text{(C-12)}$$

Equations (11) and (12) are two simultaneous equations in the two unknowns P_s and P_D. Using the experimental value of μ_d for μ in (C-12) the solution for P_s and P_D are

$$P_D = 4\%, \quad P_s = 96\%$$

The quadrupole moment Q_d can be found in the same manner as the magnetic moment,

$$\hat{Q}_d = 3\hat{z}^2 - \hat{r}^2 = (3\cos^2\theta - 1)r^2 \qquad \text{(C-13)}$$

In the c-m system, the distance of the neutron and proton from the center of mass is r/2, and only the proton contributes to Q_d. Hence,

$$\langle Q_d\rangle = \frac{1}{4}\int\phi^*(3\cos^2\theta - 1)\phi r^2 d\vec{r} \qquad \text{(C-14)}$$

In terms of spherical harmonics this becomes,

$$\langle Q_d\rangle = \frac{1}{4}\sqrt{\frac{16\pi}{5}}\int\phi^* r^2 Y_2^0\, d\vec{r}$$

$$\langle Q_d\rangle = \frac{1}{4}\sqrt{\frac{16\pi}{5}}\int\Big[u^2 \mathcal{Y}^{*\,1}_{011}\, Y_2^0\, \mathcal{Y}^{1}_{011} + uw\Big(\mathcal{Y}^{*\,1}_{011}\, Y_2^0\, \mathcal{Y}^{1}_{211} + \mathcal{Y}^{1}_{011}\, Y_2^0 \mathcal{Y}^{*\,1}_{211}\Big) + w^2 \mathcal{Y}^{*\,1}_{211} + Y_2^0\, \mathcal{Y}^{1}_{211}\Big]d\vec{r}.$$

The first term represents the pure $^3S_1$ contribution and when integrated over the solid angle it is zero because of spherical symmetry. The next terms in parentheses are hermitian conjugates of each other and the total can be written as

$$\frac{1}{2}\sqrt{\frac{16\pi}{5}}\int uw\,\mathcal{Y}^{*}_{011}\,Y^{0}_{2}\,\mathcal{Y}_{211}\,d\vec{r}$$

which after angular integration gives

$$\frac{1}{\sqrt{50}}\int_0^\infty uwr^2\,dr.$$

The third term comes from the $^3D_1$ state and gives

$$-\frac{1}{20}\int_0^\infty w^2r^2\,dr.$$

Hence

$$\langle Q_d\rangle = \frac{\sqrt{2}}{10}\int_0^\infty uwr^2\,dr - \frac{1}{20}\int_0^\infty w^2r^2\,dr \qquad \text{(C-15)}$$

To go further, explicit solutions for the radial wave functions u(r) and w(r) are needed. Some examples of Q_d for specific numerical solutions u and w are listed in Table III.

APPENDIX D

THE BREIT OR BRICKWALL FRAME

The Breit frame is a Lorentz frame in which either $\vec{k}_1 + \vec{k}_2'$ or, $\vec{p}_1 + \vec{p}_2'$ vanish, where in an elastic two-body collision, $\vec{k}_1$, $\vec{p}_1$ are incident particle 3-momentum and $\vec{k}_2'$, $\vec{p}_2'$ are outgoing particle 3-momentum. The somewhat odd notation stems from traditional techniques in elastic scattering theory and dispersion relations, particularly the Mandelstam representation. Consider Figure D-1. The convention is that all four-momentum are ingoing. This has the advantage that one may consider any two of the four to be the incoming particles and the other two as outgoing ones; the physical momentum of the outgoing particles is then the negative of the one used in Figure D-1.

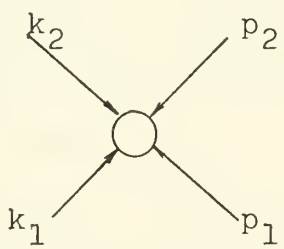

Figure D-1

The physical momentum of an outgoing particle is denoted by a prime. For example, if the particle corresponding to the arrow with k_2 is outgoing, it has physical momentum $k_2' = -k_2$.

Apply a Lorentz transformation to the scattering event such that $\vec{k}_1 + \vec{k}_2 = 0$. Thus, four-momentums k_1 and k_2' have the form ($\hbar = c = 1$)

$$k_1 = (\omega,\vec{k}), \quad k_2' = (\omega,-\vec{k}) \tag{D-1}$$

From conservation of energy it follows that the energies of the p particle before and after the collision, ε_1 and ε_2' must be equal. Hence $|\vec{p}_1| = |\vec{p}_2'|$ and

$$p_1 = (\varepsilon,\vec{p}_1), \quad p_2' = (\varepsilon,\vec{p}_2') \tag{D-2}$$

with

$$|\vec{p}_1| = |\vec{p}_2| = p = \sqrt{\varepsilon^2 - m^2}$$

Since scattering is elastic $k_1 - k_2' = p_2' - p_1$ and it follows

$$k_1 - k_2' = (0,2\vec{k}) = p_2' - p_1 = (0,\vec{p}_2' - \vec{p}_1) \tag{D-3}$$

$2\vec{k}$ the three momentum transfer. Equation (1) (2) and (3) yield the following picture. Both particles seem to be reflected on a hard wall, the k particle perpendicularly and the particle at some angle

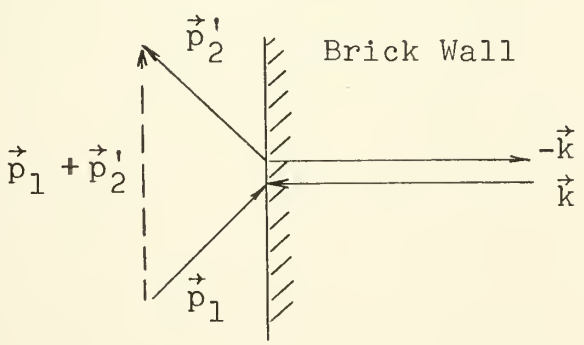

Figure D-2

In the c-m system the energies ε and ω of the p and k particles are not independent, but they are in this system. Therefore they are convenient to use as variables. In this system the four momentum transfer is very simple:

$$q^2 = (k_1 - k_2')^2 = (0, 2\vec{k})^2 = - |2\vec{k}|^2 = -\vec{q}^2$$

i.e., it is the three momentum transfer.

LIST OF REFERENCES

1. Drickey, D. J. and Hand, L. N., Phys. Rev. Letters 9, 521, 1962.
2. Casper, B. M. and Gross, F., Phys. Rev. 155, 1607, 1967.
3. Jankus, V. Z., Phys. Rev. 102, 1586, 1956.
4. Jones, H. F., Nuovo Cimento 26, 790, 1962.
5. Gourdin, M., Nuovo Cinento 35, 1105, 1965.
6. Adler, R. J. and Drell, S. D., Phys, Rev. Letters 13, 349, 1964.
7. Adler, R. J., Phys. Rev. 141, 1499, 1966.
8. Gross, F., Phys. Rev. 134, B405, 1964.
9. Gross, F., Phys Rev. 136, B140, 1964.
10. Gross, F., Phys Rev. 140, B410, 1965.
11. Gross, F., Phys Rev. 142, 1025, 1966.
12. Hughes, D. J., Pile Neutron Research, Addison Wesley Publishing Company, Cambridge, Mass., 1953.
13. Foldy, L. L., Phys. Rev. 87, 693, 1952.
14. Havens, W., Rabi, I. I., and Rainwater, L. J., Phys. Rev. 72, 634, 1947.
15. Hughes, D., Harvey, J. A., Goldberger, M. D. and Stafue, M. J., Phys. Rev. 90, 497, 1953.
16. Krohn, V. E., Ringo, G. R., Phys, Rev. 148, 1303, 1966.
17. Fermi, E., and Marshall, L., Phys. Rev. 72, 1139, 1947.
18. Glendenning, N. K., and Kramer, G., Phys. Rev. 126, 2159, 1962.
19. Signell, P. S., and Marshak, R. E., Phys.Rev.106, 832, 1957.
20. Gammel, J. L., and Thaler, R. M., Phys. Rev. 107, 1337, 1957.

21. Hamada, T., Progr. Theoret. Phys. (Kyoto) 24, 126, 1960.

22. Hamada, T., and Johnston, I. D., Nuc. Phys. 34, 382, 1962.

23. Feshbach, H. and Lomon, E., Ann. of Physics (US) 48, 94, 1968.

24. Rarita, W. and Schwinger, J., Phys. Rev. 59, 436, 1941.

25. Foldy, L. L., Phys. Rev. 87, 688, 1952.

26. Yennie, D., Levy, M., and Ravenhall, D., Rev. Mod. Phys. 29, 144, 1957.

27. Hand, L. N., Miller, D. G. and Wilson, R., Rev. Mod. Phys. 35, 335, 1963.

28. de Vries, C., Hofstadter, R., Johansson, A. and Herman, R., Phys. Rev. 134, B848, 1964.

29. Scotti, A. and Wong, D. Y., Phys. Rev. 138, B145, 1965.

30. Chew, G. F., Karplus, R., Gasiorowicz, S. and Zachariasen, F., Phys. Rev. 110, 265, 1958.

31. Lehmann, P., Taylor, R. and Wilson, R., Phys. Rev. 126, 1183, 1962.

32. Glaser, V. and Jaksic, B., Nuovo Cimento 5, 1197, 1957.

33. Erickson, E., Thesis, Stanford University.

34. Van, J., Nuovo Cimento 30, 1100, 1963.

35. Gourdin, M., Nuovo Cimento 33, 1391, 1964.

36. Cutkosky, R. E., Proc. of the 1960 Annual Conference on High Energy Physics at Rochester, 236, Interscience Publishers Inc., New York, 1960.

37. Chilton, F. and Uhrhane, F., High Energy Physics Laboratory Report 454, Stanford University (unpublished).

38. Midgarden, P. S., Naval Postgraduate School Thesis, December 1957.

39. Gordon, R., Naval Postgraduate School Thesis, June 1968.

40. Crannel, H. and Suelzle, L., Nuc. Instr. and Methods 44, 133, 1966.

41. Tsai, Y., Phys. Rev. 122, 1898, 1961.

42. Bethe, H. A. and Ashkin, J., Experimental Nuclear Physics, John Wiley and Sons, Inc., New York, 1953.

43. Schwinger, J., Phys. Rev. 75, 898, 1949.

44. Gordon, J., Naval Postgraduate School Thesis, June 1970.

45. Adler, R. J., Thesis, Stanford University, unpublished.

46. Elias, J., Friedman, J., Hartman, G., Kendall, H., Sogard, M. Van Speybroeck, L., and de Pagter, J. K., Phys. Rev.

INITIAL DISTRIBUTION LIST

		No. Copies
1.	Defense Documentation Center Cameron Station Alexandria, Virginia 22314	2
2.	Library Naval Postgraduate School Monterey, California 93940	2
3.	Professor F. A. Bumiller, 61Bw Department of Physics Naval Postgraduate School Monterey, California 93940	1
4.	LCDR Jake W. Stewart, Jr. USS KING (DLG-10) Fleet Post Office, San Francisco California 96601	1

DOCUMENT CONTROL DATA - R & D

(Security classification of title, body of abstract and indexing annotation must be entered when the overall report is classified)

ORIGINATING ACTIVITY (Corporate author)

Naval Postgraduate School
Monterey, California 93940

2a. REPORT SECURITY CLASSIFICATION

Unclassified

2b. GROUP

REPORT TITLE

ELASTIC ELECTRON SCATTERING MEASUREMENTS OF THE NEUTRON CHARGE FORM FACTOR AT VERY LOW MOMENTUM TRANSFERS

DESCRIPTIVE NOTES (Type of report and inclusive dates)

Ph.D. Thesis; June 1970

AUTHOR(S) (First name, middle initial, last name)

Jake W. Stewart, Jr., Lieutenant Commander, United States Navy

REPORT DATE

June 1970

7a. TOTAL NO. OF PAGES

135

7b. NO. OF REFS

46

CONTRACT OR GRANT NO.

PROJECT NO.

9a. ORIGINATOR'S REPORT NUMBER(S)

9b. OTHER REPORT NO(S) (Any other numbers that may be assigned this report)

DISTRIBUTION STATEMENT

This document has been approved for public release and sale; its distribution is unlimited.

SUPPLEMENTARY NOTES

12. SPONSORING MILITARY ACTIVITY

Naval Postgraduate School
Monterey, California 93940

ABSTRACT

Measurements of the ratio of the neutron-proton electric form factors, G_{E_n}/G_{E_p}, were made from elastic electron-deuteron scattering to a precision of approximately 1 to 2% for the range of momentum transfers, q^2 of $0.10 \leq q^2 \leq 0.8$ F^{-2}, and for electron scattering angles of 45° to 120°. It was found that within experimental errors the slope as determined from the ratio, G_{E_n}/G_{E_p}, agrees with the thermal neutron-electron interaction slope when relativistic corrections and proper deuteron wave functions are applied to the electron-deuteron scattering results.

KEY WORDS	LINK A		LINK B		LINK C	
	ROLE	WT	ROLE	WT	ROLE	WT
CHARGE FORM FACTOR						
NEUTRON						
ELECTRON SCATTERING						
DEUTERON						

Thesis
S7144 Stewart
c.1
Elastic electron scattering measurements of the neutron charge form factor at very low momentum transfers.
119015